Doctoral Dissertation

Preparation and Gas Permeation Properties of AEI, CHA Zeolite Membranes as well as these Zeolites filled Mixed Matrix Membranes

（AEI 型と CHA 型のゼオライト膜およびこれらのゼオライトを用いた Mixed Matrix Membrane の作製とガス透過特性）

WU TING

呉 婷

Division of Environmental Science and Engineering

Graduate School of Science and Engineering

Yamaguchi University

山口大学大学院理工学研究科環境共生系専攻

2018/3

Abstract

Gas separation is an important process in the field of chemical engineering and usually achieves by some energy-intensive processes such as absorption, adsorption and distillation. In the view of worldwide sustainable development, and chemical industry demands low costs and high efficient processes. Membrane based gas separation provides an alternate way to those energy-intensive processes due to less-environment impact, lower energy consumption and more efficiency. Polymer membranes are widely used in gas separation processes while the low performance as described in Robeson plot limited its application. Zeolite membranes are being developed and display much higher performance over polymer membranes. Recently, the CHA zeolite membranes attract much attention in natural gas separations. AEI type zeolites, similar to CHA type zeolites, own a 3D pore structure system with the size of ~0.38nm that close to the kinetic diameter of light gases, indicating the ability for light gas separation by membrane processes. At the same time, mixed matrix membranes (MMMs), with less expensive and medium performance compared to zeolite membranes, are intensively investigated those years.

With this respect, we devoted our attention to prepare and investigate gas permeation properties of AEI and CHA zeolite membranes as well as AEI-type, CHA-type zeolites filled mixed matrix membranes. This thesis can be divided into seven Chapters. Chapter 1 is the overview of membrane based gas separation processes and the corresponding gas separation membranes as well as some importance applications.

In Chapter 2, three AEI type AlPO-18 zeolites with crystal sizes of 300 to 700 nm, one CHA type SSZ-13 zeolite of ~400 nm and six CHA type SAPO-34 zeolites with crystal sizes range from 0.1 to 3 μm were prepared by using different gel compositions.

In Chapter 3, AlPO-18 membranes were prepared by using combined TEAOH and DIPEA templates, single TEAOH template and single DIPEA template, respectively. AlPO-5 impurity was formed by using n(DIPEA) from 1.0 to 1.2 when synthesized at 478K for 48h. The corresponding gas permeation properties were also investigated. The as-synthesized AlPO-18 membranes through combined TEAOH and DIPEA templates displayed moderate CO_2 single gas permeance with lowest CO_2/CH_4 ideal selectivity. The obtained AlPO-18 membranes by single TEAOH template displayed highest

CO$_2$/CH$_4$ selectivity however lowest CO$_2$ gas permeance. The AlPO-18 membrane prepared with single DIPEA template displayed highest CO$_2$ single gas permeance and moderate CO$_2$/CH$_4$ ideal selectivity. Meanwhile, gas permeation properties of both pure and impure AlPO-18 membranes were affected by measuring conditions of temperature and pressure. CO$_2$ and N$_2$ single gas permeances decreased dramatically by increasing temperature, while CH$_4$ single gas permeance was almost independent of temperature. Pressure also decreased CO$_2$ single gas permeance however slightly increased both N$_2$ and CH$_4$ single gas permeances.

In Chapter 4, two types CHA zeolite membranes (SAPO-34 and SSZ-13) are used for CO$_2$/CH$_4$, N$_2$/CH$_4$, and CO$_2$/i-butane separations at both low (270 and 350kPa) and high (1.73MPa) pressures. The SSZ-13 membranes were more selective, with CO$_2$/CH$_4$ separation selectivity as high as 280 and N$_2$/CH$_4$ separation selectivity of 12 at 270 kPa feed pressure. The CO$_2$/i-butane separation selectivities were greater than 500,000 for SAPO-34 membranes but were smaller for SSZ-13 membranes (2,800-20,000) due to concentration polarization and possible O-ring sealing. SSZ-13 membranes separated CO$_2$/CH$_4$ mixtures with higher selectivity (> 200 at high pressure) than SAPO-34 membranes, but their permeances were only ~10% of the SAPO-34 membrane permeances because the SSZ-13 membranes are thicker. The effects of propane impurity with the different concentrations on the SAPO-34 and SSZ-13 membranes for both CO$_2$/CH$_4$ and N$_2$/CH$_4$ are discussed. Propane continuously decreases CO$_2$ and N$_2$ permeances for both SSZ-13 and SAPO-34 membranes at low pressures, but permeances decreased ten times faster for SAPO-34 membranes. Propane only changed selectivities slightly but steady state was not reached after seven days.

In Chapter 5, gas permeation properties on PESU based flat mixed matrix membranes by filling CHA type SAPO-34, SSZ-13 and AEI type AlPO-18 zeolites were investigated. CHA type zeolites loaded PESU-MMMs showed higher gas separation performance than AEI type zeolites loaded PESU-MMMs. The PESU-MMMs by incorporating homogeneous SAPO-34-3 with the crystal size of 200 nm and SSZ-13 with the crystal size of 400 nm showed a continuous interface with less defects. SAPO-34 as the filler showed higher ideal selectivity and SSZ-13 as the filler displayed higher single gas permeability. Moreover, CO$_2$ single gas permeability and CO$_2$/CH$_4$ ideal selectivity was increased by increasing the filler loading from 20 wt.% to 30 wt.% for SAPO-34 with 200nm crystals size.

In Chapter 6, gas permeation properties on 6FDA-TrMPD (PI) based flat mixed matrix

membranes by filling both homogeneous and heterogeneous SAPO-34 zeolites were investigated. Single gas permeability was dramatically improved by filling both homogeneous and heterogeneous zeolites along with decreasing a little ideal selectivity. Single gas permeability was improved as increasing the filler loading with 20 wt.%, 30 wt.% and 40 wt.%. Higher permeability membrane can be obtained by loading homogeneous zeolites. Meanwhile, using milling method to prepare 6FDA-TrMPD (PI)/SAPO-34 MMMs can improve both CO_2 single gas permeability and CO_2/CH_4 selectivity.

Finally, Chapter 7 summarized the main contents of this thesis.

要旨

ガス分離は化学工学の分野で重要なプロセスであり、通常、吸収、吸着、蒸留などのエネルギー集約的なプロセスで行なわれている。持続可能な発展の観点から、化学産業は低コストと高効率の分離プロセスを求めている。膜ベースのガス分離は、環境への影響とエネルギー消費が少なく、効率が高いため、エネルギー集中型のプロセスに代わる方法を提供する。ポリマー膜はガス分離プロセスで使用されているが、Robeson プロットに記載されているように性能が高くなくその用途が限定される。これに対しゼオライト膜はポリマー膜よりもはるかに高い性能を示す。この中でも近年、CHA 型ゼオライト膜が天然ガス分離用に多くの注目を集めている。CHA 型ゼオライトに類似した AEI 型ゼオライトは約 0.38nm の 3 次元細孔構造を有する。これは軽質ガスの分子サイズに近く、膜プロセスによる軽質ガス分離能力を持つ。また、混合マトリックス膜（MMM）はゼオライト膜と比較して安価で中程度の性能を有し、近年盛んに研究されている。

このような状況において本研究では、AEI 型と CHA 型のゼオライト膜およびこれらのゼオライトを用いた Mixed Matrix Membrane の作製とガス透過特性を検討した。本論文は 7 つの章で構成されている。

第 1 はガス分離プロセスで使用されるガス分離膜とその応用に関する概要である。

第 2 章では、300nm~700nm の結晶サイズを有する AEI 型 AlPO-18 ゼオライト 3 種類、400nm の CHA 型 SSZ-13 ゼオライト 1 種類と 100nm~3μm の CHA 型 SAPO-34 ゼオライト 6 種類の調製方法について考察した。

第 3 章では、2 種類のテンプレート TEAOH と DIPEA を混合した合成溶液、TEAOH のみの合成溶液と DIPEA のみの合成溶液をそれぞれ使用して AlPO-18 膜を製膜した。n（DIPEA）＝1.0 と 1.2 を用いて 48 時間 478K で合成した場合に不純物の AlPO-5 が生成した。これらのガス透過特性も検討した。2 種類のテンプレート TEAOH と DIPEA を混合した溶液で作製した AlPO-18 膜は CO_2/CH_4 理想選択性が最も低く、CO_2 単ガス透過速度は 2 番目の性能を示した。TEAOH のみを使用して得られた AlPO-18 膜は最も高い CO_2/CH_4 理想選択性を

示したが、最も低い CO_2 単ガス透過速度を示した。DIPEA のみを使用して調製した AlPO-18 膜は、最も高い CO_2 単ガス透過速度および 2 番目の CO_2/CH_4 理想選択性を示した。純粋な AlPO-18 膜と不純物が含まれる AlPO-18 膜の両方のガス透過特性は、温度および圧力の影響を受けた。CO_2、N_2 の単一ガス透過速度は温度上昇によって顕著に減少したが、CH_4 単一ガス透過速度は温度にほとんど依存しなかった。また、圧力は CO_2 単一ガス透過速度を減少させたが、N_2 および CH_4 単一ガス透過速度をわずかに増加させた。

第 4 章では、低圧（270 と 350kPa）と高圧(1.73MPa)の条件下で測定を行った。2 種類の CHA 型 SAPO-34 と SSZ-13 ゼオライト膜を用いて CO_2/CH_4、N_2/CH_4 及び CO_2/i-butane ガス透過特性を検討した。高い選択性の SSZ-13 膜は供給圧力 350kPa で CO_2/CH_4 分離性 280 及び N_2/CH_4 分離性 12 を有していた。SAPO-34 膜について、CO_2/i-ブタン分離選択性は 500,000 以上であった。SSZ-13 膜では、濃度分極と O リングシールの問題のため、CO_2/i-ブタン分離選択性は 2,800-20,000 であった。SSZ-13 膜は、SAPO-34 膜よりも高い選択性（>200）で CO_2/CH_4 混合気体を分離したが、SSZ-13 の膜が厚くなるので、それらのパーミアンスは、SAPO-34 の膜パーミアンスのわずか約 10%であった。CO_2/CH_4 と N_2/CH_4 分離でのプロパンの影響を SAPO-34 膜及び SSZ-13 膜について検討した。プロパンが低い圧力で、SSZ-13 および SAPO-34 膜の両方において CO_2 と N_2 パーミアンスは連続的に減少した。プロパンを含まないものと比較してパーミアンスは SAPO-34 膜に関して 10 倍速く減少した。プロパンを含む場合は、わずかに選択性が変化したが、7 日後でも定常状態には到達しなかった。

第 5 章では、PESU に CHA 型 SAPO-34、SSZ-13 または AEI 型 AlPO-18 ゼオライトを混合した平膜 (MMMs) のガス透過特性を調べた。CHA 型ゼオライトを用いた PESU-MMM は、AEI 型ゼオライトを用いた PESU-MMM よりも高いガス分離性能を示した。結晶サイズ 200nm の均一な SAPO-34-3 および結晶サイズ 400nm の SSZ-13 を含有した PESU-MMM は、欠陥の少ない連続的な界面を示した。充填材の SAPO-34 はより高い理想選択性を示し、SSZ-13 はより高い単一ガス透過率をもたらした。また、200nm の結晶サイズを有する SAPO-34 について、充填量を 20wt.%から 30wt.%に増加させることにより、CO_2 単一ガス透過率および CO_2/CH_4 理想選択性が増加した。

第 6 章では、6FDA-TrMPD（PI）に CHA 型 SAPO-34 ゼオライト充填した平膜のガス透過特性を調べた。単一のガス透過率は、ゼオライトを充填することによって改善されたが、理想選択性は少し低下した。一方、充填材が 20 wt.%、30 wt.%、40 wt.%と増加するにつれて、単一ガス透過率は改善された。しかし、ゼオライトを充填することで、より高い透過性能膜を得ることができ、6FDA-TrMPD（PI）/SAPO-34 MMM に粉砕法を用いて製膜することによって、CO_2 単一ガス透過率および CO_2/CH_4 選択性を改善することができた。

第 7 章ではこの研究の結論をまとめた。

Contents

Chapter 1 Introduction

1.1 Membranes for gas separation

The gas separation technology by using membrane-based materials has attracted much attentions in a plenty of chemical industrial processes since last century during 1980s [1–8]. Back to the past centuries, the gas transport properties were firstly observed by Mitchell through the balloons that made by the natural rubber-India rubber, and in 1860, the remarkable contribution was obtained by Thomas Graham, who later described the basic principle concept and theory of gas transportation with nonporous polymer membranes for gas separation in 1866 [9]. Since then, a plenty of researches were performed for the gas separation through membranes, and until approximately in 1970s, the commercial industrial by gas separation membranes were established. The membrane-based gas separation processes were grown exponentially following [10,11]. In recent 30 years, the membrane-based gas separations have already made a big progress and showed a competitive strength compared with the well-established process such as pressure swing adsorption [12–14], absorption [15] and cryogenic distillation [16–18] due to the energy-saving, low capital cost, environment friendly and easy-operation effects [4,8,19–23]. The membranes-based gas separation process showed a broad application in many industrial processes, such as CO_2/CH_4 and N_2/CH_4 separation in natural gas, O_2/N_2 separation in air separation, CO_2/N_2 separation from post-combustion gases and H_2 purification from the mixtures with N_2 or hydrocarbons in petrochemical industrial.

Figure 1 shows the schematic gas separation process through membrane. One can easily go through while the other one cannot. The perfect gas separation properties with both high permeability and selectivity are the key point for gas separation membranes. At the same time, the good thermal, hydrothermal, chemical-resistance and stability are also important for membranes in gas separation industries. There are varieties types of membrane classifications according to the different chemical and physical properties.

In this thesis, the gas separation membranes are cataloged into three groups based on the nature of the membranes materials: polymer membrane, inorganic membrane and mixed matrix membrane.
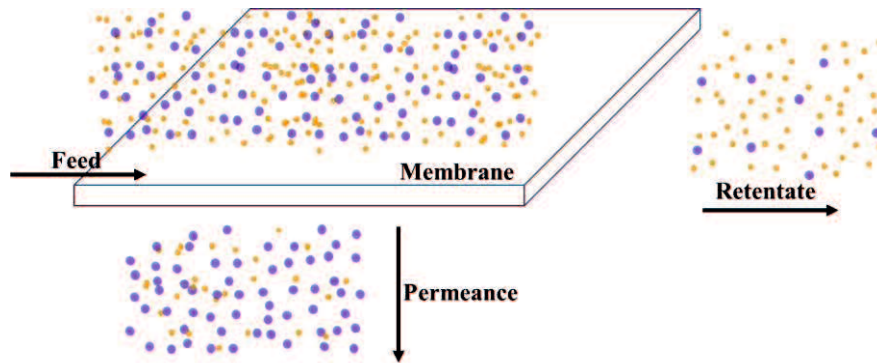
Figure 1 The schematic gas separation process of membrane.

1.1.1 Polymer membranes

The first successful membrane-based practical gas separation application was performed by polymer membrane and built in 1979-1980 by Monsanto [8]. Since then, many industrial gas separation applications were performed by using polymer membranes. According to the properties, the polymer membranes can be classified into rubbery and glassy polymers. Figure 2 described some examples of the polymer membranes for gas separations in the industrial applications. Polymer membranes [7,19,24–28] with the good processability, low operating cost, high flexibility and scalability [29], currently dominate the membrane-based gas separation markets [30] and show attractivities for air, hydrogen and CO_2 separations. Gas separations by polymer membranes have been studied for over decades and lots of polymers have been investigated as the membrane materials till now, while, so far, the potential and capable polymer membrane materials for industrial gas separations are limited [31]. Table 1 summarized some current membrane materials used for the actual industrial gas separations applications [19,29]. Both rubbery and glassy polymers can be used as the promising materials for the gas separation membranes, such as the rubbery polymer-silicon rubbery [32,33]and the glassy polymers [7,26,34] for example cellulose acetate

[35–37], polysulfone [27,38–40] and polymides [41–43].
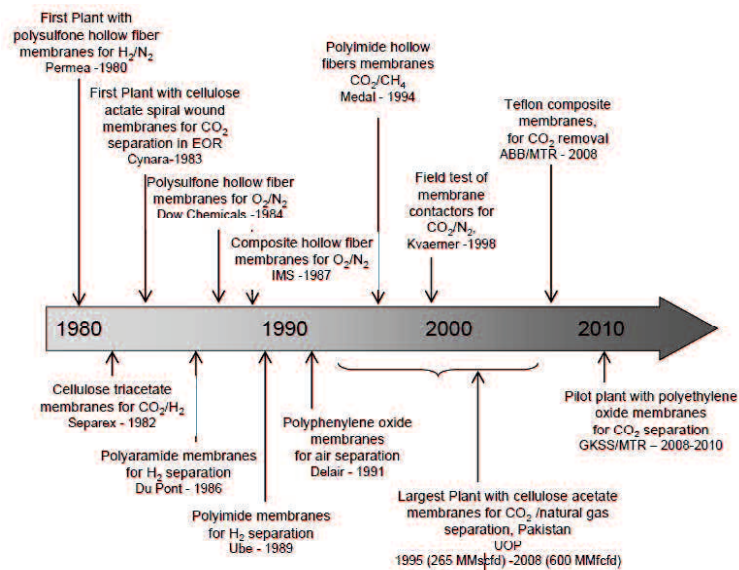
Figure 2 Industrial application by polymer membranes for gas separations [44].

However, some disadvantages limited the gas separation application by polymer membranes, such as lower thermal, chemical stability and poor resistance to the contaminants. what's more, the trade-off between permeability and selectivity described in the Robeson plot [26,34] for polymeric membranes are also limited the further improvement in the gas separation industrial.

Table 1 Industrial application of principal companies and membrane materials for gas separations [29].

Polymer type	Polymer materials	Company
Glassy	Polysulfone	Permea (air separation)
Glassy	Polysulfone, Polymide	Grasys
Glassy	Polymides	MEDAL(air liquid separation)
Glassy	Polymide	Ube
Glassy	Cellulose acetate	Separex (UOP)
Glassy	Ethyl cellulose	Air Liquid
Glassy	Tetrabromopolycarbonate	Generon
Rubbery	Silicon rubber	MTR
Rubbery	Poly(phenylene oxide)	Aquila

As with the relative low capital costs and ability that can be applied into a variety of applications [19], polymeric membranes still exhibit the big chance to apply for the gas separations market, and the combination of both good permeability and selectivity, as well as good stability of polymeric membranes is the main point for industrial

3

application [45].

1.1.2 Inorganic membranes

Inorganic membranes were developed since before 1945, as so far, the inorganic membranes were widely investigated and played a significant role in numerous gas separation applications [21]. Inorganic membranes are a kind of membrane that made of a series of materials like zeolite, silica, ceramic, carbon, oxides, metals and so on, which have higher selectivity and permeability and can bear much severer operating conditions such as higher chemical resistance [46] compared with polymer membranes [47,48]. Figure 3 shows the structure of the inorganic membranes according to Ismail [21]. The inorganic membranes can be classified into two categories based on the structure properties: dense and porous membranes, and base on the pore structure, the porous membranes can be distributed into asymmetric and symmetric membranes [21,49]. The dense membranes are studied less due to the lower permeability [21] and higher cost compared with the porous membranes. In recent years, the porous inorganic membranes, such as the zeolite membranes and carbon molecular sieve membranes, as with the uniform, molecular-sized pore properties and excellent thermal, chemical stabilities, meanwhile with a much higher permeability and stability, displayed a widespread and intensive studies in gas separation processes. And for the porous inorganic membranes, one of the key parameter is the pore size. According to the IUPAC definition of the pore diameter, the inorganic membranes can be classified into three types: microporous membrane with the pore diameter less than 2nm, mesoporous membrane with the pore size in the range from 2nm to 50nm, the microporous membrane with the pore lager than 50nm. For separating small-molecular gases, the microporous membranes will be more effective. For examples, the zeolite membranes: SAPO-34 membranes [50–55], SSZ-13 membranes [56–60], AlPO-18 membranes [61–63], T membranes [64,65], DDR membranes [66–68] and NaY membrane [69] show good separations for CO_2/CH_4 separation.
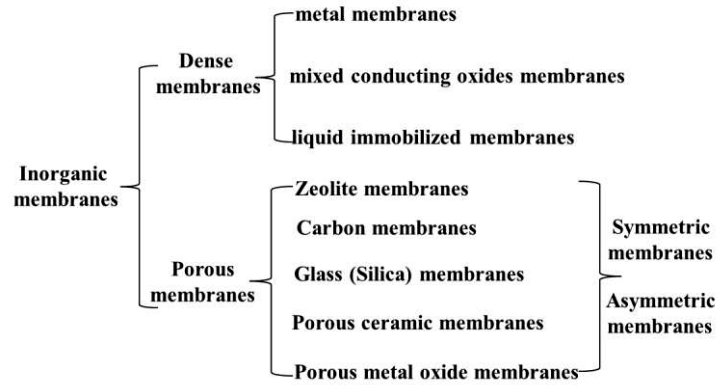
Figure 3 Structure of inorganic membranes [21].

However, since the inorganic membranes show good gas separation performances that above the trade-off between permeability and selectivity, the inorganic membranes still face some problems that restricted scale up for gas separation industrial because of the poor reproducibility, the difficult of making defect-free layers and fabricating cost.

1.1.3 Mixed matrix membranes

Mixed Matrix Membranes (MMMs), which is comprised by embedding inorganic fillers into a polymeric matrix, indicating one of the alternative candidate to overcome these limitations between polymer and inorganic membranes for gas separation. The Mixed Matrix Membranes(MMMs) were first reported in 1970s by Paul et al when filling 5A zeolite into a rubbery polydimethylsiloxane membrane [70], a delay time lag was investigated between different diffusions in CO_2 and CH_4 on the polydimethylsiloxane-based 5A MMMs. And the numerous efforts have been made since from the first investigation of the MMMs, and a lot of intensive researches were acquired in recent years [20,71–78].

The ideal Mixed Matrix Membranes (MMMs) were developed by combining both the advantages of polymer matrix and the inorganic fillers, which can be own the flexible properties of the polymer as well as the higher permeability and selectivity of inorganic fillers [72]. Figure 4 shows the structure and schematic diagram of various morphologies of MMMs. In theoretical, there are only two phases in the MMMs and defect-free, while, the properties of the incorporated fillers and the connection with the matrix polymer will affect the properties of the nearby polymer, hence affect the

MMMs gas separation properties. The nonideal MMMs morphologies were also showed in Figure 4. Since the poor adhesion between the filler and the polymer matrix, the packing configuration of the vicinity polymer, the polymer chain dynamic and conformation, the force between the filler and the nearby polymer, the agglomeration of filler all-over affect the configuration of the morphologies of the all MMMs, and in some degree decrease the MMMs permeability or selectivity. The non-ideal morphologies normally can be classified into three types which described in Figure 4: the interfacial voids, the rigidified polymer layer and some pore blockages within the fillers [71,72,79]. The MMMs are normally classified into three different types according to the literatures: solid-polymer MMMs, liquid polymer MMMs and solid-liquid-polymer MMMs [79,80], and there are only few studies working on the liquid-polymer and solid-liquid-polymer MMMs [80–84], and most attentions were focus on solid-polymer membranes. The conventional fillers for solid-polymer MMMs were zeolites [76,85–87], CMS [88,89] and silica [74,90–92]. Meanwhile, some new materials such as carbon nanotubes [93] and MOFs [78] were adopted to be new fillers and the modification by changing the surface properties of the filler to improve the interfacial connections as new strategies in order to improve the gas separation properties of Mixed Matrix Membranes.
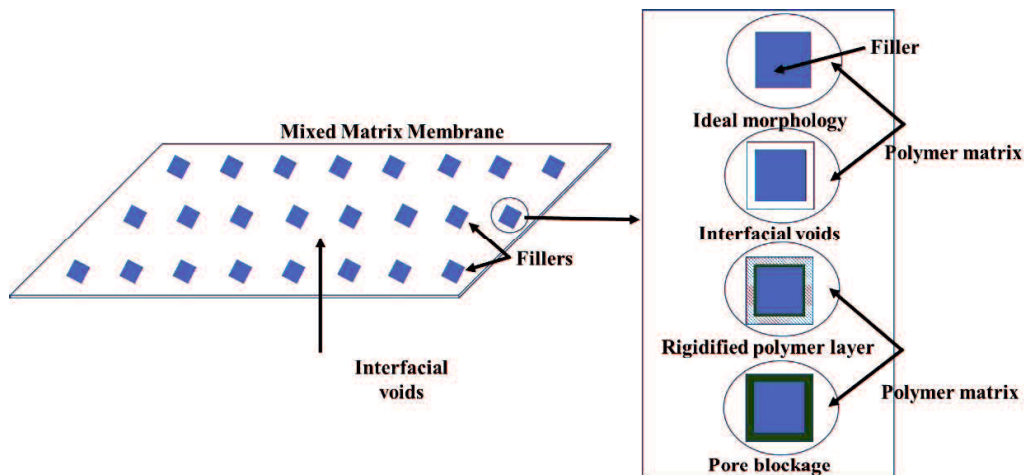
Figure 4 Structure and schematic diagram of various morphologies of Mixed Matrix Membranes.

1.2 Separation mechanism

The gas mixtures can be separate through the membranes based on the different gas permeability through the membranes. The permeability of different gases components was calculated as the permeate flux through the effective area of the membrane under its partial pressure. And the selectivity was calculated by the ratio of the permeance with different components.

According to the properties of the membranes, in general, two categories can be roughly described for the membranes for gas separation. Figure 5 illustrates the four gas transport mechanisms that used to describe the gas transportation properties that through the porous (viscous flow, Knudsen diffusion, molecular sieving) and nonporous (solution diffusion) membranes.
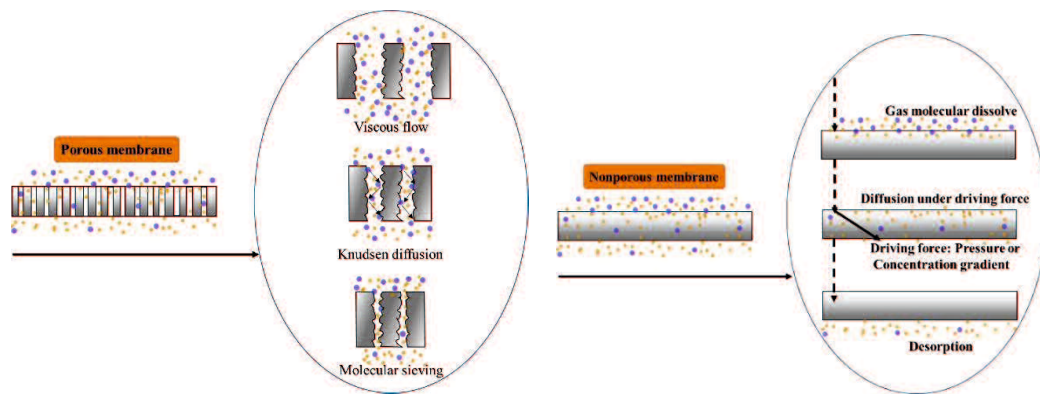
Figure 5 Gas transport mechanism for the gas separation membrane.

Viscous flow: The viscous flow happens if the porous membranes have the relatively large pore sizes range from 0.1-10μm, which is much bigger than the gas molecules, there are no separations when the gas permeate through the viscous flow.

Knudsen diffusion: The Knudsen diffusion usually takes place as the porous membranes have a pore size smaller than 50nm [6], and the pores in the membrane layers are in the same size or smaller in diameter than the mean free path of the gas molecules. The two gases that separated by Knudsen diffusion was basically based on the difference between these two gases molecular weights, which is proportional to the inverse square root ratio of the molecular weights [7,94]. The Knudsen selectivity for

some selected gas pairs and the gases properties were summarized in Table 2.

Table 2 Gas properties and calculated selectivity based on Knudsen diffusion.

Gas	Molecular weight	Kinetic diameter(Å)	Gas pairs	Knudsen selectivity
He	4	2.60	H_2/O_2	4.00
H_2	2	2.89	H_2/N_2	3.74
O_2	32	3.46	H_2/CO_2	4.69
N_2	28	3.64	H_2/CH_4	2.83
CO_2	44	3.30	CO_2/N_2	0.80
CH_4	16	3.80	CO_2/CH_4	0.60
n-C_4H_{10}	58	4.69	N_2/CH_4	0.76
i-C_4H_{10}	58	5.28	O_2/N_2	0.94
SF_6	146	5.50		

Molecular sieving: When the pores of the membranes that are similar to the molecular sizes that to be separated, then the separation can be achieved by molecular sieving, that is, as the membrane pore size between the diameter of two different gases, the smaller gas molecules can pass through the membrane, while the larger molecules are excluded [6,7,20,94].

Solution diffusion: For the nonporous membranes, the gas transportation is quite different from that of porous membranes, which is mostly based on the solution-diffusion transport mechanism: the permeants dissolve first in the membrane and then diffuse through the membrane.

The solution-diffusion transport mechanism can be described in three steps [6,94] also shown in Figure 5. Firstly, the gas molecules condensed and dissolved on the surface of the membrane layer, secondly, the activated diffusion through the membrane layer happened under the driving force that is pressure or concentration gradient [29]; thirdly, the gas molecules desorbed in the other side of the membrane.

In the solution-diffusion membrane, both the solubility and the diffusivity determine the permeability, which can be formulated as

$P = D\ S$

The solubility favors the more condensable gases while the diffusivity favors the smaller gases [28,95]. The gas transportation is more complicated for the practical

application, which may combine of the mechanisms above.

1.3 Gas separation applications

Membrane based gas separations have received many intensive studies and shown great potential applications in lots of domains of industry processes. Table 3 listed some principal developed gas separations that was summarized by Yampolskii [3,19] the details were discussed below:

Table 3 Gas separation application.

Application	Gas pairs	Knudsen selectivity	Status
H_2 purification	H_2/O_2	4.00	Various H_2 recovery applications in refineries, petrochemical and ammonia plants
	H_2/N_2	3.74	
	H_2/CO_2	4.69	
	H_2/CH_4	2.83	
CO_2 separation	CO_2/N_2	0.80	Separate CO_2 from natural gas and flue gas
	CO_2/CH_4	0.60	
	N_2/CH_4	0.76	Natural gas purification
Air separation	O_2/N_2	0.94	Obtain grade N_2 or O_2 enriched air
	O_2/Ar	1.12	

1.3.1 H_2 purification

H_2 is considered as a clean, efficiency and environmental-friendly energy as its combustion products only contains water [94]. Separation and purification of H_2 displayed a significant effect on the energy security, air pollution and the global climate change. The first large-scale commercial application of H_2 separation by membrane was established in the separation hydrogen from N_2, CH_4 and Ar in ammonia industry [5]. As a small and non-condensable gas, H_2 is easily permeate through membranes when compared with other gases. Up to now, various large scale H_2 recover applications established and lied in the industrial of ammonia synthesis, refinery, syngas and the petrochemical plants. It is necessary to separate H_2 from CH_4, CO, CO_2 etc. H_2 separation by membrane was firstly focus on the polymer membranes due to the quite high diffusion coefficient [94], polymeric membranes still exhibit a widely application in H_2 recovery industries with high selectivity currently, while the thermal stability

under high temperatures still limit the polymer membranes' application. Many research groups also investigated the inorganic membranes for H_2 separation. Li et al [95] and Nathan et al [96] reviewed the Hydrogen separation inorganic membranes including porous and dense membranes. The H_2 selective porous inorganic membrane includes zeolite membranes, silica membranes, carbon based membranes, metal organic frameworks (MOFs) membranes and the amorphous metal oxide membranes; the dense inorganic membranes like Metallic Membranes [96].

1.3.2 CO_2 separation

Removal of CO_2 from flue gas steam was first adopting as a way to mitigate the effect of greenhouse [97]. As with the industrial development that lead to a huge increase consumption in fossil fuel and natural gas, CO_2, by far, has become the main cause of global warming, which should be a big urgent to separate from fuel gas and natural gas. In recent years, membrane technology has been investigated to prevent the greenhouse emissions with the advantage of lower power consumption [98]. The main areas to release the greenhouse effect is to separate CO_2 from N_2, in the other hand, one of the important application for separating CO_2 is to separate CO_2 from the natural gas. As the main contaminate in natural gas, it will decrease the heat value of the natural gas, meanwhile, for the gas transportation process, the pipeline will be corrosive when CO_2 exists in the presence of moisture. Many types membrane materials are studied for CO_2 separation, the first one is the polymeric membrane. In the early time, the cellulose acetate and its derivatives formed with a thin dense selective layer are used for CO_2 separation [99]. However, due to the plasticization effects, the polymeric membranes are easy to lose the flux of CO_2. Since the polymeric membranes are the widely used materials, there are still somehow imperfect to meet the criterion of current membrane separation process. Improvements still need to be made for CO_2 separation. The inorganic membranes, because of the high temperature stability, indicated a much attractive attention for CO_2 separation, till now, especially for the zeolite membranes, for instances, as T [64], DDR [68], SAPO-34 [50,52–54], Si-CHA [100], SSZ-13

10

[56,60], SAPO-17 as well as AlPO-17 [101], AlPO-18 [62,63] membranes are widely investigated for CO_2 separation. The zeolite membranes showed both high CO_2/CH_4 selectivity and CO_2 permeability that are above to the upper bound of the Roberson plot that is commonly used to compare polymers membranes [34]. Meanwhile, mixed matrix membranes [77,87] are also showed the separation properties to separate CO_2.

1.3.3 Air separation

Separate enriched nitrogen and oxygen from the air has a significant effect on the chemical industry [102]. As with the economical and configuration consideration, membrane-based gas separation processes own the advantages compared with the traditional and conventional separation method such as cryogenic distillation and absorption. Since the first effective air separation membranes that separate the O_2 from N_2 with the selectivity of 4, a big progress that improved the O_2/N_2 selectivity from 8 to 12 without losing the permeation rate have already made through membranes separation, which might reduce the cost [5]. However, the main studies for O_2/N_2, separation are polymeric membranes. and only some particular polymeric membranes can adopt for this separation, commercially available polymeric membranes are still underground [103].

1.4 Thesis overview

In this thesis, we will prepare the AEI, CHA zeolite membranes and AEI, CHA zeolites filled mixed matrix membranes and study the gas permeation properties of those prepared zeolite membranes and mixed matrix membranes. The gas permeation properties of AEI zeolite membranes are studied by using different templates TEAOH and DIPEA. For the CHA zeolite membranes, the effects of propane in feed for CO_2/CH_4 and N_2/CH_4 separation are investigated. The mixed matrix membranes are prepared with loading AlPO-18, SAPO-34 and SSZ-13 zeolites into PESU and 6FDA-TrMPD polymer matrix.

(1) Chapter 1

It describes the critical background of the subjects in this thesis. It provides the overview of gas separation and the main gas separation membranes. Gas separation mechanisms and the membrane for gas separation applications are also reviewed.

(2) Chapter 2

The AEI-type AlPO-18 and CHA-type SAPO-34 and SSZ-13 zeolites are prepared. Different crystals sizes zeolites have been obtained by changing the synthesis parameters.

(3) Chapter 3

The AEI type AlPO-18 zeolite membranes are fabricated by using the crystals prepared in Chapter 2 as seeds. Effects of the single and combined templates on the synthesis of the AlPO-18 zeolite membranes are investigated. The as-synthesized AlPO-18 zeolite membranes are applied for gas permeation test. Effects of temperature and pressure on the gas permeation properties of those AlPO-18 zeolite membranes are discussed.

(4) Chapter 4

Two types CHA zeolite membranes (SAPO-34 and SSZ-13) are used for CO_2/CH_4, N_2/CH_4, and CO_2/i-butane separations at both low (270 and 350kPa) and high (1.73MPa) pressures. The effects of propane impurity with the different concentrations on the SAPO-34 and SSZ-13 membranes for both CO_2/CH_4 and N_2/CH_4 are discussed.

(5) Chapter 5

CHA and AEI zeolites are used as filler to prepare the flat self-supported PESU-based mixed matrix membranes (MMMs). The effects of the crystals sizes and the loading amount on the gas permeation properties of the MMMs are discussed.

(6) Chapter 6

CHA type SAPO-34 zeolites are used as filler to incorporate into 6FDA-TrMPD (PI) polymer matrix to prepare the self-supported mixed matrix membranes (MMMs). The effects of the crystals sizes and the loading amount on the gas permeation properties of the MMMs are discussed.

(7) Chapter 7

A summary of this dissertation and future work are also proposed.

References

[1]   A. Brunetti, P. Bernardo, E. Drioli, G. Barbieri, Membrane Engineering: Progress and Potentialities in Gas Separations, John Wiley & Sons, Ltd, (2010) 279-312.

[2]   Y. Yampolskii, B.D. Freeman, Membrane Gas Separation, John Wiley & Sons, 2010.

[3]   G. Maier, Gas Separation with Polymer Membranes, Angewandte Chemie International Edition. 37 (1998) 2960–2974.

[4]   P. Bernardo, E. Drioli, G. Golemme, Membrane gas separation: A review/state of the art, Industrial and Engineering Chemistry Research. 48 (2009) 4638-4663.

[5]   R.W. Baker, Future Directions of Membrane Gas Separation Technology, Industrial and Engineering Chemistry Research. 41 (2002) 1393-1411.

[6]   M. Freemantle, Membranes for gas separation, Chemical & Engineering News. 83 (2005) 49-57.

[7]   K. Ghosal, B.D. Freeman, Gas separation using polymer membranes: an overview, Polymers for Advanced Technologies. 5 (1994) 673-697.

[8]   R.W. Baker, B.T. Low, Gas Separation Membrane Materials: A Perspective, Macromolecules. 47 (2014) 6999-7013.

[9]   T. Graham, On the Absorption and Dialytic Separation of Gases by Colloid Septa, Philosophical Transactions of the Royal Society of London. 156 (1866) 399-439.

[10]   D.F. Sanders, Z.P. Smith, R. Guo, L.M. Robeson, J.E. McGrath, D.R. Paul, B.D. Freeman, Energy-efficient polymeric gas separation membranes for a sustainable future: A review, Polymer. 54 (2013) 4729-4761.

[11]   P. Pandey, R.S. Chauhan, Membranes for gas separation, Progress in polymer science, 26 (2001) 853-893.

[12]   E.S. Kikkinides, R.T. Yang, S.H. Cho, Concentration and recovery of carbon dioxide from flue gas by pressure swing adsorption, Industrial and Engineering Chemistry Research. 32 (1993) 2714-2720.

[13]   M.T. Ho, G.W. Allinson, D.E. Wiley, Reducing the Cost of CO_2 Capture from

Flue Gases Using Pressure Swing Adsorption, Industrial and Engineering Chemistry Research. 47 (2008) 4883-4890.

[14]   K.T. Chue, J.N. Kim, Y.J. Yoo, S.H. Cho, R.T. Yang, Comparison of Activated Carbon and Zeolite 13X for CO_2 Recovery from Flue Gas by Pressure Swing Adsorption, Industrial and Engineering Chemistry Research. 34 (1995) 59-598.

[15]   B. Zhu, Q. Liu, Q. Zhou, J. Yang, J. Ding, J. Wen, Absorption of Carbon Dioxide from Flue Gas using Blended Amine Solutions, Chemical Engineering & Technology. 37 (2014) 635-642.

[16]   K. Maqsood, J. Pal, D. Turunawarasu, A.J. Pal, S. Ganguly, Performance enhancement and energy reduction using hybrid cryogenic distillation networks for purification of natural gas with high CO_2 content, Korean Journal of Chemical Engineering. 31 (2014) 1120-1135.

[17]   D.Y.C. Leung, G. Caramanna, M.M. Maroto-Valer, An overview of current status of carbon dioxide capture and storage technologies, Renewable and Sustainable Energy Reviews. 39 (2014) 426-443.

[18]   Y. Kansha, A. Kishimoto, T. Nakagawa, A. Tsutsumi, A novel cryogenic air separation process based on self-heat recuperation, Separation and Purification Technology. 77 (2011) 389-396.

[19]   Y. Yampolskii, Polymeric Gas Separation Membranes, Macromolecules. 45 (2012) 3298-3311.

[20]   W.J. Koros, R. Mahajan, Pushing the limits on possibilities for large scale gas separation: Which strategies?, Journal of Membrane Science. 175 (2000) 181-196.

[21]   A.F. Ismail, L.I.B. David, A review on the latest development of carbon membranes for gas separation, Journal of Membrane Science. 193 (2001) 1-18.

[22]   S.M. Saufi, A.F. Ismail, Fabrication of carbon membranes for gas separation - A review, Carbon. 42 (2004) 241-259.

[23]   D. Jiang, V.R. Cooper, S. Dai, Porous Graphene as the Ultimate Membrane for Gas Separation, Nano Letters. 9 (2009) 4019-4024.

[24]   P.M. Budd, K.J. Msayib, C.E. Tattershall, B.S. Ghanem, K.J. Reynolds, N.B.

McKeown, D. Fritsch, Gas separation membranes from polymers of intrinsic microporosity, Journal of Membrane Science. 251 (2005) 263-269.

[25] B.D. Freeman, Basis of Permeability/Selectivity Tradeoff Relations in Polymeric Gas Separation Membranes, Macromolecules. 32 (1999) 375-380.

[26] L.M. Robeson, Correlation of separation factor versus permeability for polymeric membranes, Journal of Membrane Science. 62 (1991) 165-185.

[27] C.E. Powell, G.G. Qiao, Polymeric CO_2/N_2 gas separation membranes for the capture of carbon dioxide from power plant flue gases, Journal of Membrane Science. 279 (2006) 1-49.

[28] W.J. Koros, G.K. Fleming, Membrane-based gas separation, Journal of Membrane Science. 83 (1993) 1-80.

[29] H.A. Mannan, H. Mukhtar, T. Murugesan, R. Nasir, D.F. Mohshim, A. Mushtaq, Recent Applications of Polymer Blends in Gas Separation Membranes, Chemical Engineering & Technology. 36 (2013) 1838-1846.

[30] D.F. Sanders, Z.P. Smith, R. Guo, L. M. Robeson, J. E. McGrath, D. R. Paul, B. D. Freeman, Energy-efficient polymeric gas separation membranes for a sustainable future: A review, Polymer. 54 (2013) 4729-4761.

[31] P.M. Budd, N.B. McKeown, Highly permeable polymers for gas separation membranes, Polymer Chemistry. 1 (2010) 63-68.

[32] W.L. Robb, Thin silicon membranes-their permeation properties and some applications, Annals of the New York Academy of Sciences. 146 (1968) 119-137.

[33] R.M. Barrer, H.T. Chio, Solution and diffusion of gases and vapors in silicone rubber membranes, Journal of Polymer Science Part C: Polymer Symposia. 10 (2007) 111-138.

[34] L.M. Robeson, The upper bound revisited, Journal of Membrane Science. 320 (2008) 390-400.

[35] A.Y. Houde, B. Krishnakumar, S.G. Charati, S.A. Stern, Permeability of dense (homogeneous) cellulose acetate membranes to methane, carbon dioxide, and their mixtures at elevated pressures, Journal of Applied Polymer Science. 62 (1996) 2181-2192.

[36] M.D. Donohue, B.S. Minhas, S.Y. Lee, Permeation behavior of carbon dioxide-methane mixtures in cellulose acetate membranes, Journal of Membrane Science. 42 (1989) 197-214.

[37] P.K. Gantzel, U. Merten, Gas Separations with High-Flux Cellulose Acetate Membranes, Industrial & Engineering Chemistry Process Design and Development. 9 (1970) 331-332.

[38] A.F. Ismail, L.P. Yean, Review on the development of defect-free and ultrathin-skinned asymmetric membranes for gas separation through manipulation of phase inversion and rheological factors, Journal of Applied Polymer Science. 88 (2003) 442-451.

[39] M.A. Aroon, A.F. Ismail, M.M. Montazer-Rahmati, T. Matsuura, Morphology and permeation properties of polysulfone membranes for gas separation: Effects of non-solvent additives and co-solvent, Separation and Purification Technology. 72 (2010) 194-202.

[40] A.F. Ismail, I.R. Dunkin, S.L. Gallivan, S.J. Shilton, Production of super selective polysulfone hollow fiber membranes for gas separation, Polymer. 40 (1999) 6499-6506.

[41] T.H. Kim, W.J. Koros, G.R. Husk, K.C. O'Brien, Relationship between gas separation properties and chemical structure in a series of aromatic polyimides, Journal of Membrane Science. 37 (1988) 45-62.

[42] M.R. Coleman, W.J. Koros, Isomeric polyimides based on fluorinated dianhydrides and diamines for gas separation applications, Journal of Membrane Science. 50 (1990) 285-297.

[43] A.B. Fuertes, D.M. Nevskaia, T.A. Centeno, Carbon composite membranes from Matrimid and Kapton polyimides for gas separation, Microporous and Mesoporous Materials. 33 (1999) 115-125.

[44] P. Bernardo, G. Clarizia, 30 Years of Membrane Technology for Gas Separation, Chemical Engineering Transactions. 32 (2013) 1999-2004.

[45] L. Robeson, Polymer membranes for gas separation, Current Opinion in Solid State and Materials Science. 4 (1999) 549-552.

[46] A.B. Shelekhin, A.G. Dixon, Y.H. Ma, Theory of gas diffusion and permeation in inorganic molecular-sieve membranes, AIChE Journal. 41 (1995) 58-67.

[47] N. Kosinov, J. Gascon, F. Kapteijn, E.J.M. Hensen, Recent developments in zeolite membranes for gas separation, Journal of Membrane Science. 499 (2016) 65-79.

[48] H. Verweij, Inorganic membranes, Current Opinion in Chemical Engineering. 1 (2012) 156-162.

[49] Y.S. Lin, Microporous and dense inorganic membranes: Current status and prospective, Separation and Purification Technology. 25 (2001) 39-55.

[50] S. Li, J.L. Falconer, R.D. Noble, Improved SAPO-34 Membranes for CO_2/CH_4 Separations, Advanced Materials. 18 (2006) 2601-2603.

[51] S Li, J. L.Falconer, Richard D.Noble, SAPO-34 membranes for CO_2/CH_4 separation, Journal of Membrane Science. 241 (2004) 121-135.

[52] M.A. Carreon, S. Li, J.L. Falconer, R.D. Noble, Alumina-Supported SAPO-34 Membranes for CO_2/CH_4 Separation, Journal of the American Chemical Society. 130 (2008) 5412-5413.

[53] J.C. Poshusta, V.A. Tuan, E.A. Pape, R.D. Noble, J.L. Falconer, Separation of light gas mixtures using SAPO-34 membranes, AIChE Journal. 46 (2000) 779-789.

[54] S. Li, J.G. Martinek, J.L. Falconer, R.D. Noble, T.Q. Gardner, High-Pressure CO_2/CH_4 Separation Using SAPO-34 Membranes, Industrial and Engineering Chemistry Research. 44 (2005) 3220-3228.

[55] R. Zhou, E.W. Ping, H.H. Funke, J.L. Falconer, R.D. Noble, Improving SAPO-34 membrane synthesis, Journal of Membrane Science. 444 (2013) 384-393.

[56] Y. Zheng, N. Hu, H. Wang, N. Bu, F. Zhang, R. Zhou, Preparation of steam-stable high-silica CHA (SSZ-13) membranes for CO_2/CH_4 and C_2H_4/C_2H_6 separation, Journal of Membrane Science. 475 (2015) 303-310.

[57] B. Liu, R. Zhou, N. Bu, Q. Wang, S. Zhong, B. Wang, H. Kita, Room-temperature ionic liquids modified zeolite SSZ-13 membranes for CO_2/CH_4 separation, Journal of Membrane Science. 524 (2017) 12-19.

[58] N. Kosinov, C. Auffret, G.J. Borghuis, V.G.P. Sripathi, E.J.M. Hensen, Influence of the Si/Al ratio on the separation properties of SSZ-13 zeolite membranes, Journal of Membrane Science. 484 (2015) 140-145.

[59] T. Wu, M.C. Diaz, Y. Zheng, R. Zhou, H.H. Funke, J.L. Falconer, R.D. Noble, Influence of propane on CO_2/CH_4 and N_2/CH_4 separations in CHA zeolite membranes, Journal of Membrane Science. 473 (2015) 201-209.

[60] N. Kosinov, C. Auffret, C. Gücüyener, B.M. Szyja, J. Gascon, F. Kapteijn, E.J.M. Hensen, High flux high-silica SSZ-13 membrane for CO_2 separation, Journal of Materials Chemistry A. 2 (2014) 13083-13092.

[61] T. Wu, B. Wang, Z. Lu, R. Zhou, X. Chen, Alumina-supported AlPO-18 membranes for CO_2/CH_4 separation, Journal of Membrane Science. 471 (2014) 338-346.

[62] B. Wang, N. Hu, H. Wang, Y. Zheng, R. Zhou, Improved AlPO-18 membranes for light gas separation, Journal of Materials Chemistry A. 3 (2015) 12205-12212.

[63] M.L. Carreon, S. Li, M.A. Carreon, AlPO-18 membranes for CO_2/CH_4 separation, Chemical Communications. 48 (2012) 2310-2312.

[64] Y. Cui, H. Kita, K. Okamoto, Preparation and gas separation performance of zeolite T membrane, Journal of Materials Chemistry. 14 (2004) 924-932.

[65] Y. Cui, H. Kita, K. Okamoto, Preparation and gas separation properties of zeolite T membrane, Chemical Communications. 0 (2003) 2154-2155.

[66] T. Tomita, K. Nakayama, H. Sakai, Gas separation characteristics of DDR type zeolite membrane, Microporous and Mesoporous Materials. 68 (2004) 71-75.

[67] M. Kanezashi, J. O'Brien-Abraham, Y.S. Lin, K. Suzuki, Gas permeation through DDR-type zeolite membranes at high temperatures, AIChE Journal. 54 (2008) 1478-1486.

[68] S. Himeno, T. Tomita, K. Suzuki, K. Nakayama, K. Yajima, S. Yoshida, Synthesis and Permeation Properties of a DDR-Type Zeolite Membrane for Separation of CO_2/CH_4 Gaseous Mixtures, Industrial and Engineering Chemistry Research. 46 (2007) 6989-6997.

[69] Y. Hasegawa, T. Tanaka, K. Watanabe, B.H. Jeong, K. Kusakabe, S. Morooka,

Separation of CO_2-CH_4 and CO_2-N_2 systems using ion-exchanged fau-type zeolite membranes with different Si/Al ratios, Korean Journal of Chemical Engineering. 19 (2002) 309-313.

[70] D.R. Paul, D.R. Kemp, The diffusion time lag in polymer membranes containing adsorptive fillers, Journal of Polymer Science. 41 (2007) 79-93.

[71] P.S. Goh, A.F. Ismail, S.M. Sanip, B.C. Ng, M. Aziz, Recent advances of inorganic fillers in mixed matrix membrane for gas separation, Separation and Purification Technology. 81 (2011) 243-264.

[72] T.S. Chung, L.Y. Jiang, Y. Li, S. Kulprathipanja, Mixed matrix membranes (MMMs) comprising organic polymers with dispersed inorganic fillers for gas separation, Progress in Polymer Science. 32 (2007) 483-507.

[73] R.M. and, W.J. Koros, Factors Controlling Successful Formation of Mixed-Matrix Gas Separation Materials, Industrial and Engineering Chemistry Research. 39 (2000) 2692-2696.

[74] J. Ahn, W.J. Chung, I. Pinnau, M.D. Guiver, Polysulfone/silica nanoparticle mixed-matrix membranes for gas separation, Journal of Membrane Science. 314 (2008) 123-133.

[75] M.A. Aroon, A.F. Ismail, T. Matsuura, M.M. Montazer-Rahmati, Performance studies of mixed matrix membranes for gas separation: A review, Separation and Purification Technology. 75 (2010) 229-242.

[76] D. Bastani, N. Esmaeili, M. Asadollahi, Polymeric mixed matrix membranes containing zeolites as a filler for gas separation applications: A review, Journal of Industrial and Engineering Chemistry. 19 (2013) 375-393.

[77] G. Dong, H. Li, V. Chen, Challenges and opportunities for mixed-matrix membranes for gas separation, Journal of Materials Chemistry A. 1 (2013) 4610-4630.

[78] H.B. Tanh Jeazet, C. Staudt, C. Janiak, Metal-organic frameworks in mixed-matrix membranes for gas separation, Dalton Transactions. 41 (2012) 14003-14027.

[79] H. Vinh-Thang, S. Kaliaguine, Predictive Models for Mixed-Matrix Membrane

Performance: A Review, Chemical Reviews. 113 (2013) 4980-5028.

[80]   M. Rezakazemi, A. Ebadi Amooghin, M.M. Montazer-Rahmati, A.F. Ismail, T. Matsuura, State-of-the-art membrane based CO_2 separation using mixed matrix membranes (MMMs): An overview on current status and future directions, Progress in Polymer Science. 39 (2014) 817-861.

[81]   Y.C. Hudiono, T.K. Carlisle, J.E. Bara, Y. Zhang, D.L. Gin, R.D. Noble, A three-component mixed-matrix membrane with enhanced CO_2 separation properties based on zeolites and ionic liquid materials, Journal of Membrane Science. 350 (2010) 117-123.

[82]   L. Hao, P. Li, T. Yang, T.S. Chung, Room temperature ionic liquid/ZIF-8 mixed-matrix membranes for natural gas sweetening and post-combustion CO_2 capture, Journal of Membrane Science. 436 (2013) 221-231.

[83]   R. Shindo, M. Kishida, H. Sawa, T. Kidesaki, S. Sato, S. Kanehashi, K. Nagai, Characterization and gas permeation properties of polyimide/ZSM-5 zeolite composite membranes containing ionic liquid, Journal of Membrane Science. 454 (2014) 330-338.

[84]   E. Santos, E. Rodríguez-Fernández, C. Casado-Coterillo, Á. Irabien, Hybrid Ionic Liquid-Chitosan Membranes for CO_2 Separation: Mechanical and Thermal Behavior, International Journal of Chemical Reactor Engineering. 14 (2016) 713-718.

[85]   Y. Li, T.S. Chung, C. Cao, S. Kulprathipanja, The effects of polymer chain rigidification, zeolite pore size and pore blockage on polyethersulfone (PES)-zeolite A mixed matrix membranes, Journal of Membrane Science. 260 (2005) 45-55.

[86]   Z. Huang, Y. Li, R. Wen, M. May Teoh, S. Kulprathipanja, Enhanced gas separation properties by using nanostructured PES-Zeolite 4A mixed matrix membranes, Journal of Applied Polymer Science. 101 (2006) 3800-3805.

[87]   K.C. Khulbe, T. Matsuura, C.Y. Feng, A.F. Ismail, Recent development on the effect of water/moisture on the performance of zeolite membrane and MMMs containing zeolite for gas separation; review, RSC Advanced. 6 (2016) 42943-

42961.

[88] D.Q. Vu, W.J. Koros, S.J. Miller, Mixed matrix membranes using carbon molecular sieves: I. Preparation and experimental results, Journal of Membrane Science. 211 (2003) 311-334.

[89] W.A.W. Rafizah, A.F. Ismail, Effect of carbon molecular sieve sizing with poly(vinyl pyrrolidone) K-15 on carbon molecular sieve-polysulfone mixed matrix membrane, Journal of Membrane Science. 307 (2008) 53-61.

[90] J. Ahn, W.J. Chung, I. Pinnau, J. Song, N. Du, G.P. Robertson, M.D. Guiver, Gas transport behavior of mixed-matrix membranes composed of silica nanoparticles in a polymer of intrinsic microporosity (PIM-1), Journal of Membrane Science. 346 (2010) 280-287.

[91] B. Zornoza, C. Téllez, J. Coronas, Mixed matrix membranes comprising glassy polymers and dispersed mesoporous silica spheres for gas separation, Journal of Membrane Science. 368 (2011) 100-109.

[92] R. Xing, W.S.W. Ho, Crosslinked polyvinylalcohol-polysiloxane/fumed silica mixed matrix membranes containing amines for CO_2/H_2 separation, Journal of Membrane Science. 367 (2011) 91-102.

[93] A.F. Ismail, P.S. Goh, S.M. Sanip, M. Aziz, Transport and separation properties of carbon nanotube-mixed matrix membrane, Separation and Purification Technology. 70 (2009) 12-26.

[94] G.Q. Lu, J.C. Diniz da Costa, M. Duke, S. Giessler, R. Socolow, R.H. Williams, T. Kreutz, Inorganic membranes for hydrogen production and purification: A critical review and perspective, Journal of Colloid and Interface Science. 314 (2007) 589-603.

[95] H. Li, K. Haas-Santo, U. Schygulla, R. Dittmeyer, Inorganic microporous membranes for H_2 and CO_2 separation-Review of experimental and modeling progress, Chemical Engineering Science. 127 (2015) 401-417.

[96] N.W.Ockwig, T.M. Nenoff, Membranes for Hydrogen Separation, Chemical Reviews. 107 (2007) 4078-4110.

[97] P.A. Webley, Adsorption technology for CO_2 separation and capture: a

perspective, Adsorption. 20 (2014) 225-231.

[98]   M.H. Nematollahi, A.H.S. Dehaghani, V. Pirouzfar, E. Akhondi, Mixed matrix membranes comprising PMP polymer with dispersed alumina nanoparticle fillers to separate CO_2/N_2, Macromolecular Research. 24 (2016) 782-792.

[99]   J. Mustafa, M. Farhan, M. Hussain, CO_2 Separation from Flue Gases Using Different Types of Membranes, Journal of Membrane Science & Technology. 6 (2016) 153.

[100] K. Kida, Y. Maeta, K. Yogo, Preparation and gas permeation properties on pure silica CHA-type zeolite membranes, Journal of Membrane Science. 522 (2017) 363-370.

[101] S. Zhong, N. Bu, R. Zhou, W. Jin, M. Yu, S. Li, Aluminophosphate-17 and silicoaluminophosphate-17 membranes for CO_2 separations, Journal of Membrane Science. 520 (2016) 507-514.

[102] R.S. Murali, T. Sankarshana, S. Sridhar, Air Separation by Polymer-based Membrane Technology, Separation & Purification Reviews. 42 (2013) 130-186.

[103] A. Fernández-Barquín, C. Casado-Coterillo, S. Valencia, A. Irabien, Mixed Matrix Membranes for O_2/N_2 Separation: The Influence of Temperature, Membranes. 6 (2016) 28.

Chapter 2 Preparation and Characterization of CHA and AEI Zeolites

2.1 Introduction

Zeolites are one of the kind of crystalline microporous structure materials that consisted of TO_4 tetrahedral units by sharing all the neighbor oxygen atoms to form regular cavities and channels in molecular dimensions [1–3], and T mostly equals to Si and Al atoms, it can be replaced by other heteroatoms like B, Mg, Ca, Ti, Be etc [1]. Different zeolites own the uniform and periodic pore structures, unique and particular pore sizes and specific surface areas, which have been widely used for catalysis, absorbent and separation [4]. In 1980s, a new class of crystalline materials, zeolite-like aluminophosphates (AlPOs) materials, were reported by Wilson et al [5]. The AlPOs crystalline own microporous structures that were only built with TO_4 tetrahedral units of equimolar AlO_4^- and PO_4^+ tetrahedral, which formed a neutral open-framework and without ion-exchange ability [6]; and the silicoaluminophosphates (SAPOs), are the same class materials as AlPOs, while the T atoms were partially substituted by Si [7]. Among the AlPOs and SAPOs materials, the SAPO-34 [8–12] and AlPO-18 [13,14] have already attracted much attentions for light gas separations such as CO_2/CH_4, N_2/CH_4, H_2/CH_4 and CO_2/N_2 during these years.

SAPO-34 and AlPO-18 zeolites, have the similar structural properties with a little difference in ring arrangement [15,16]. Thus made SAPO-34 has the structure of CHA and AlPO-18 has a structure of AEI [2]. The Pore architecture of CHA and AEI framework were shown in Figure 2-1 and Figure 2-2, respectively. Both of CHA and AEI-type zeolites have a three-dimensional pore system constructed by 8-membered intersecting channels, and formed a pore with a diameter of 0.38 nm [2]. The pore properties of CHA and AEI framework indicate SAPO-34 and AlPO-18 are good candidates for CO_2 (kinetic diameter of 0.33 nm), N_2 (kinetic diameter of 0.364 nm) and CH_4 (kinetic diameter of 0.38 nm) separation.

Another aluminosilicate zeolite SSZ-13, owns the same CHA framework as SAPO-

34 [2], while without PO_4^+ tetrahedral in the structure, the difference in SAPO-34 and SSZ-13 structure may display different gas permeation properties in gas separation process.
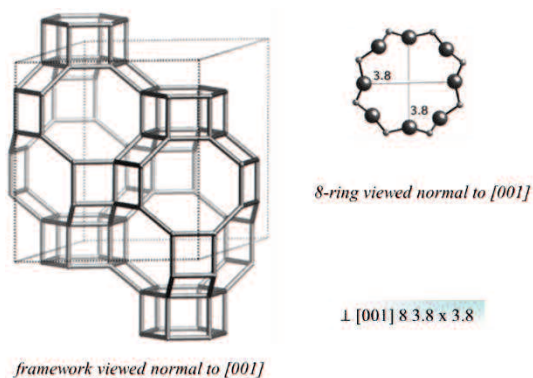
Figure 2.1 Pore architecture of SAPO-34 and SSZ-13 (CHA-type) [2].
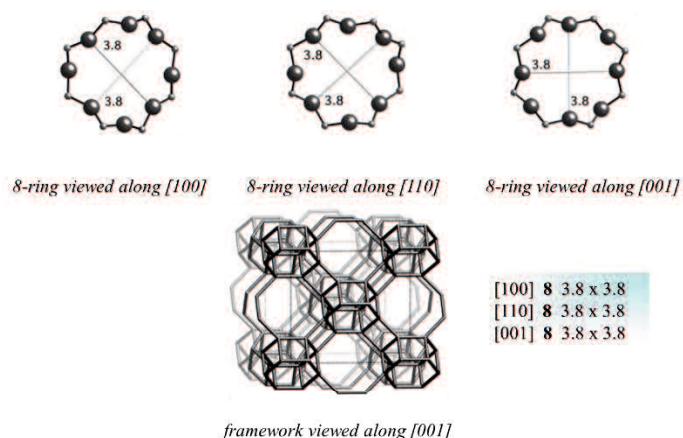
Figure 2.2 Pore architecture of AlPO-18 (AEI-type) [2].

In this work, we prepared both CHA type SAPO-34, SSZ-13 zeolites and AEI type AlPO-18 zeolites. One SSZ-13 and some SAPO-34 and AlPO-18 zeolites were obtained. The effect of single or combined templates and the corresponding synthesis conditions were investigated for preparing different sizes AlPO-18 and SAPO-34 zeolites.

2.2 Experimental

2.2.1 Synthesis of SSZ-13 crystals

SSZ-13 zeolites were synthesized according to Hudson et al. [17]. First was to prepare the structure-directing agent (SDA): N, N, N-trimethyl-1-adamantanamine

iodide (TMAAI).

10g 1-adamantanamine (97%, Sigma-Aldrich) was firstly dissolved into 24.8 g methanol (99.7%, Wako), and 9 g of tributylamine (98.5%, Wako) was added into the solution, stirred for 15 min, then added 28.4 g of methyl iodide (99.5% Wako) in a drop-wise fashion under ice bath condition. The final solution was stirred for another 5 days at room temperature. At last, precipitated the final solution with 100 mL of diethyl ether (Wako) by further 30 min, stirred to get the product. The obtained product was then wash with 200ml diethyl ether and dried at room temperature overnight.

SSZ-13 zeolite was prepared by mixing 5 g of sodium silicate (Sigma-Aldrich) and 0.16 g of NaOH (97%, Wako) to 12 g water. Stirred at room temperature for 15 min; later, added 0.5 g of NH4-Y zeolite (Wako) to the solution and stirred for 30 min. Next, added 0.8 g prepared of N, N, N-trimethyl-1-adamantanamine iodide (TMAAI) and stirred for another 30 min, transferred the resulting solution into Teflon-lined autoclaves and synthesized at 423K with rotation rate of~15 r/min for 6 days. The products were then centrifuged at 3500 rpm for 30 min and washed with DI water, dried overnight in an oven at 323 K for 1 day. Then calcined under air atmosphere at 823K for 8h.

2.2.2 Synthesis of SAPO-34 crystals

Two synthesis routes were adopted to prepare SAPO-34 through different gel compositions.

Route 1 was synthesized by single template TEAOH with the gel composition of $1Al_2O_3:2P_2O_5:0.6SiO_2:4TEAOH:75H_2O$ similar as the procedure of Thomas Bein et al. [18], $Al(i-C_3H_7O)_3$ (98%, Sigma-Aldrich), TEAOH (35% aqueous solution, TCI and Sigma-Aldrich) and deionized water were mixed well and stirred for 2-3 h to form a homogeneous solution. Then Si source (TM-40,40%, Sigma-Aldrich; AS-40, 40%, Sigma-Aldrich; TEOS, 98%, Sigma-Aldrich) were added slowly and stirred for another 2-3h, then the H_3PO_4 (85% aqueous solution, TCI) was added in a drop-wise fashion and the resulting solution was stirred for a period of time at room temperature. Then the final gel was transferred to a Teflon-lined autoclave. The stationary hydrothermal synthesis was carried out in an oven at 453 K for 4-12 h and 473K for 12h.

Route 2 was prepared with using combined templates of TEAOH and DIPEA with the gel composition of $1Al_2O_3:1P_2O_5:0.6SiO_2:1.5TEAOH:0.5DIPEA:75H_2O$. Firstly, mixing $Al(i-C_3H_7O)_3$ (98%, Sigma-Aldrich), H_3PO_4 (85% aqueous solution, TCI and Sigma-Aldrich) and distilled water for 3 h, following added Si source (TEOS, 98%, Sigma-Aldrich), stirred for another 3h, then TEAOH (35% aqueous solution, Sigma-Aldrich) was added and stirred for 30min, finally added the DIPEA (99%, Wako), then the resulting solution was stirred for 12h at room temperature. The final gel was at last transferred to a Teflon-lined autoclave and synthesized in an oven at 473K for 12 or 24h.

After synthesis, the SAPO-34 seeds were centrifuged at 3500 rpm for 40 min and washed with DI water. The resulting SAPO-34 seeds were dried overnight in an oven at 323 K for one day. Then calcined under air atmosphere at 823K for 8h with the increasing and cooling rate of 10K/min until neutral. The powders were dried and saved in an oven at 353 K for later experiments.

2.2.3 Synthesis of AlPO-18 crystals

Three AlPO-18 crystals were synthesized with the previously-described procedure [14,19,20]. In a typical synthesis, $Al(i-C_3H_7O)_3$ (98%, Sigma-Aldrich), TEAOH (35% aqueous solution) and deionized water were mixed and stirred for 1 h to form a homogeneous solution. Then H_3PO_4 (85% aqueous solution, TCI) was added in a drop-wise fashion and the resulting solution was stirred for 2 h at room temperature. The final gel had a molar composition that described in Table 2-1 and was transferred to a Teflon-lined autoclave. The stationary hydrothermal synthesis was carried out in an oven at 423 K for 20 h. After the reaction mixture cooled below 343 K, the seeds were centrifuged at 3500 rpm for 40 min and washed with DI water. The resulting AlPO-18 seeds were dried overnight in an oven at 323 K. and then calcined under air atmosphere at 823K for 8h with the increasing and cooling rate of 10K/min.

Table 2-1. Synthesis conditions of AlPO-18 zeolites.

Zeolite	Gel composition	Aged time(h)	Syn. Conditions
AlPO-18-1	$1Al_2O_3:3.16P_2O_5:6.32$ TEAOH:186H_2O	2	423K, 20h
AlPO-18-2	$1Al_2O_3:1P_2O_5:1.8$ TEAOH: 60H_2O:2IPA	2	423K, 20h
AlPO-18-3	$1Al_2O_3:1P_2O_5:1.8$ TEAOH:60H_2O	2	423K, 20h

2.2.3 Characterization

The morphologies of as-synthesized CHA-type (SAPO-34 and SSZ-13) and AEI-type AlPO-18 were determined by a field emission scanning electron microscope (FE-SEM, JEOL JSM 6335F) at an acceleration voltage of 5KV. The crystallinity of CHA-type (SAPO-34 and SSZ-13) and AEI-type AlPO-18 were identified by X-ray diffraction (XRD, SHIMADZU XRD-6100) using a Shimadzu XD-3 diffractometer with Cu-Ka radiation at a scanning range of 2θ=5~45° and a scanning rate of 4°/min.

2.3 Results and discussion

2.3.1 SSZ-13 crystals

Figure 2-3 was the SEM image and corresponding XRD Pattern of CHA-type aluminosilicate SSZ-13 zeolites, pure SSZ-13 zeolites were successfully prepared, and the SSZ-13 crystals exhibited the typical SSZ-13 peaks and displayed the similar near-cubic morphology as reported by Zheng et al [21] but smaller crystal size with the homogenous size of ~400 nm according to the SEM images.
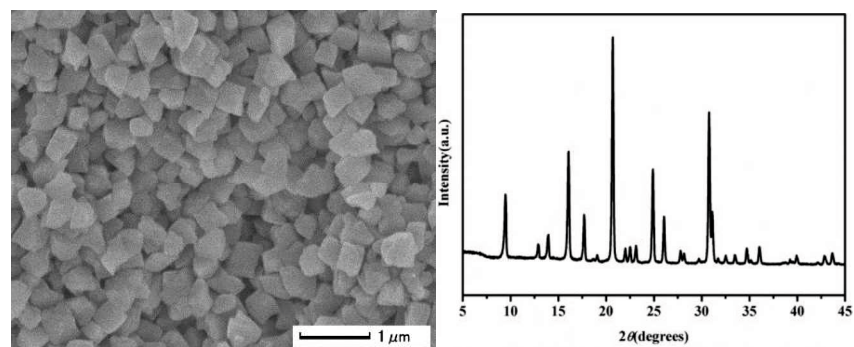
Figure2-3 SEM image of SSZ-13 zeolites and corresponding XRD pattern.

2.3.2 SAPO-34 crystals

The properties of obtained silicoaluminophosphates SAPO-34 zeolites by using single TEAOH template were summarized in Table 2-2. The corresponding XRD patterns were shown in Figure 2-4.

Table 2-2. Properties of prepared SAPO-34 zeolites by single TEAOH template.

Zeolite	TEAOH	Si source	Syn. Temp.	Syn. Time	XRD result	Crystals size
SAPO-34-1	TCI	AS-40	180°C	4	SAPO-5	-
SAPO-34-2	TCI	AS-40	180°C	7	SAPO-5	-
SAPO-34-3	TCI	TEOS	180°C	7	Amorphous	-
SAPO-34-4	TCI	TM-40	180°C	4	Amorphous	-
SAPO-34-5	TCI	TM-40	180°C	7	Amorphous	-
SAPO-34-6	Aldrich	TEOS	180°C	4	SAPO-34	~100nm
SAPO-34-7[1]	Aldrich	TEOS	180°C	4	SAPO-34	~150nm

1: add 0.2 wt.% SAPO-34-6 before hydrothermal synthesis

By using the gel composition of $1Al_2O_3:2P_2O_5:0.6SiO_2:4TEAOH:75H_2O$, pure SAPO-34 zeolites as Heyden et al described [20] are difficult to obtain when we use the TEAOH from TCI company. SAPO-5 impurity was formed when use AS-40 as Silicon source under 180°C for 4h or 7h, which can be seen from Figure 2-4a. And after changing the silicon source to TM-40 or TEOS, no crystals were formed, which can be seen from the XRD in Figure 2-4b. While, when use the template from Sigma-Aldrich, by using TEOS as silicon source, synthesized at 180°C only for 4h, pure SAPO-34 crystals were obtained (Figure 2-4a). The zeolites displayed the characteristic SAPO-34 peak.
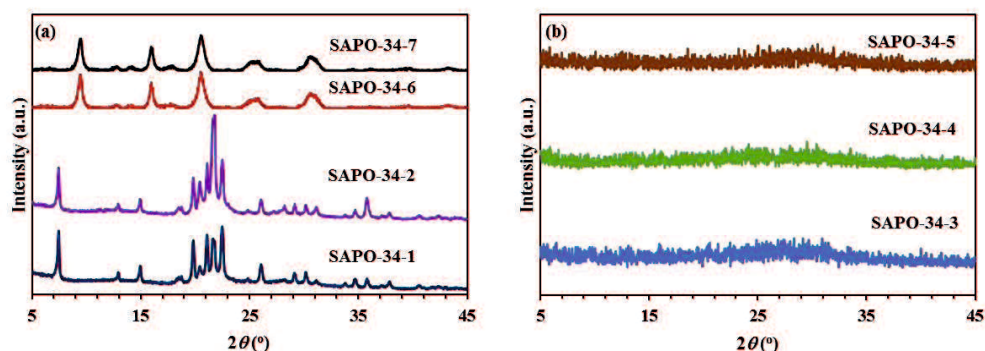
Figure2-4 XRD patterns of SAPO-34 zeolites prepared by single TEAOH template.

Figure 2-5 shows the SEM images of the as-synthesized SAPO-34-6 and SAPO-34-7 zeolites. SAPO-34-7 were prepared by adding 0.2 wt.% SAPO-34-6 into the gel solution, stirred for 30min before the hydrothermal treatment. Pure SAPO-34 zeolites can be obtained after adding the SAPO-34-6 as seeds. The crystals morphologies did not change, meanwhile, the crystals become a little bigger (~150nm) compared with the SAPO-34-6 (~100nm) zeolites.
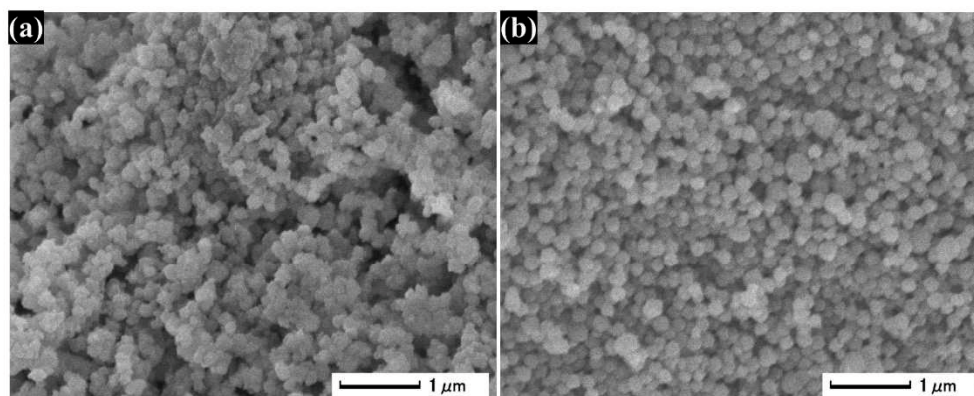
Figure 2-5 SEM images of SAPO-34 zeolites prepared by single TEAOH template:(a) SAPO-34-6, (b) SAPO-34-7.

SAPO-34 zeolites with different crystal sizes were also prepared by using combined TEAOH and DIPEA templates at 200°C for 12-24h with the gel composition of $1Al_2O_3:1P_2O_5:0.6SiO_2:1.5TEAOH:0.5DIPEA: 75H_2O$. The properties of the obtained SAPO-34 zeolites were shown in Table 2-3, the corresponding XRD patterns are shown in Figure 2-6.

Table 2-3. Properties of prepared SAPO-34 zeolites by combined TEAOH and DIPEA templates.

Zeolite	TEAOH	Si source	Syn. Temp.	Syn. Time	XRD result	Crystals size
SAPO-34-8	TCI	TEOS	200	12	SAPO-34	~3μm
SAPO-34-9	TCI	TEOS	200	24	SAPO-34	~3μm
SAPO-34-8-2	Aldrich	TEOS	200	12	SAPO-34	~100-500nm
SAPO-34-10	Aldrich	TEOS	200	12	SAPO-34	~200nm

By using the combined TEAOH and DIPEA templates, pure SAPO-34 zeolites with the characteristic peak same as reported [2] were obtained through the DIPEA from different companies, however the crystals sizes are extremely different. The SEM

images of the as-synthesized SAPO-34 zeolites by combined templates are shown in Figure 2-7.
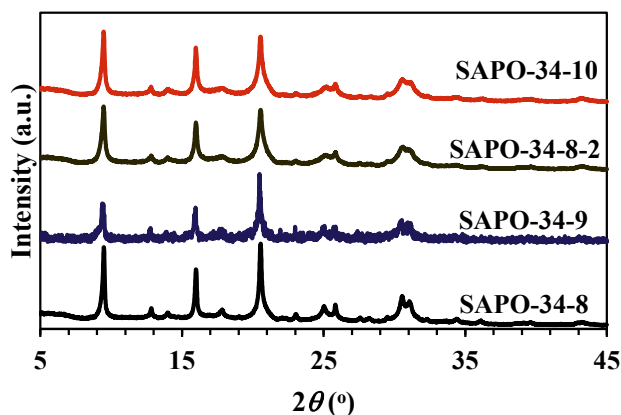
Figure 2-6 The XRD patterns of SAPO-34 zeolites prepared by combined TEAOH and DIPEA templates.

SAPO-34 zeolites SAPO-34-8 prepared with TEAOH from TCI company at 180°C for 12h showed a spherical morphology with the crystal size of ~3μm (Figure 2-7a), which was aggregated by the cubic crystals with the size of ~ 500nm (Figure 2-7b). And the crystals size almost keeps stable when increasing the synthesis time from 12h to24h (Figure 2-7c and Figure 2-7d). However, SAPO-34-8-2 (Figure 2-7e and Figure 2-7f) prepared with the combined templates TEAOH (Sigma-Aldrich, 35%) and DIPEA (Wako, 99%) showed a both spherical and cubic morphology along with a crystal size range from 100nm to 500nm, which is total different from SAPO-34-8. Meanwhile, SAPO-34-10 (Figure 2-7g and Figure 2-7h) added 0.2% SAPO-34-8 (crystals prepared with 35% TEAOH purchased from TCI Company) as seeds and prepared with dual templates displayed also a spherical shape crystal with a size of ~200nm. For SAPO-34-8-2 and SAPO-34-10, under the same synthesis temperature and synthesis time, only with adding a little seeded obtained SAPO-34 with totally different crystals sizes and morphologies.
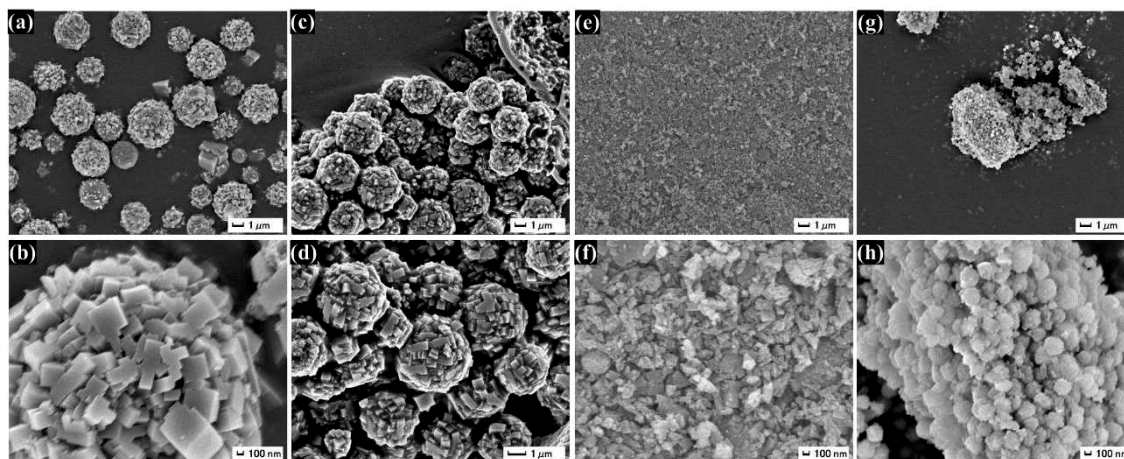
Figure 2-7 The SEM images of SAPO-34 zeolites prepared by combined TEAOH and DIPEA templates. (a) and (b) SAPO-34-8, (c) and (d) SAPO-34-9, (e) and (f) SAPO-34-8-1, (g) and (h) SAPO-34-10.

2.3.3 AlPO-18 crystals

AlPO-18 zeolites with different crystal sizes were also prepared by using different gel compositions as shown in Table 2-1. The properties of as-synthesized AlPO-18 were summarized in Table 2-4, the corresponding XRD patterns were shown in Figure 2-8.

Table 2-4. Properties of prepared AlPO-18 zeolites from different gel composition.

Zeolite	Gel composition	XRD result	Crystals size
AlPO-18-1	$1Al_2O_3:3.16P_2O_5:6.32\ TEAOH:186H_2O$	AlPO-18	300nm
AlPO-18-2	$1Al_2O_3:1P_2O_5:1.8\ TEAOH:\ 60H_2O:2IPA$	AlPO-18	300-500nm
AlPO-18-3	$1Al_2O_3:1P_2O_5:1.8\ TEAOH:60H_2O$	AlPO-18	500-700nm
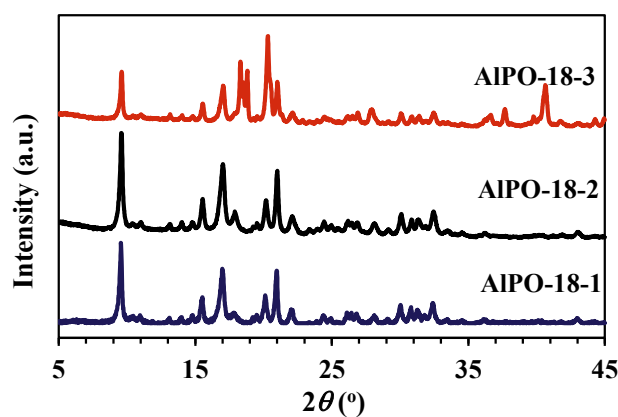
Figure 2-8 The XRD patterns of prepared AlPO-18 zeolites from different gel composition.

The XRD patterns as shown in Figure 2-8 confirmed the pure AlPO-18 zeolites were

formed. The SEM images were displayed in Figure 2-9.

The AlPO-18 zeolites with the gel composition of $1Al_2O_3{:}3.16P_2O_5{:}6.32$ TEAOH:186H$_2$O displayed the sheet-like crystals morphology with the size of ~300nm, by using the gel composition of $1Al_2O_3{:}1P_2O_5{:}1.8$ TEAOH:60H$_2$O, bigger AlPO-18 zeolites with the size of ~500-700nm were obtained, while, some amorphous can be found from the SEM images in Figure 2-9e and Figure 2-9f. And after adding some IPA into the gel solution, the amorphous still exists.

Meanwhile, the AlPO-18 zeolites by TEAOH from TCI company by using the same composition as described in Table 2-1 were also prepared, while, no crystals formed.
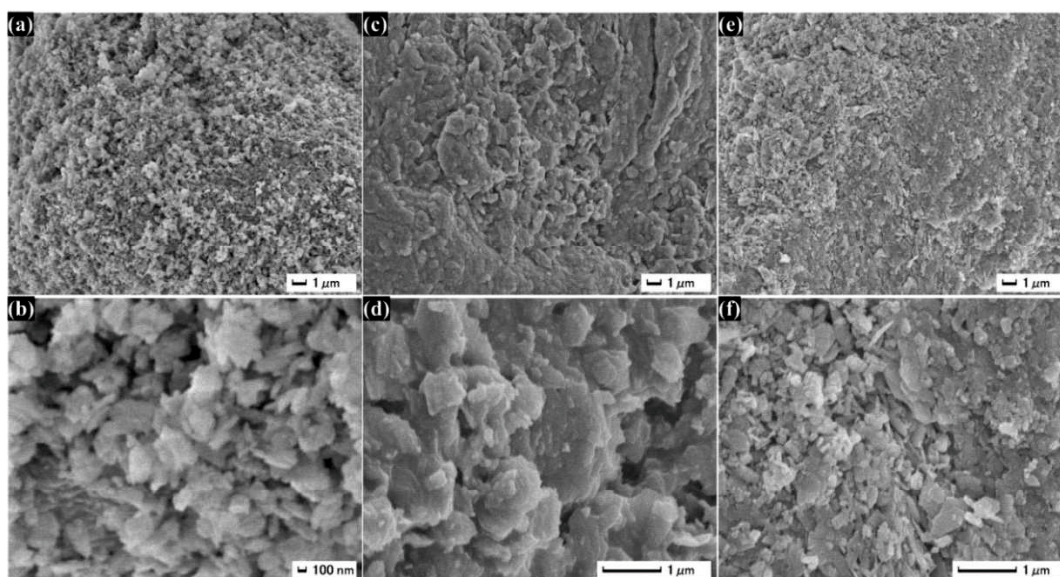
Figure 2-9 The SEM images of AlPO-18 zeolites. (a) and (b) AlPO-18-1, (c) and (d) AlPO-18-2, (e) and (f) AlPO-18-3.

The synthesis conditions and the properties of zeolites SAPO-34, SSZ-13 and AlPO-18 used for later discussions were summarized in Table 2-5. Four SAPO-34 zeolites with the crystals sizes range from 100nm to 500nm, one SSZ-13 zeolite of ~400nm and three AlPO-18 zeolites with the crystals sizes of 300-700nm were successful prepared.

Table 2-5. Synthesis conditions and properties of SAPO-34, SSZ-13 and AlPO-18 zeolites.

Zeolite	Gel composition	Syn. condition	Crystal shape	Size (nm)
SAPO-34 zeolite				
SAPO-34-6	$1Al_2O_3:2P_2O_5:0.6SiO_2:4TEAOH:75H_2O$	453K, 4h	spherical	~100
SAPO-34-8[1]	$1Al_2O_3:1P_2O_5:0.6SiO_2:1.5TEAOH:0.5$ DIPEA: $75H_2O$	473K, 12h	spherical aggregated by cubic	~3000
SAPO-34-8-2	$1Al_2O_3:1P_2O_5:0.6SiO_2:1.5TEAOH:0.5$ DIPEA: $75H_2O$	473K, 12h	spherical + cubic	~100-500
SAPO-34-10	$1Al_2O_3:1P_2O_5:0.6SiO_2:1.5TEAOH:0.5$ DIPEA: $75H_2O$ (add 0.2wt.% SAPO-34-8)	473K, 12h	spherical	~200
SSZ-13 zeolite				
SSZ-13	-	423K, 6d	near-cubic	~400
AlPO-18 zeolite				
AlPO-18-1	$1Al_2O_3:3.16P_2O_5:6.32TEAOH:186H_2O$	423K, 20h	sheet-like	300
AlPO-18-2	$1Al_2O_3:1P_2O_5:1.8TEAOH:60H_2O:2IPA$	423K, 20h		300-500
AlPO-18-3	$1Al_2O_3:1P_2O_5:1.8TEAOH:60H_2O$	423K, 20h	sheet-like	500-700

1: TEAOH from TCI company.

2.4 Conclusions

Two SAPO-34 zeolites with the crystals sizes of 100 and 150nm and three AlPO-18 zeolites with the crystals sizes of 300-700nm were successful prepared by using single TEAOH template from Sigma-Aldrich through the gel composition reported. When changing the TEAOH from TCI company, AlPO-5 or amorphous were formed. Meanwhile, when using dual templates of TEAOH and DIPEA to prepare the SAPO-34 zeolite, the morphologies were totally different when using the TEAOH from TCI and Sigma-Aldrich. One SSZ-13 zeolite of near-cubic morphology with the crystals size of ~400nm were successfully obtained by using home-made single TMAAI template.

References

[1]   S.M. Auerbach, K.A. Carrado, P.K. Dutta, Handbook of zeolite science and technology, Taylor & Francis Group. 2003.

[2]   C. Baerlocher, L.B. McCusker, D. Olson, Atlas of zeolite framework types, 6th revised edition , Elsevier, Amsterdam. 2007.

[3]   D.W. Breck, Zeolite molecular sieves: structure, chemistry, and use, Wiley. 1973.

[4]   P.A. Jacobs，E.M. Flanigen，J.C. Jansen，Herman van Bekkum, Introduction to zeolite science and practice, Elsevier. 2001.

[5]   S.T. Wilson, B.M. Lok, C.A. Messina, T.R. Cannan, E.M. Flanigen, Aluminophosphate molecular sieves: a new class of microporous crystalline inorganic solids, Journal of the American Chemical Society. 104 (1982) 1146-1147.

[6]   Y. Hasegawa, C.Abe, T. Ikeda, K. Sato, Influence of change in the unit cell parameters on permeation properties of AEI-type zeolite membrane, Journal of Membrane Science. 499 (2016) 538-543.

[7]   S.Mintova, VERIFIED SYNTHESES OF ZEOLITIC MATERIALS Third Revised Edition, Published on behalf of the the Synthesis Commission of the International Zeolite Association. 2016.

[8]   S. Li, J.L. Falconer, R.D. Noble, SAPO-34 membranes for CO_2/CH_4 separation, Journal of Membrane Science. 241 (2004) 121-135.

[9]   M.A. Carreon, S. Li, J.L. Falconer, R.D. Noble, Alumina-Supported SAPO-34 Membranes for CO_2/CH_4 Separation, Journal of the American Chemical Society. 130 (2008) 5412-5413.

[10]   S. Li, C.Q. Fan, High-Flux SAPO-34 Membrane for CO_2/N_2 Separation, Industrial and Engineering Chemistry Research. 49 (2010) 4399-4404.

[11]   S. Li, Z. Zong, S.J. Zhou, Y. Huang, Z. Song, X. Feng, R. Zhou, H.S. Meyer, M. Yu, M.A. Carreon, SAPO-34 Membranes for N_2/CH_4 separation: Preparation, characterization, separation performance and economic evaluation, Journal of Membrane Science. 487 (2015) 141-151.

[12] Y. Huang, L. Wang, Z. Song, S. Li, M. Yu, Growth of High-quality, thickness-reduced zeolite membranes towards N_2/CH_4 separation using high-aspect-ratio seeds, Angewandte Chemie International Edition. 127 (2015) 10993-10997.

[13] Z. Zong, S.K. Elsaidi, P.K. Thallapally, M.A. Carreon, Highly Permeable AlPO-18 Membranes for N_2/CH_4 Separation, Industrial and Engineering Chemistry Research. 56 (2017) 4113-4118.

[14] T. Wu, B. Wang, Z. Lu, R. Zhou, X. Chen, Alumina-supported AlPO-18 membranes for CO_2/CH_4 separation, Journal of Membrane Science. 471 (2014) 338-346.

[15] Y. Wang, S.L. Chen, Y.J. Jiang, Y.Q. Cao, F. Chen, W.K. Chang, Y.L. Gao, Influence of template content on selective synthesis of SAPO-18, SAPO-18/34 intergrowth and SAPO-34 molecular sieves used for methanol-to-olefins process, RSC Advanced. 6 (2016) 104985-104994.

[16] D. Zhao, Y. Zhang, Z. Li, Y. Wang, J. Yu, Synthesis of SAPO-18/34 intergrowth zeolites and their enhanced stability for dimethyl ether to olefins, RSC Advanced. 7 (2017) 939-946.

[17] M.R. Hudson, W.L. Queen, J.A. Mason, D.W. Fickel, R.F. Lobo, C.M. Brown, Unconventional, highly selective CO_2 adsorption in zeolite SSZ-13, Journal of the American Chemical Society. 134 (2012) 1970-1973.

[18] H. Van Heyden, S. Mintova, T. Bein, Nanosized SAPO-34 synthesized from colloidal solutions, Chemistry of Materials. 20 (2008) 2956-2963.

[19] M. Vilaseca, S. Mintova, V. Valtchev, T.H. Metzger, T. Bein, Synthesis of colloidal AlPO4-18 crystals and their use for supported film growth, Journal of Materials Chemistry. 13 (2003) 1526-1528.

[20] H. van Heyden, S. Mintova, T. Bein, AlPO-18 nanocrystals synthesized under microwave irradiation, Journal of Materials Chemistry. 16 (2006) 514–518.

[21] Y. Zheng, N. Hu, H. Wang, N. Bu, F. Zhang, R. Zhou, Preparation of steam-stable high-silica CHA (SSZ-13) membranes for CO_2/CH_4 and C_2H_4/C_2H_6 separation, Journal of Membrane Science. 475 (2015) 303-310.

Chapter 3 Preparation and Gas Permeation Properties of AEI Zeolite Membranes

3.1 Introduction

The separation of CH_4 from other components, such as N_2 and CO_2, typically present in natural gas wells is of importance since both decrease the energy content of the gas and CO_2 is corrosive in the presence of moisture. Carbon dioxide can be removed with amine scrubbers or polymer membranes. The amine scrubbers require high pressure and thus they are relatively expensive, and the selectivity of polymer membranes decreases at high pressure due to the plasticization from dissolved CO_2. Cryogenic distillation allows the separation of N_2 but energy costs are high [1]. Membrane separation with inorganic membranes that have molecular-sized pore and good thermal, hydrothermal stabilities are thus of interest for natural gas separation because energy requirements are low and they are not susceptible to plasticization. Several types of microporous membranes such as T [2], DDR [3], SAPO-34 [4,5], Si-CHA [6], SSZ-13 [5,6], SAPO-17 as well as AlPO-17 [7], AlPO-18 [8,9] and the MOF material ZIF-8 [10] have been investigated for CO_2 separation. The SAPO-34 [1,5,11–13], SSZ-13 [5], and AlPO-18 [14] zeolite membranes as well as carbon molecular membranes [15] have high CO_2/CH_4 selectivities and N_2/CH_4 selectivities that are above to the upper bound of the Roberson plot that is commonly used to compare polymers membranes [16].

AlPO-18 is an aluminophosphate with the AEI-type framework that is formed from equimolar AlO_4^- and PO_4^+ tetrahedral units. It has three-dimensional, electrically neutral pores with a diameter of 3.8 Å indicated that it has the potential for separating CO_2 (3.3Å) and N_2 (3.64Å) from CH_4 (3.8Å) by molecular sieving. The Carreon group [14,17] prepared the AlPO-18 membrane with the template TEAOH and showed that those membranes can separate both CO_2/CH_4 and N_2/CH_4 mixtures. The CO_2/CH_4 separation was further improved by Wang et al [8] with a CO_2 permeance of ~1940GPU

with the same template TEAOH. This permeance was still lower than the highest permeances reported for SAPO-34 membranes [4] but the N_2 fluxes for N_2/CH_4 separation [14] were higher than those previously reported for SAPO-34 membranes. However, the N_2/CH_4 selectivity was lower than that of the SAPO-34 membranes [12]. In this work, we prepared the AEI-type AlPO-18 membranes with both TEAOH and N, N-diisopropylethylamine (DIPEA) as a single or combined template. Herein, the effect of synthesis parameters such as the gel composition, synthesis temperature, synthesis time, and the supports were investigated on preparing the AlPO-18 membranes. And these membranes were applied for the gas permeations, meanwhile, the effects of temperature and pressure on the gas permeation properties for AlPO-18 membranes were also investigated here.

3.2 Experimental

3.2.1 Synthesis of AlPO-18 membranes with combined templates TEAOH and DIPEA

The AEI-type AlPO-18 membranes were prepared by secondary growth on the outside of a series of tubes with the gel composition of $1.0Al_2O_3$: $1.0P_2O_5$:0.3TEAOH:1.8DIPEA: $120H_2O$, where the DIPEA is N, N-diisopropylethylamine. The gel solution was prepared by mixing the $Al(i-C_3H_7O)_3$ (98%, Sigma-Aldrich), H_3PO_4 (85% aqueous solution, Wako) and deionized water and stirred for 3 h at room temperature to form a homogeneous solution. Then the DIPEA (99%, Wako) was added in a drop-wise fashion and stirred for another 3h. Finally added the TEAOH into the solution. The resulting solution was then stirred overnight. The rub-coating seeded mullite supports were placed vertically into an autoclave and the synthesis gel was slowly added. Zeolite growth was carried out under hydrothermal conditions 453K for 72h. Here, the AEI- type AlPO-18 crystals were used as the seed to rub-coat onto the porous tubes. The AlPO-18 crystals were prepared as described previously [8,9] and introduced in Chapter 2. The as-synthesized membranes were washed under running tap water for 10 min, then rinsed soaked in running tap water until the soaking solution was clear. The membranes then were dried in an oven at 353K

before calcination. The membranes were calcined in air at 753 K for 6 h with heating and cooling rates of 0.5 K/min.

3.2.2 Synthesis of AlPO-18 membranes with single template TEAOH

The AEI-type AlPO-18 membranes were prepared by secondary growth on the outside of a series of tubes with the gel composition of $1.0Al_2O_3$: $1.0P_2O_5$: $1.8TEAOH$: $120H_2O$ as described before [9]. The gel solution was prepared by mixing the Al(i-$C_3H_7O)_3$ (98%, Sigma-Aldrich), H_3PO_4 (85% aqueous solution, Wako) and deionized water and stirred for 3 h at room temperature to form a homogeneous solution. Then the TEAOH (35% aqueous solution, Sigma-Aldrich) was added drop-wise and stirred in 3h. The resulting solution was then stirred for more 6h. The rub-coating seeded supports were placed vertically into an autoclave and the synthesis gel was slowly added. Zeolite growth was carried out under hydrothermal conditions 488K for a period of time. Here, the AEI- type AlPO-18 crystals were used as the seed to rub-coat onto the porous tubes. The as-synthesized membranes were washed under running tap water for a 10 mins, then soaked in running tap water until the soaking solution was clear. The membranes then were dried in an oven at 353K before calcination. The membranes were calcined in air at 753 K for 6 h with heating and cooling rates of 0.5 K/min.

3.2.3 Synthesis of AlPO-18 membranes with single template DIPEA

The AEI type AlPO-18 membranes were prepared by secondary growth on the outside of porous tubes (12 mm OD, 9 mm ID) with the gel composition of $1.0Al_2O_3$: $1.0P_2O_5$: $1.0DIPEA$: $120H_2O$, where the DIPEA is N, N-diisopropylethylamine. The gel solution was prepared by mixing the Al(i-$C_3H_7O)_3$ (98%, Sigma-Aldrich), H_3PO_4 (85% aqueous solution, Wako) and deionized water and stirred for 3 h at room temperature to form a homogeneous solution. Then the DIPEA (99%, Wako) was added drop-wise. The resulting solution was then stirred for more 12h. The rub-coating seeded mullite supports were placed vertically into an autoclave and the synthesis gel was slowly added. Zeolite growth was carried out under hydrothermal conditions at 478K for 48h. Here, the AEI- type AlPO-18 crystals were used as the seed to rub-coat onto

the porous tubes. The as-synthesized membranes were washed under running tap water for a 10 mins, then rinsed soaked in running tap water until the soaking solution was clear. The membranes then were dried in an oven at 353K before calcination. The membranes were calcined in air at 753 K for 6 h with heating and cooling rates of 0.5 K/min.

3.2.4 Characterization

The morphologies of as-synthesized AEI type membranes were determined by a field emission scanning electron microscope (FE-SEM, JEOL JSM 6335F) at an acceleration voltage of 5KV and some membranes were characterized by using a field emission scanning electron microscopy (FE-SEM, Hitachi SU8020) at acceleration voltages of 5KV. The crystallinity of the AEI type AlPO-18 membranes was identified by X-ray diffraction (XRD, SHIMADZU XRD-6100) using a Shimadzu XD-3 diffractometer with Cu-Ka radiation at a scanning range of 2θ=5~45° and a scanning rate of 4°/min.

3.2.5 Gas permeation

Single gas permeation of He, H$_2$, CO$_2$, O$_2$, N$_2$, CH$_4$, CF$_4$ and SF$_6$ was measured between 298K and 473K using the time-lag method with fixed-volume apparatus as described by Cui et al [2] and vacuum on the permeate side [18]. The membranes were mounted in a stainless-steel cell and sealed with 4 rubber O-rings and 2 stainless steel O-rings on both ends. The Area of the membranes was 18.9 cm^2. Before the permeation measurements, the membrane was degassed at 473K for 20h. For the permeation measurements, the test gas was introduced to the feed side with a back-pressure regulator. The pressure increase on the fixed-volume permeate side due to the gas permeation was monitored with a pressure transducer after closing the vacuum line to the permeate volume. The permeances Pi were then calculated from the pressure increament and the known cell volume on the permeate side. Ideal selectivity (α_{AB}) for different gas pairs were calculated as the ratio of the single-gas permeances:

α_{AB}=P_A/P_B

3.3 Results and discussion

3.3.1 Gas permeation properties of AlPO-18 membranes by combined templates TEAOH and DIPEA

The AlPO-18 zeolite membranes prepared on a series of porous supports with using the gel composition of $1.0Al_2O_3$: $1.0P_2O_5$: $0.3TEAOH$: $1.8DIPEA$: $120H_2O$ were summarized in Table 3-1. Three different kinds of alumina support with different pore sizes and the synthesis time were adopted to investigate the effects on the gas permeances of the as-synthesized AlPO-18 zeolite membranes. Those AlPO-18 membranes prepared at 453K for 72h displayed the characteristic peak of AEI type AlPO-18 membrane, which were confirmed by XRD characterization in Figure 3-1, the pure AEI type AlPO-18 membranes with the characteristic XRD peak of 2θ at $9.5°$ [8,9] can be successfully obtained on these three different supports with 453K, 72h. While for short time of 48h, it is difficult to form the crystals on the surface of the macro-porous support.

Table 3-1 AlPO-18 zeolite membranes prepared with different synthesis conditions.

Membrane	α-Al₂O₃ Support	Synthesis conditions	Phase
a-1	(F tube) (pore size 1.25μm)	453K,48h	AEI
a-2	(F tube) (pore size 1.25 μm)	453K,48h	AEI
a-3	(YUA-08) (pore size 90 nm/1.75 μm)	453K,72h	AEI
a-4	(NS-1) (pore size 100 nm)	453K,72h	AEI
a-5	(F tube) (pore size 1.25 μm)	453K,72h	AEI
a-6	(NS-1) (pore size 100 nm)	453K,72h	AEI
a-11[1]	(mullite) (pore size 1.25 μm)	453K,72h	AEI
a-12[1]	(mullite) (pore size 1.25 μm)	453K,72h	AEI

[1]: mullite support.
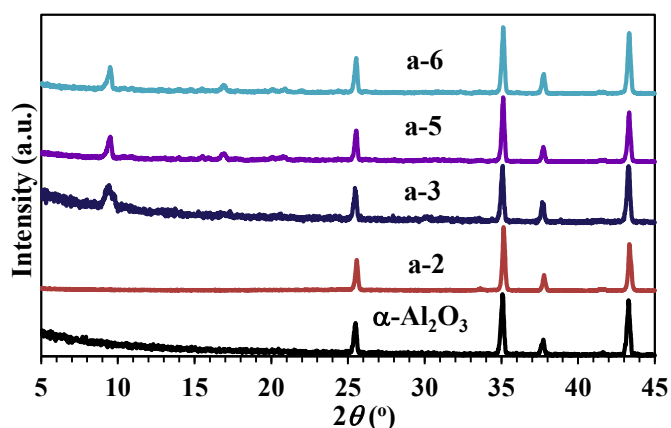
Figure 3-1 XRD patterns of AlPO-18 membranes prepared with different synthesis conditions.

Single gas permeances of He, H_2, CO_2, O_2, N_2 and CH_4 were measured at 0.1MPa and 308K by vacuum method as a function of the gas kinetic diameter, and were shown in Figure 3-2. The single gas permeances were increased in the order of $H_2>CO_2>He>O_2>N_2>CH_4$, since the AlPO-18 crystals has a strong adsorption on CO_2 [9]. H_2 shows the highest single gas permeance, which is different from our previous studies [8,9]. It may be the reason of many defects formed with the membranes as the defect has counteract effects on the gas permeance for CO_2.
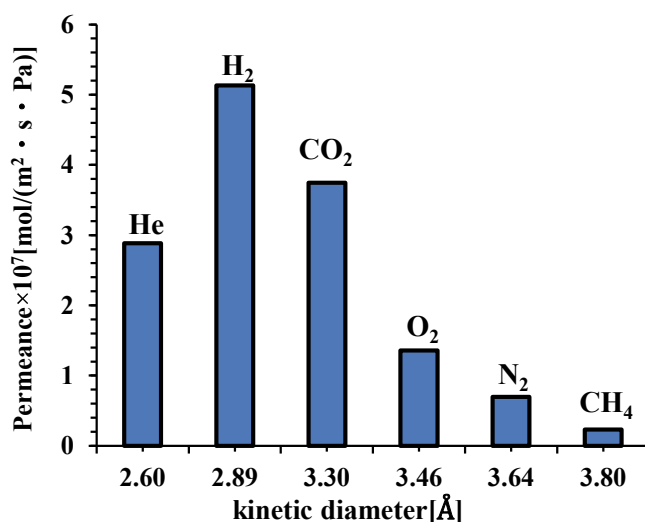
Figure 3-2 Single gas permeances under vacuum method as a function of the kinetic diameter for a-6 prepared with 150nm pore size support.

Figure 3-3 compared the CO_2, CH_4 gas permeation properties by different measuring methods: vacuum method and pressure differential method, at the same time, compared the membrane gas permeation properties before and after desorption. After 20h desorption under 473K, both CO_2 and CH_4 single gas permeances increased

compared with the permeance before desorption, it may result from the residual components such as bonded H_2O [19,20] that stacked into the pores and some defects, which finally in somehow increased the ideal selectivity before desorption. Meanwhile, the gas measurement by using vacuum method and without using vacuum method are also investigated as in Figure 3-3. Both the CO_2 and CH_4 single gas permeances are lower compared with using vacuum method, it may be the effect of concentration polarization [21,22]. Concentration polarization maybe released when performed the membrane by vacuum method. It's a big problem when measuring the membrane with pressure differential method, and will lower the gas permeation properties. What's more, the CO_2 single gas permeance was almost 10 times higher as the recently reported AlPO-18 membrane since the CO_2/CH_4 ideal selectivity was much lower [8], meanwhile, the membrane fabricated on two-layer support (YU-A08) also showed 3-4 times higher of CO_2 single gas permeance than prepared on NS-1 support.
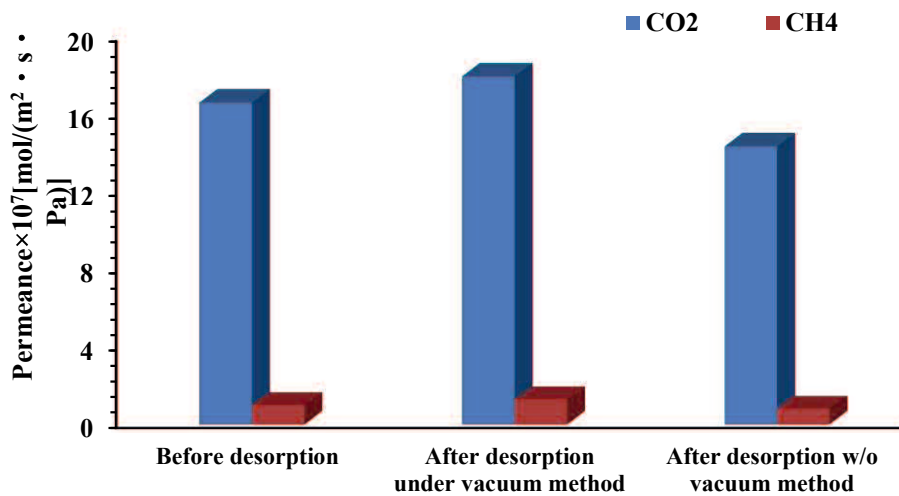
Figure 3-3 Effect of measuring method for AlPO-18 membrane (a-3) fabricated on YU-A08 support.

CO_2 and CH_4 gas permeation properties of the as-synthesized AlPO-18 membranes were summarized in Table 3-2, it is difficult to form the selected AlPO-18 membranes on macro-porous supports (F tube) at 453K with both 48h and 72h. Meanwhile, it also cannot prepare the AlPO-18 membranes on the macro-porous mullite supports. It may result from the small crystals seeds that go into the inside of the support. When prepared the membranes on the NS-1 supports, the membranes displayed a CO_2 single gas permeance ranges from 3.7-5.3 x 10^{-7} mol/(m^2 s Pa) with the CO_2/CH_4 ideal selectivity

with the range of 8.7-16.1. The membrane with highest CO_2 single gas permeance was obtained when fabricated the AlPO-18 membrane on the two-layer smallest pore size support. The membrane shows the CO_2 single gas permeance of 18 x 10^{-7} mol/(m^2 s Pa) with the CO_2/CH_4 ideal selectivity of 13.7. Membrane prepared with the combined TEAOH and DIPEA templates displayed a highest CO_2 single gas permeance for the current reported AlPO-18 membranes [8,9,17] but the selectivity is much lower. Since only few studies on the AlPO-18 membranes for gas separation, it still shows the potential ability to separate light gases, especially for CO_2/CH_4 separation as with the quite well pore structure with the pore size of 0.38nm.

Table 3-2 CO_2 and CH_4 gas permeance properties of AlPO-18 membranes prepared with combined templates.

Membrane	α-Al$_2$O$_3$ Support	Permeance [10^{-7} mol/(m^2 s Pa)]		Ideal Selectivity
		CO$_2$	CH$_4$	
a-1	(F tube) (pore size 1.25μm)	Leak		Leak
a-2	(F tube) (pore size 1.25μm)	Leak		Leak
a-3	(YUA-08) (pore size 90nm/1.75μm)	18.04	1.32	13.7
a-4	(NS-1) (pore size 100nm)	5.293	0.606	8.74
a-5	(F tube) (pore size 1.25μm)	Leak		Leak
a-6	(NS-1) (pore size 100nm)	3.746	0.232	16.1
a-11[1]	(mullite) (pore size 1.33μm)	Leak		Leak
a-12[1]	(mullite) (pore size 1.33μm)	Leak		Leak

[1]: mullite support.

Figure 3-4 shows the SEM images of the AlPO-18 membranes prepared on different supports. It is obvious to see the plate-like crystals with the crystal size of ~1.0 μm was formed on surface of α-Al$_2$O$_3$ supports, and the crystals on the surface were not compact that may lead to some defects. Many small gaps were easily found on the surface. F tube with a pore size of 1.25μm, which is similar to the crystal size itself, many crystals go into the inner of the support (Figure 3-4d). This made it difficult to form a continuous membrane layer. For the membrane prepared on NS-1 support

(Figure 3-4a and Figure 3-4b), the crystals on the surface were big enough compared with the support pore size. The membrane was formed with the thickness of about 1-1.5μm. While, the membrane still was not compact, which may be the reason for the low selectivity. But for the membrane prepared on mullite support (Figure 3-4e and f), since the crystals on the surface are a little bigger (Figure 3-4e) than on α-Al$_2$O$_3$ supports (Figure 3-4a and c), a selective continuous layer still does not form which can be easily see from the cross section in Figure 3-4f. The pore size of mullite support is ~1.33μm that may lead no selective membrane.
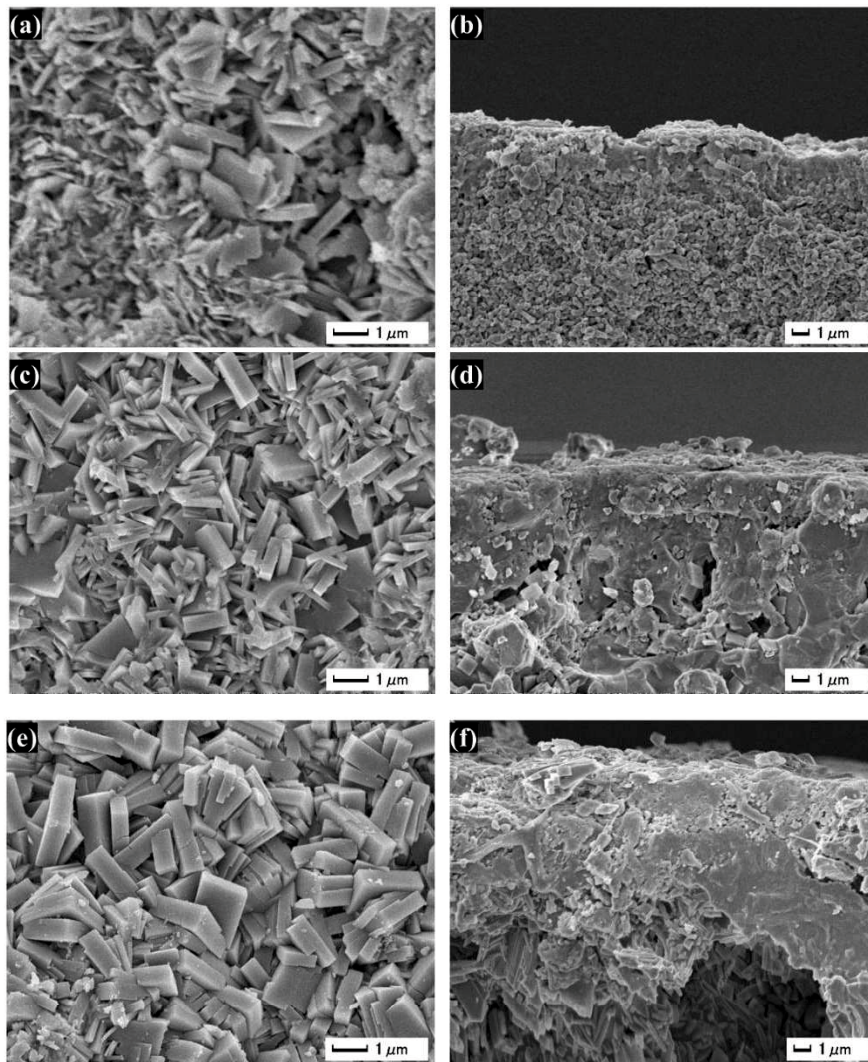
Figure 3-4 SEM images of the AlPO-18 membranes prepared on different supports by combined templates under 473K for 72h. (a) and (b): NS-1 support. (c) and (d): F-tube support. *(e) and (f): mullite support.

Herein, For the AlPO-18 membranes prepared with combined TEAOH and DIPEA templates, since high permeance membrane can be obtained, while, the selectivity is still much lower compared with the current AlPO-18 membranes. In order to improve the gas permeation properties of the AlPO-18 membrane, we try to prepare the AlPO-18 membrane with using single TEAOH or DIPEA template.

3.3.2 Gas permeation properties of AlPO-18 membranes by single template TEAOH

TEAOH as the conventional template for preparing AlPO-18 zeolites [23–26] and membranes [8,9,14,17]. Previously, we already successfully prepared the AlPO-18 zeolite membranes on macro-porous α-Al_2O_3 supports (average pore size:1.25μm) with the gel composition of 1.0Al_2O_3: 1.0P_2O_5: 1.8TEAOH: 120H_2O. Those AlPO-18 membranes showed the average CO_2 gas permeance of 1.8 x 10^{-7} mol/(m^2 s Pa) with the CO_2/CH_4 selectivity of 101. Here, we try to prepare the AlPO-18 membrane on macro-porous mullite support (average pore size of 1.33μm) under the gel composition of 1.0Al_2O_3: 1.0P_2O_5: 1.8TEAOH: 120H_2O, and increase 2h more to form the AlPO-18 membranes.
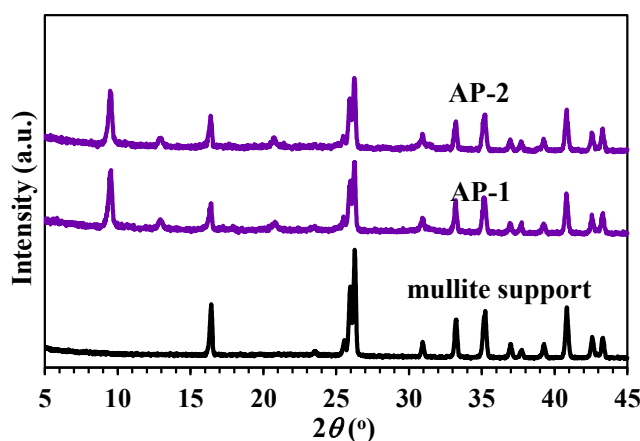
Figure 3-5 XRD patterns of mullite support and the AlPO-18 membrane by single TEAOH template.

Two AlPO-18 membranes were prepared on mullite supports and the corresponding XRD patterns were shown in Figure 3-5. Both two membranes displayed the characteristic peaks with 2θ=9.6º, 12.7º, 16º, and 21º, which is consistence with the our previous reported AlPO-18 membrane [8,9], indicated the pure and non-preferred orientation AlPO-18 membrane also can be formed onto mullite supports.
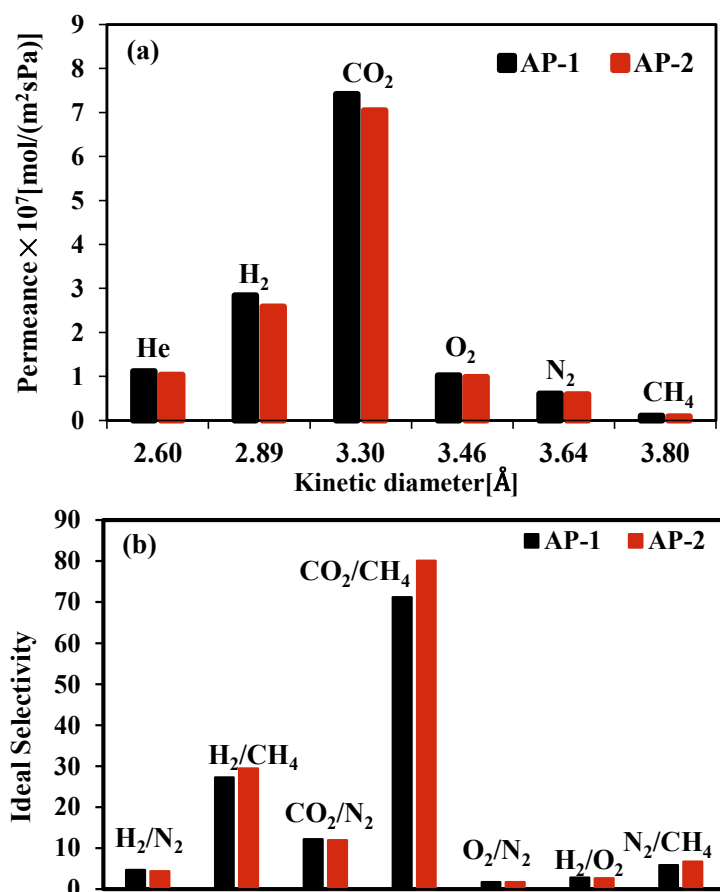
Figure 3-6 The single gas permeance (a) and ideal selectivity (b) of AlPO-18 membranes on mullite supports with single TEAOH template.

Single gas permeances of He, H_2, CO_2, O_2, N_2 and CH_4 measured at 308K and 0.11MPa feed pressure by vacuum method are shown in Figure 3-6a as a function of their kinetic diameters. Permeances decrease in the order of $CO_2>H_2>He>O_2>N_2>CH_4$, which was consistent with our previous study for pure AEI-type AlPO-18 membranes prepared on α-Al_2O_3 supports [9]. Since the CO_2 here shows the highest single gas permeance compared with other five gases, it should be less defects on the surface compared with using combined templates. Figure 3-6b is the ideal selectivity for the gas pairs of H_2/N_2, H_2/CH_4, CO_2/N_2, CO_2/CH_4, O_2/N_2, H_2/O_2 and N_2/CH_4. Both two membranes displayed high CO_2 single gas permeances, the AlPO-18 membrane prepared here shows high CO_2 single gas permeance of 7.0 x 10^{-7} mol/(m^2 s Pa) with the CO_2/CH_4 ideal selectivity with the range of 71.2-80.1. The membranes also displayed a high N_2/CH_4 ideal selectivity range from 5.85-6.71, which is higher than the reported AlPO-18 membranes [14] however lower N_2 permeance ranges of (0.59-

$0.61) \times 10^{-7}$ mol/(m^2 s Pa).

Table 3-3 Apparent activation energy of AlPO-18 membrane (AP-2) by single TEAOH template.

Membrane	Apparent activation energy Ea. (kJ/mol)				
	H$_2$	CO$_2$	O$_2$	N$_2$	CH$_4$
AP-2	-2.53	-12.69	-7.51	-7.30	-0.75
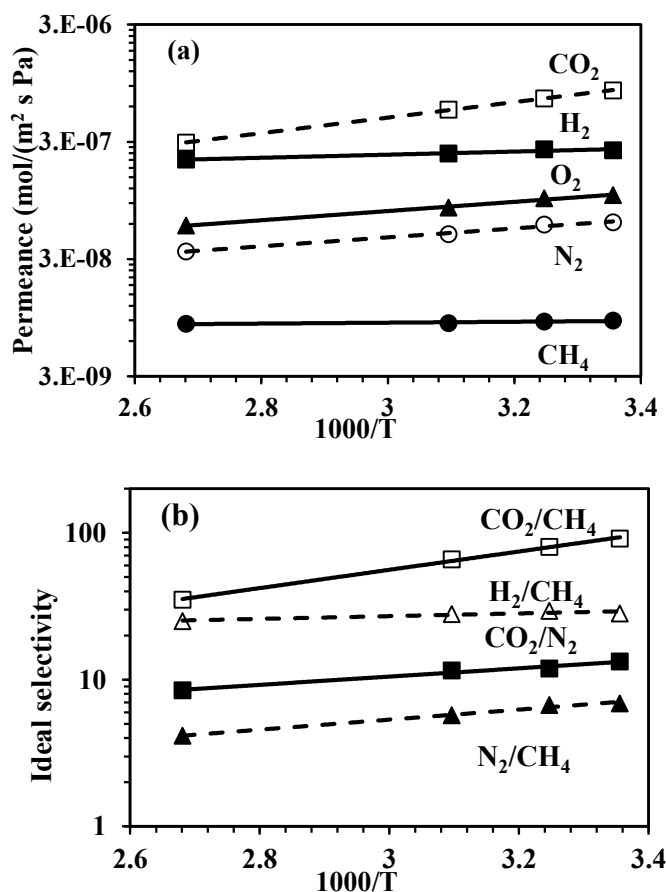
Figure 3-7 Temperature dependence on single gas permeance (a) and ideal selectivity (b) for AlPO-18 membrane (AP-2) prepared with single TEAOH template. Pressure drop was 0.11MPa.

The effect of temperature on gas permeation properties for AlPO-18 membrane (AP-2) is shown in Figure 3-7, single gas permeances of H$_2$, CO$_2$, O$_2$, N$_2$, CH$_4$ five gases continuously decreased with increasing temperature from 298K to 373K (Figure 3-7a), which finally decreased the CO$_2$/CH$_4$, H$_2$/CH$_4$, CO$_2$/N$_2$, N$_2$/CH$_4$ ideal selectivity (Figure 3-7b).

The apparent activation energies of H_2, CO_2, O_2, N_2 and CH_4 permeate through AlPO-18 membrane were calculated by the Arrhenius equation, which was shown in Table 3-3. CO_2 shows the highest apparent activation energy with -12.69 kJ/mol, which indicated the strong adsorption for CO_2 on AlPO-18 membrane. CH_4 has a kinetic diameter of 0.38nm, which is similar as the pore size of AlPO-18 zeolite membrane. A negative activation energy of -0.75 kJ/mol was obtained. It indicates few defects with the as-synthesized AlPO-18 membrane.
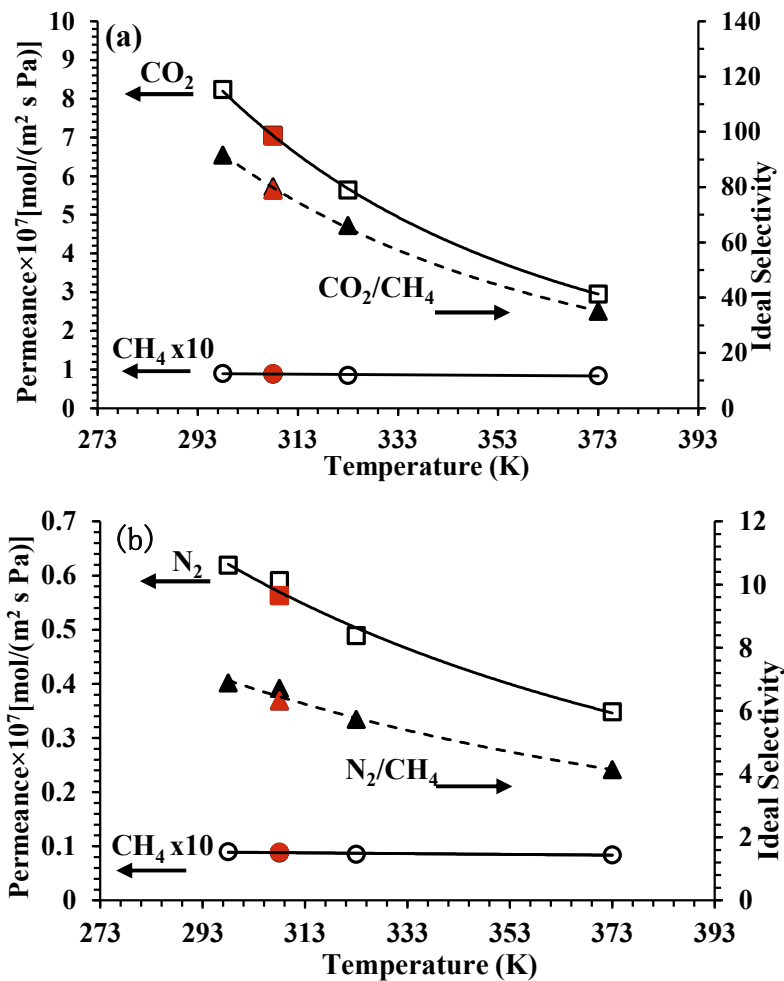
Figure 3-8 Temperature dependence on AlPO-18 membrane (AP-2) for CO_2/CH_4 (a) and N_2/CH_4 (b) separation by vacuum method. Pressure drop was 0.11MPa. Red symbols are measured after one-round test.

For natural gas separation, as the main contaminates in natural gases are CO_2 and N_2, which will decrease the heat value of natural gas, also, CO_2 will lead to corrosion when transportation process under moisture [5], the temperature dependence on CO_2/CH_4 and N_2/CH_4 separation properties for AlPO-18 membrane are shown in Figure

3-8. Both CO_2 and N_2 single gas permeance decreased dramatically when increasing the temperature from 298K to 373K, while CH_4 single gas permeance almost keep stable. The CO_2 single gas permeance decreased from 8.24 x 10^{-7} mol/(m^2 s Pa) to 2.95 x 10^{-7} mol/(m^2 s Pa) along with the CO_2/CH_4 ideal selectivity decrease from 91.7 to 35.1 (Figure 3-8a). And the N_2 single gas permeance decreased from 0.62 x 10^{-7} mol/(m^2 s Pa) to 0.35 x 10^{-7} mol/(m^2 s Pa) with the N_2/CH_4 ideal selectivity decrease from 6.9 to 4.1 (Figure 3-8b). Meanwhile, after 373K measurement, CO_2 and N_2 single gas permeances are 7.04 x 10^{-7} mol/(m^2 s Pa) and 0.56 x 10^{-7} mol/(m^2 s Pa) with the CO_2/CH_4 and N_2/CH_4 ideal selectivity of 79 and 6.3 at 308K, 0.11MPa, which is restored to the similar gas permeation properties as fresh one, indicated a good thermo-stability of AlPO-18 membrane.
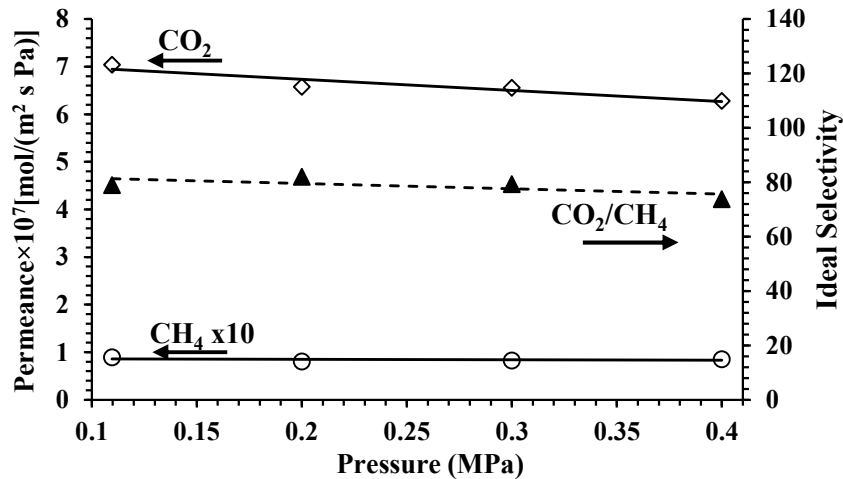
Figure 3-9 Pressure dependence on AlPO-18 membrane (AP-2) for CO_2/CH_4 separation by vacuum method. Temperature was 308K.

Figure 3-9 shows the effect of pressure on CO_2/CH_4 gas permeation properties, the CO_2 single gas permeance decreased continuously from 0.11MPa to 0.4MPa, while CH_4 single gas permeance is relative constant, which result in a slight decrease for CO_2/CH_4 ideal selectivity. This phenomenon is similar as in SAPO-34 zeolite membranes [27,28], due to both AlPO-18 membrane and SAPO-34 membrane belong to the aluminophosphate material and have the same pore size of 0.38nm. Figure 3-10 is the SEM images of the AlPO-18 membrane, the AlPO-18 membrane has a selective layer of~ 10μm that consist of the crystals size of ~8μm, which is similar as prepared on the microporous alumina support with the same gel composition [9].
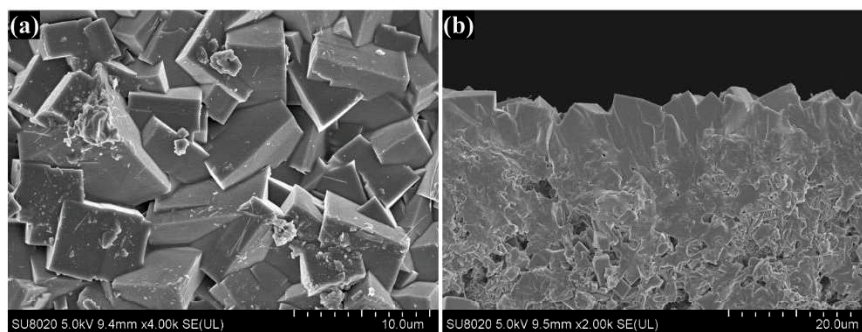
Figure 3-10 Surface (a) and cross-sectional (b) images of AlPO-18 membrane prepared by single TEAOH template on mullite support.

The gas permeation properties of seven AlPO-18 membranes prepared by single TEAOH template fabricated on mullite supports are shown in Table 3-4. The AlPO-18 membrane can obtain gas permeance that higher that the current AlPO-18 membrane of CO_2 [8,17] and higher N_2/CH_4 selectivity [14], while the reproducibility was not as good as that prepared on alumina support [9]. Here, the defect is difficult to control when fabricating those AlPO-18 membranes on mullite support.

Table 3-4 Reproducibility of AlPO-18 membranes by single TEAOH template prepared on mullite supports (308K, ΔP=0.11MPa).

Membrane	Permeance [10^{-7}mol/(m^2 s Pa)]				Ideal Selectivity (α) [-]			
	H_2	CO_2	N_2	CH_4	H_2/CH_4	CO_2/N_2	CO_2/CH_4	N_2/CH_4
AP-1	2.84	7.42	0.610	0.104	27.2	12.2	71.2	5.85
AP-2	2.59	7.05	0.591	0.088	29.4	11.9	80.1	6.71
AP-3	1.81	3.40	0.445	0.256	7.1	7.6	13.3	1.74
AP-4	3.11	4.83	0.700	0.232	13.4	6.9	20.8	3.02
AP-5	2.31	4.58	0.508	0.233	9.9	9.0	19.6	2.18
AP-6	1.56	2.61	0.396	0.255	6.1	6.6	10.2	1.55
AP-7	2.10	3.74	0.496	0.104	20.2	7.5	36.0	4.77

XRD was performed to investigate the reason of bad reproducibility. Figure 3-11 shows the XRD patterns of those reproduced AlPO-18 membranes, unfortunately, the impurities were found on those bad permeation AlPO-18 membranes. The impure phase has the characteristic peaks with $2\theta=7.5°$, which represents the AFI phase AlPO-5. AlPO-5, has the AFI-type framework, is another microporous aluminophosphate with

one-dimensional, cylindrical pores with a diameter of 7.3 Å that was much bigger than CO_2 (3.3Å), N_2 (3.64Å) and CH_4 (3.8Å) and thus permeances of AlPO-5 membranes are much higher but selectivities are low [29].
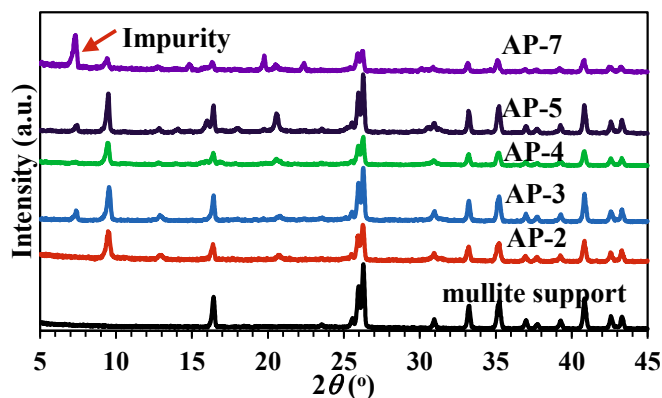
Figure 3-11 XRD patterns of reproduced AlPO-18 membranes by single TEAOH template.

Figure 3-12 illustrates SEM images of the impure AlPO-18 membrane, it is easily found the AFI-type AlPO-5 impurity on the surface of the membrane, meanwhile, those AlPO-18 crystals on the surface are not well intergrowth and inhomogeneous, thus, finally formed a not continuous and unselective zeolite layer, which will result in the bad gas permeation properties.
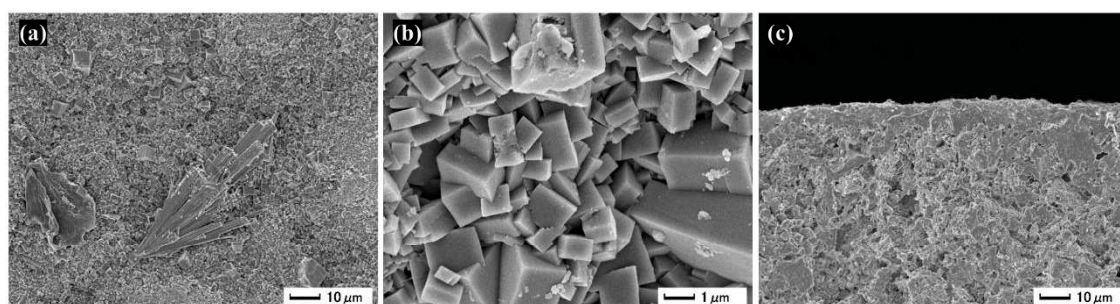
Figure 3-12 SEM images of AlPO-18 membrane (AP-4) by single TEAOH template.

In order to obtain the pure AlPO-18 membrane, two AlPO-18 membranes (AP-8 and AP-9) were prepared with using the single TEAOH template from different company (35%, TCI). Gas permeation properties of the as-synthesized AlPO-18 membranes were illustrated in Table 3-5, and the corresponding XRD patterns were shown in Figure 3-13. AP-1 and AP-2 use the TEAOH template from Sigma-Aldrich, AP-8 and AP-9 use the TEAOH template from TCI.

Table 3-5 Gas permeation properties of AlPO-18 membrane prepared by different TEAOH on mullite supports (308K, ΔP=0.11MPa).

Membrane	Permeance [10^{-7}mol/(m^2 s Pa)]				Ideal Selectivity (α) [-]			
	H_2	CO_2	N_2	CH_4	H_2/CH_4	CO_2/N_2	CO_2/CH_4	N_2/CH_4
AP-1	2.84	7.42	0.610	0.104	27.2	12.2	71.2	5.85
AP-2	2.59	7.05	0.591	0.088	29.4	11.9	80.1	6.71
AP-8	0.606	1.644	0.117	0.033	18.5	14.0	50.1	3.57
AP-9	0.746	1.738	0.148	0.039	18.9	11.8	44.1	3.75

Since the selectivities of the membranes were improved when changed the TEAOH, while, the single gas permeances of CO_2 were decreased from ~7 to ~1.7 x10^{-7}mol/(m^2 s Pa), and the impurity of AFI-type AlPO-5 was still existed in the prepared membrane (as shown in Figure 3-13), thus lower the permeation properties.
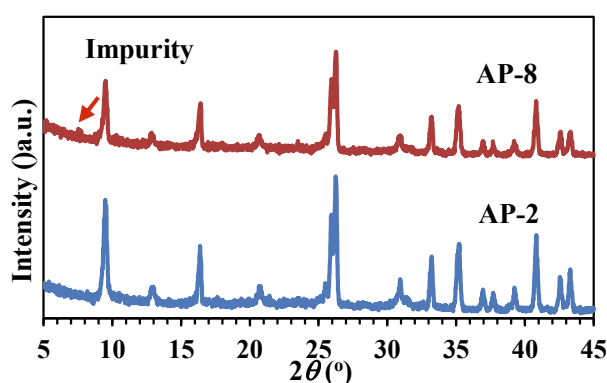
Figure 3-13 XRD patterns of AlPO-18 membranes prepared from different TEAOH template.

Herein, For the AlPO-18 membranes prepared with single TEAOH template on mullite support, since high permeance and selectivity membrane can be obtained, while, the reproducibility is not good, at the same time, impurity is formed and difficult to control when prepared on mullite supports, thus finally decreased the gas permeation properties of the TEAOH prepared AlPO-18 membranes.

3.3.3 Gas permeation properties of AlPO-18 membranes by single template DIPEA

The AlPO-18 zeolite membranes prepared on a series of porous supports by single DIPEA template with the gel composition of 1.0Al_2O_3: 1.0P_2O_5: x DIPEA: 120H_2O under 478K from 36h to 60h were summarized in Table 3-6, the n (DIPEA) ranges from 1.0 to 1.8, when prepared the AlPO-18 membranes at 478K for 48h. Pure AlPO-18 membranes were only obtained when n (DIPEA)=1.8; while, when the synthesis time reduced to 36h or extended to 60h for n (DIPEA)=1.0 or 1.2, pure AlPO-18 membranes

were also formed. Details of the AlPO-18 membranes with the n (DIPEA) were discussed and the corresponding gas permeations properties of those membranes were also investigated

Table 3-6 AlPO-18 membranes prepared with different synthesis conditions.

Membrane	Support	n (DIPEA)	Syn. Conditions	Phase
DIPEA-1	α-Al$_2$O$_3$ (F tube)	1.2	478K, 48h	AlPO-5
DIPEA-2	α-Al$_2$O$_3$ (YU-A01)	1.2	478K, 48h	AlPO-5
DIPEA-3	α-Al$_2$O$_3$ (F tube)	1.2	478K, 60h	pure
DIPEA-4	α-Al$_2$O$_3$ (YU-A01)	1.2	478K, 60h	pure
DIPEA-9	α-Al$_2$O$_3$ (YU-A08)	1.2	478K, 48h	AlPO-5
DIPEA-10	α-Al$_2$O$_3$ (YU-A08)	1.2	478K, 48h	AlPO-5
DIPEA-13	α-Al$_2$O$_3$ (YU-A08)	1.2	478K, 48h	AlPO-5
DIPEA-14	α-Al$_2$O$_3$ (YU-A08)	1.2	478K, 48h	AlPO-5
DIPEA-17	α-Al$_2$O$_3$ (F tube)	1.2	478K, 36h	pure
DIPEA-18	α-Al$_2$O$_3$ (YU-A08)	1.2	478K, 36h	pure
DIPEA-5	α-Al$_2$O$_3$ (YU-A08)	1.8	478K, 48h	pure
DIPEA-6	α-Al$_2$O$_3$ (YU-A01)	1.8	478K, 48h	pure
DIPEA-7	α-Al$_2$O$_3$ (YU-A08)	1.8	478K, 48h	pure
DIPEA-8	α-Al$_2$O$_3$ (YU-A08)	1.8	478K, 48h	pure
DIPEA-11	Mullite	1.0	478K, 48h	AlPO-5
DIPEA-12	α-Al$_2$O$_3$ (YU-A08)	1.0	478K, 48h	AlPO-5
DIPEA-15	Mullite	1.0	478K, 48h	AlPO-5
DIPEA-16	α-Al$_2$O$_3$ (F tube)	1.0	478K, 48h	AlPO-5
DIPEA-21	α-Al$_2$O$_3$ (YU-A08)	1.0	478K, 48h	AlPO-5
DIPEA-22	Mullite	1.0	478K, 36h	Pure
DIPEA-23	α-Al$_2$O$_3$ (YU-A08)	1.0	478K, 36h	Pure
DIPEA-24	Mullite	1.0	478K, 36h	Pure
DIPEA-25	α-Al$_2$O$_3$ (F tube)	1.0	478K, 36h	Pure

3.3.3.1 The AlPO-18 membranes synthesized at n(DIPEA)=1.8

The XRD patterns of AlPO-18 membranes prepared with using the gel composition of 1.0Al$_2$O$_3$: 1.0P$_2$O$_5$: 1.8DIPEA: 120H$_2$O at 478K for 48h were displayed in Figure 3-14, the characteristic peak of 2θ at 9.5° confirmed the pure AEI type AlPO-18 membranes were formed.
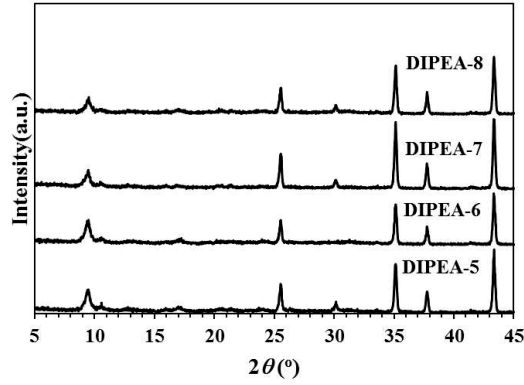
Figure 3-14 XRD patterns of AlPO-18 membranes prepared at 478K for 48h with gel composition of $1Al_2O_3:1P_2O_5:1.8$ DIPEA:$120H_2O$.

Figure 3-15 shows the SEM images of the AlPO-18 membranes prepared at n (DIPEA)=1.8, pure and intergrowth AlPO-18 crystals with the size of ~1.5μm were formed on the surface of the membrane, and a continuous zeolite layer with the thickness of ~4.5μm were easily seen from the Figure 3-15b. The sheet-like morphologies of the crystals is as same as the AlPO-18 membranes prepared with single DIPEA template by Hasegawa et al [30].
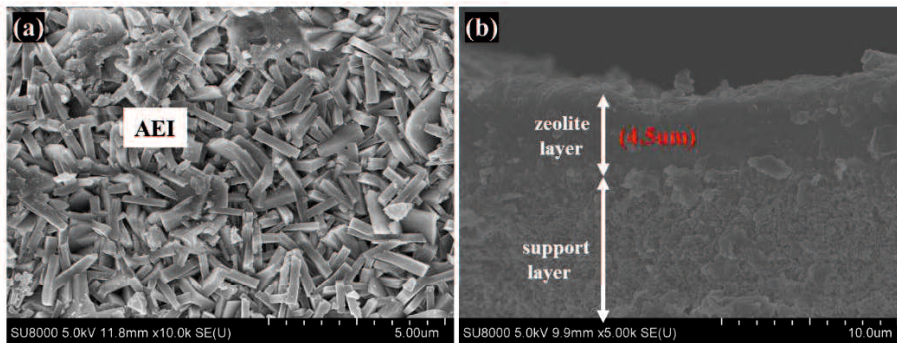
Figure 3-15 Surface (a) and cross sectional (b) images of AlPO-18 membrane (DIPEA-5) prepared with gel composition of $1Al_2O_3:1P_2O_5:1.8$ DIPEA: $120H_2O$.

Figure 3-16 shows the single gas permeances of He, H_2, CO_2, O_2, N_2 and CH_4 as a function of their kinetic diameters for the AlPO-18 membrane synthesized with n (DIPEA)=1.8, single gas permeances were consistent as the pure AlPO-18 membranes [9] with the order of $CO_2>H_2>He>O_2>N_2>CH_4$.
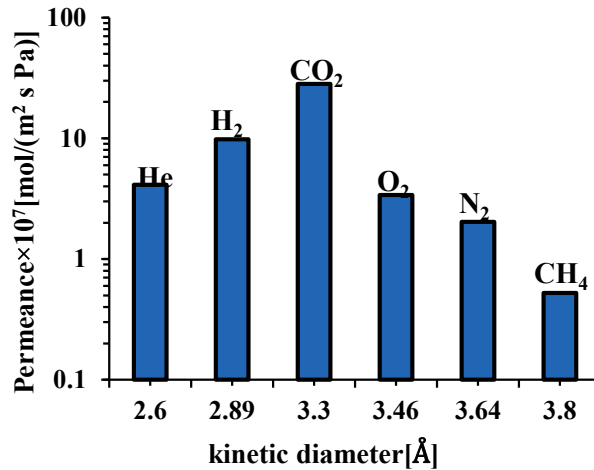
Figure 3-16 Single gas permeances as a function of the kinetic diameter of AlPO-18 membrane (DIPEA-5) performed at 308K, 0.11MPa.
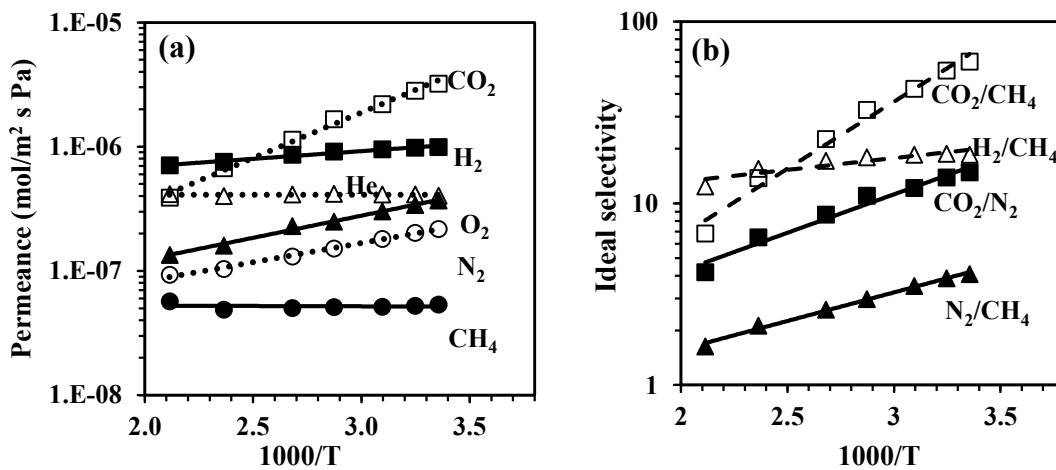
Figure 3-17 The effect of temperature on single gas permeance (a) and ideal selectivity (b) of AlPO-18 membrane (DIPEA-5) by gel composition of $1Al_2O_3$:$1P_2O_5$:1.8 DIPEA: $120H_2O$.

Figure 3-17 illustrates the gas permeances and ideal selectivity of AlPO-18 membrane (DIPEA-5) as a function of temperature, same as the membrane prepared with single TEAOH. Single gas permeances of H_2, CO_2, O_2, N_2 four gases continuously decreased with increasing temperature from 298K to 473K (Figure 3-17a). The single gas permeance of He and CH_4 almost keep stable, which finally decreased the CO_2/CH_4, H_2/CH_4, CO_2/N_2, N_2/CH_4 ideal selectivity (Figure 3-17b).

Table 3-7 shows the apparent activation energies for those six gases, CO_2 still shows the highest apparent activation energy, with -14.0 kJ/mol, while, CH_4 shows a positive activation energy of +0.11kJ/mol, which may due to the effects of the AlPO-18 membrane that same as the pure silica CHA membrane [31].

Table 3-7 Apparent activation energy of AlPO-18 membrane (DIPEA-5) by single DIPEA template.

Membrane	Apparent activation energy Ea. (kJ/mol)				
	H_2	CO_2	O_2	N_2	CH_4
DIPEA-5	-2.37	-14.0	-6.82	-5.92	+0.11
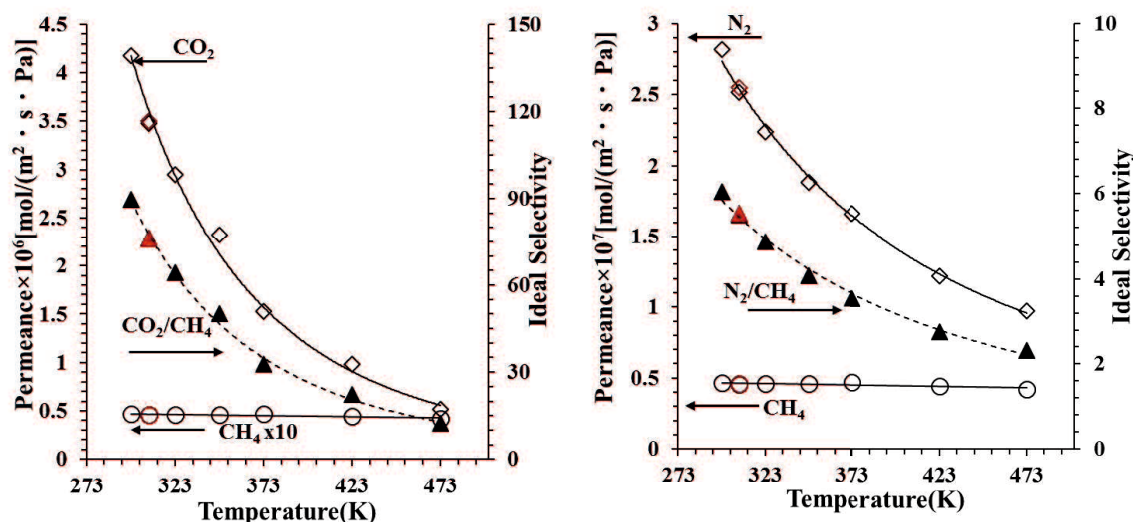
Figure 3-18 Temperature dependence on AlPO-18 membrane (DIPEA-5) for CO_2/CH_4 (left) and N_2/CH_4 (right) separation under vacuum method. Pressure drop was 0.11MPa. Red symbols are measured after one-round test.

Temperature dependence on CO_2/CH_4 and N_2/CH_4 separation properties for AlPO-18 membrane (DIPEA) are shown in Figure 3-18. For the membrane prepared with single DIPEA template, the similar gas permeation properties were found as with the membrane prepared with single TEAOH [8,9], while, the CO_2 and N_2 single gas permeances of membrane (DIPEA-5) almost increased 4 times as with here prepared with single TEAOH membrane (AP-2). Again, CO_2 and N_2 single gas permeance decreased as increasing temperature from 298K to 473K, and the single gas permeances decreased from 32.2 x 10^{-7} mol/(m^2 s Pa) to 3.89 x 10^{-7} mol/(m^2 s Pa) and 2.18 x 10^{-7} mol/(m^2 s Pa) to 0.93 x 10^{-7} mol/(m^2 s Pa), respectively. CH_4 single gas permeance also keeps stable. what's more, even under 473K, the N_2 single gas permeance (0.93 x 10^{-7} mol/(m^2 s Pa)) still higher than that (0.62 x 10^{-7} mol/(m^2 s Pa)) of membrane AP-2 measured at 298K. The AlPO-18 membrane shows quite high gas permeance of CO_2

compared with the intensively studies SAPO-34 membranes [6].

3.3.3.2 The AlPO-18 membranes synthesized at n(DIPEA)=1.2

Gas permeation properties of AlPO-18 membranes prepared with the gel composition of $1.0Al_2O_3$: $1.0P_2O_5$: 1.2DIPEA: $120H_2O$ at 478K for 36 and 48h were illustrated in Table 3-6 and details of those high gas permeation membranes were also shown in Table 3-8, the corresponding XRD patterns of the as-synthesized membranes were also displayed in Figure 3-19.

Table 3-8 Gas permeation properties of AlPO-18 membranes prepared with gel composition of $1Al_2O_3$:$1P_2O_5$:1.2 DIPEA:$120H_2O$. (308K, ΔP=0.11MPa).

Membrane			Permeance [10^{-7}mol/(m^2 s Pa)]					Ideal selectivity α [-]		
	support	phase	CO_2	N_2	CH_4	H_2	SF_6	CO_2/CH_4	N_2/CH_4	H_2/SF_6
DIPEA-9	YUA-08	AEI+AFI	35.1	2.6	0.5	12.5	0.095	75.9	5.5	132.0
DIPEA-10	YUA-08	AEI+AFI	34.8	2.5	0.5	12.0	0.082	76.2	5.5	150.0
DIPEA-13	YUA-08	AEI+AFI	34.2	2.9	1.3	11.6	0.445	25.4	2.2	26.0
DIPEA-14	YUA-08	AEI+AFI	52.1	4.4	0.9	21.7	0.229	55.1	4.6	94.8
DIPEA-17[1]	F tube	AEI	20.0	4.2	2.6	18.4	0.833	7.6	1.6	22.1
DIPEA-18[1]	YUA-08	AEI	29.8	3.1	0.7	15.5	0.117	45.0	4.6	132.1

[1]: membrane prepared at 478K for 36h.

Four AlPO-18 membranes prepared under n(DIPEA)=1.2 at 478K for 48h displayed good reproducibility as shown in Table 3-8, while, the AFI-type AlPO-5 with the characteristic peak of 2θ at 7.5° were found for all four membranes, which was proved by the XRD characterization as shown in Figure 3-19b. However, pure AlPO-18 membrane was formed when the synthesis time reduced to 36h and increased to 60h, no impurity was found in Figure 3-19a. And compared with the membranes prepared for 48h, both the membranes with 36 and 60h show a weak intensity of characteristic peak of AlPO-18.
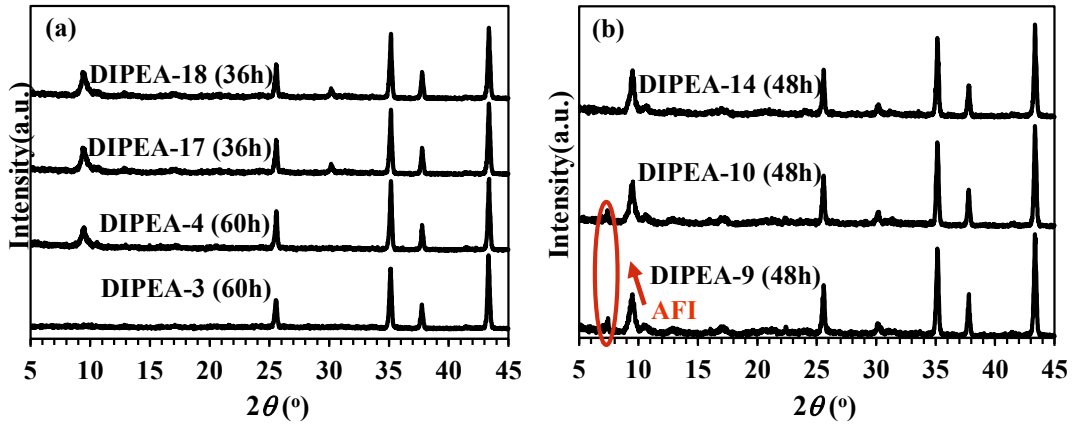
Figure 3-19 XRD patterns of AlPO-18 membranes prepared at 478K for (36-60) h with gel composition of $1Al_2O_3$:$1P_2O_5$:1.2 DIPEA:$120H_2O$.

The SEM images of the membranes prepared under n(DIPEA)=1.2 at 478K for 48h were shown in Figure 3-20, For the membranes with high gas permeation properties, a thicker selective layer with the thickness of 4-4.5μm.
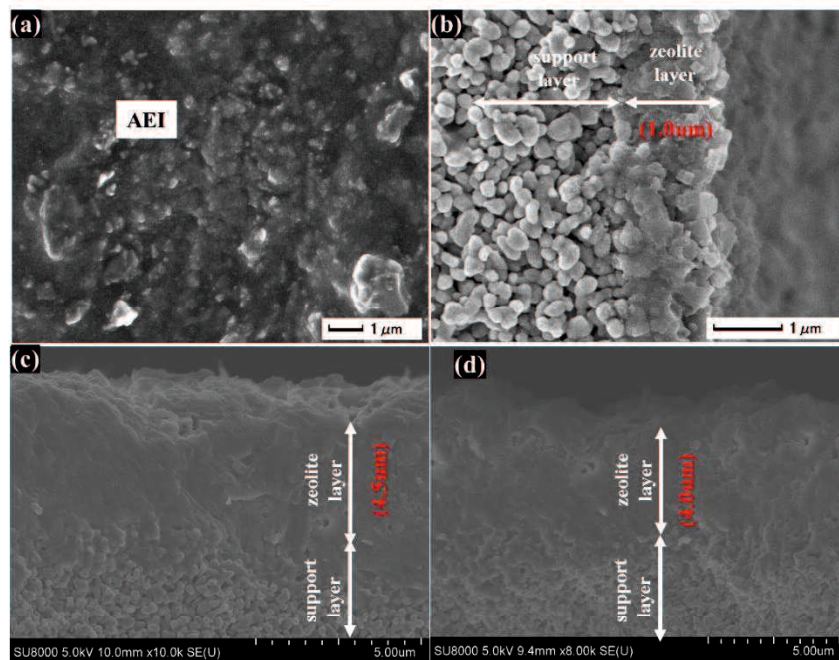
Figure 3-20 SEM images of AlPO-18 membrane for DIPEA-13 (a and b), DIPEA-9 (c) and DIPEA-10 (d) prepared with gel composition of $1Al_2O_3$:$1P_2O_5$:1.2 DIPEA: $120H_2O$.
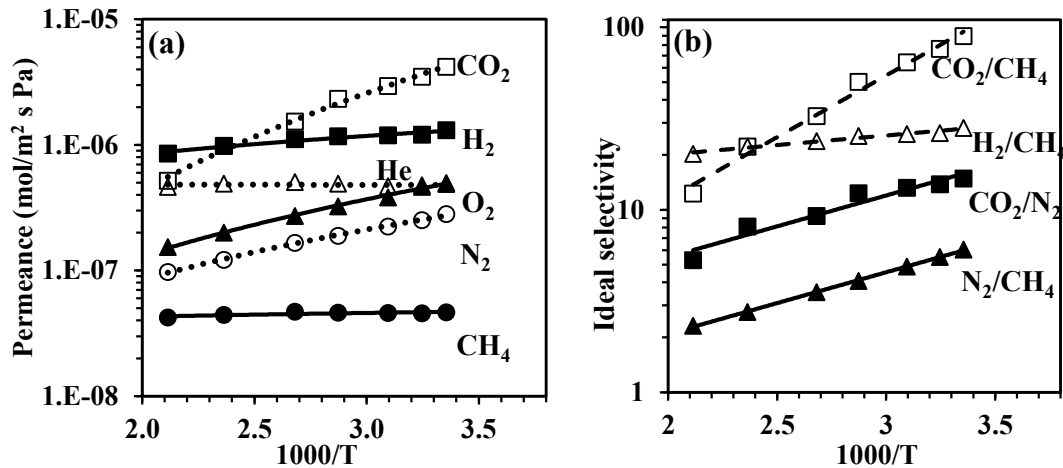
Figure 3-21 The effect of temperature on single gas permeance (a) and ideal selectivity (b) of AlPO-18 membrane (DIPEA-10) by gel composition of $1Al_2O_3:1P_2O_5:1.2DIPEA: 120H_2O$. Membrane DIPEA-10 was used to investigate the effect of temperature for the gas permeations. Single gas permeances of H_2, CO_2, O_2, N_2 four gases decreased with increasing temperature from 298K to 473K (Figure 3-21a), however, CH_4 single gas permeance did not change a lot, which resulted in the reduction of the CO_2/CH_4, H_2/CH_4, CO_2/N_2, N_2/CH_4 ideal selectivity (Figure 3-21b).
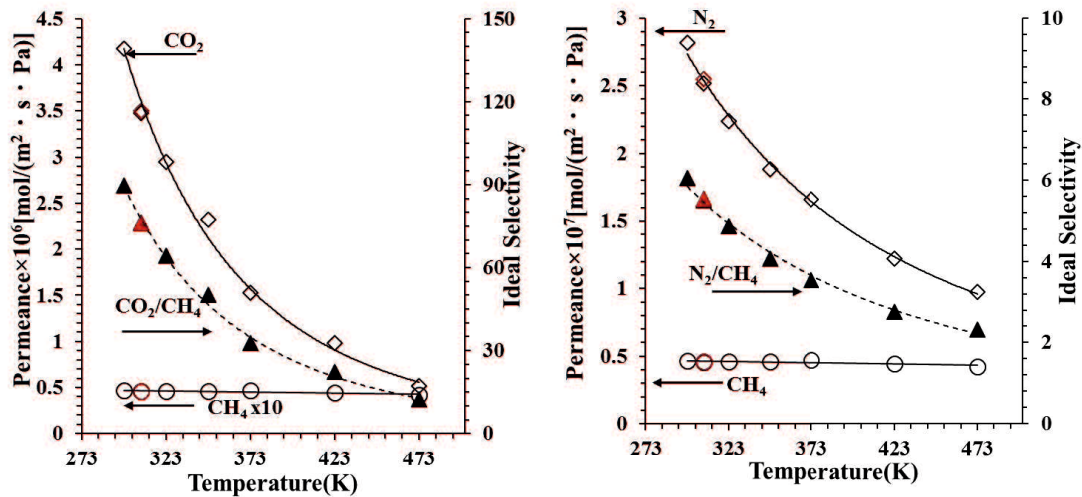
Figure 3-22 Temperature dependence on **AlPO-18** membrane (DIPEA-10) for CO_2/CH_4 (left) and N_2/CH_4 (right) separation under vacuum method. Pressure drop was 0.11MPa. Red symbols are measured after one-round test.

Meanwhile, gas permeation properties of CO_2/CH_4 and N_2/CH_4 separations as a function of temperature for AlPO-18 membrane (DIPEA-10) are shown in Figure 3-22. CO_2 single gas permeance decreased from 41.7 x 10^{-7} mol/(m^2 s Pa) to 5.17 x 10^{-7}

mol/(m^2 s Pa) and the CO_2/CH_4 ideal selectivity decreased from 89.6 to 12.3 by increasing temperature from 298K to 473K. N_2 single gas permeance decreased from 2.82 x 10^{-7} mol/(m^2 s Pa) to 0.98 x 10^{-7} mol/(m^2 s Pa) along with N_2/CH_4 decreased from 6.05 to 2.31. The AlPO-18 membrane with the AlPO-5 impurity (DIPEA-10) shows higher gas permeation properties compared with pure AlPO-18 membrane (DIPEA-5).
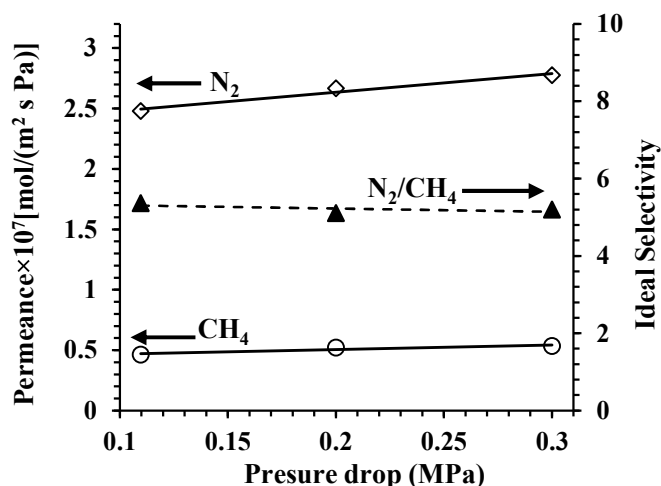
Figure 3-23 Pressure dependence on **AlPO-18** membrane (DIPEA-10) N_2/CH_4 separation under vacuum method. Temperature was 308K.

Single gas permeances of N_2 and CH_4 through membrane DIPEA-10 as a function of pressure were shown in Figure 3-23, both N_2 and CH_4 single gas permeances increased as increasing the pressure from 0.11MPa to 0.3MPa, as a result, the N_2/CH_4 ideal selectivity was almost constant.

3.3.3.3 The AlPO-18 membranes synthesized at n(DIPEA)=1.0

Table 3-9 shows the gas permeation properties of AlPO-18 membranes prepared with the gel composition of 1.0Al$_2$O$_3$: 1.0P$_2$O$_5$: 1.0DIPEA: 120H$_2$O at 478K. while, impurity was formed when performed the membranes at 478K for 48h, and the membranes prepared on the alumina supports displayed lower gas permeation properties than that on mullite supports. The membranes with the n(DIPEA) of 1.0 on the mullite supports show lower CO_2 single gas permeances and CO_2/CH_4 ideal selectivities, however, the H_2/SF_6 ideal selectivities are much higher, less defects may

form with the mullite-supported AlPO-18 membranes with the n(DIPEA)=1.0 synthesized at 478K for 48h. At the same time, the pure AlPO-18 membranes were also obtained when decreasing the synthesis time to 36h. It was also confirmed by the XRD characterization of those as-synthesized membranes showed in Figure 3-24. However, the gas permeation properties of the pure AlPO-18 membranes were not as good as with prepared by using n(DIPEA)=1.0.

Table 3-9 Gas permeation properties of AlPO-18 membranes prepared with gel composition of $1Al_2O_3:1P_2O_5:1.0$ DIPEA$:120H_2O$. (308K, $\Delta P=0.11MPa$).

Membrane			Permeance [$10^{-7}mol/(m^2\,s\,Pa)$]					Ideal selectivity α [-]		
	support	phase	CO_2	N_2	CH_4	H_2	SF_6	CO_2/CH_4	N_2/CH_4	H_2/SF_6
DIPEA-11	mullite	AEI+AFI	20.4	1.90	0.30	9.69	0.0211	67.8	6.32	460.0
DIPEA-12	YUA-08	AEI+AFI	23.3	4.42	3.91	20.87	1.3862	5.9	1.13	15.06
DIPEA-15	mullite	AEI+AFI	13.8	1.22	0.17	5.85	0.0083	79.9	7.05	700.1
DIPEA-16	F tube	AEI+AFI	17.0	8.21	9.86	27.7	-	1.7	0.83	-
DIPEA-21	YUA-08	AEI+AFI	50.2	8.12	3.97	33.8	1.2803	12.6	2.04	26.4
DIPEA-22[1]	mullite	AEI			leak				leak	
DIPEA-23[1]	YUA-08	AEI	53.4	7.62	3.06	38.0	0.8696	17.5	2.49	43.7
DIPEA-24[1]	mullite	AEI			leak				leak	
DIPEA-25[1]	F tube	AEI	22.0	4.76	2.35	20.9	-	9.3	2.0	-

[1]: membrane prepared at 478K for 36h.
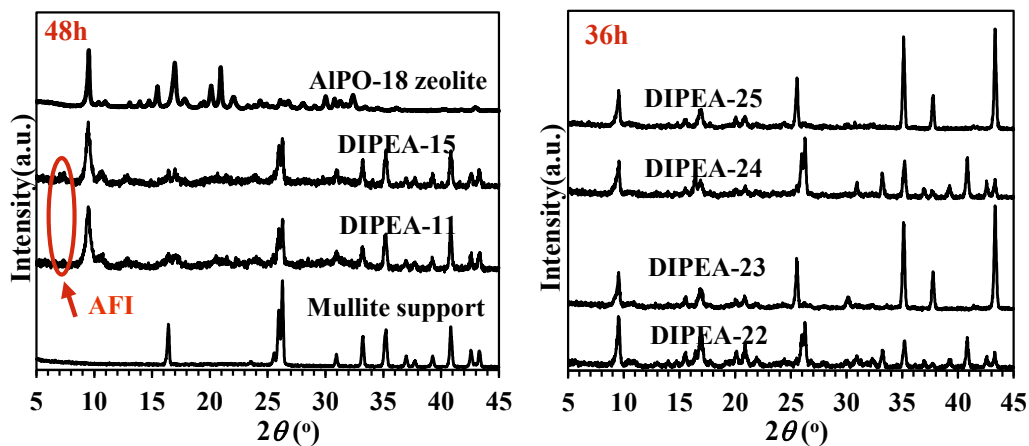
Figure 3-24 XRD patterns of AlPO-18 membranes prepared at 478K for (36-48) h with gel composition of $1Al_2O_3:1P_2O_5:1.0$ DIPEA$:120H_2O$.

As with the AFI-type impurity formed during the synthesis conditions of 478K, 48h for both n(DIPEA) of 1.0 and 1.2, the crystals collected from the bottom of the autoclaves after membrane DIPEA-11 synthesis was characterized by XRD and SEM,

it is obvious that AFI crystals with the rod-like morphology [31] formed not only on the surface of membranes, also existed in the gel solution after 48h growth.
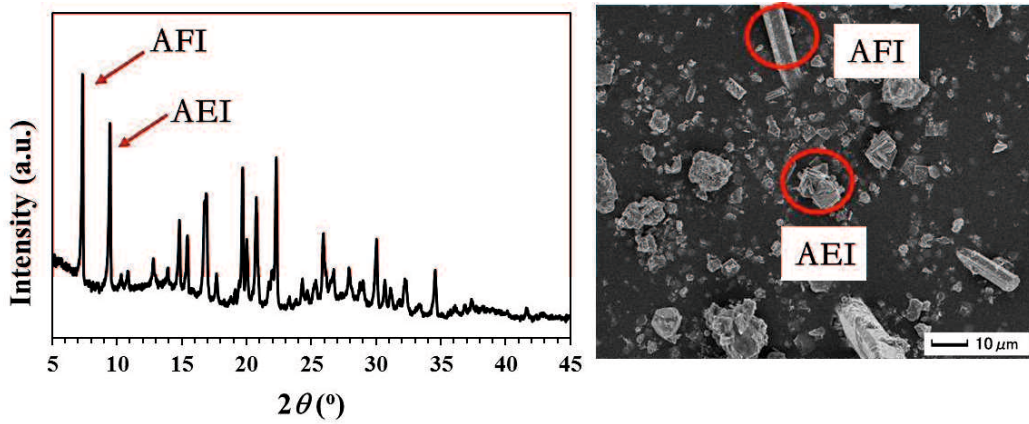
Figure 3-25 SEM images and XRD pattern of crystals collected from the bottom of the autoclave after membrane n(DIPEA=1.0) synthesis.
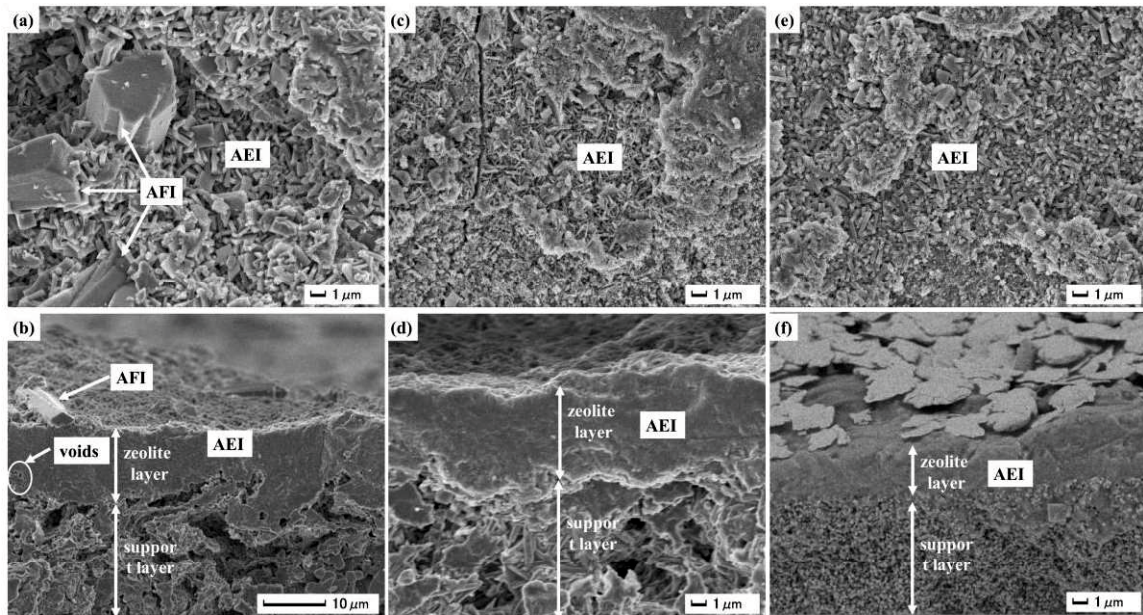
Figure 3-26 SEM images of membrane with gel composition of $1Al_2O_3:1P_2O_5:1.0$ DIPEA: $120H_2O$.
Surface (a) and cross sectional (b) of membrane prepared on mullite support with 48h
Surface (c) and cross sectional (d) of membrane prepared on mullite support with 36h
Surface (e) and cross sectional (f) of membrane prepared on α-Al_2O_3 with 36h

Figure 3-26 shows the SEM images of membranes prepared with gel composition of $1Al_2O_3:1P_2O_5:1.0$ DIPEA: $120H_2O$ under 478K for 36 and 48h on differnet supports, smaller crystals with the size less than 1μm were formed on the surface of mullite support when synthesized for 36h, as a result, the membrane formed a zeolite layer of

~7μm, which is thinner than that of membrane prepared with 48h (zeolite layer of ~ 12μm); however, when prepared with the same time of 36h, the crystals are bigger on the small pore size alumina support but with a thinner membrane layer of ~3.5μm, it may due to less seeds went into the inner pore of support with using small pore size support [32], thus big crystals and thin zeolite layer obtained.
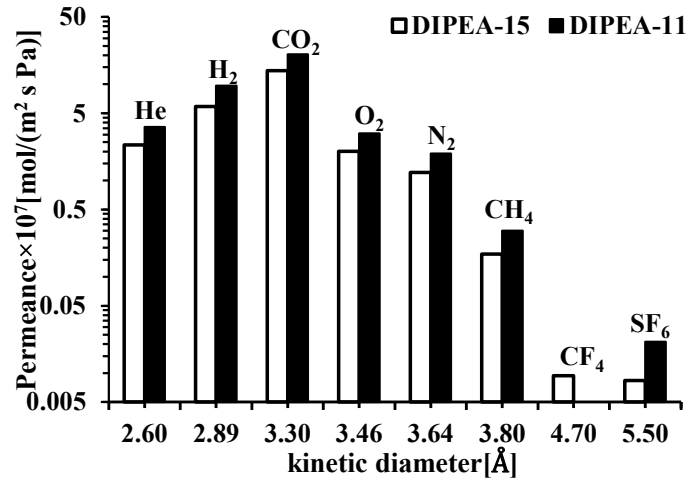
Figure 3-27 Single gas permeances as a function of the kinetic diameter of AlPO-18 membranes (DIPEA-11 and DIPEA-15) performed at 308K, 0.11MPa.

Single gas permeation properties as a function of gas kinetic diameter on two membranes fabricated on mullite supports by using n (DIPEA) of 1.0 were shown in Figure 3-27. Both of two membranes show same gas permeation trend, which were consistent as the pure AlPO-18 membrane [9] with the order of $CO_2>H_2>He>O_2>N_2>CH_4>CF_4>SF_6$. Since CF_4 (kinetic diameter:0.47nm) and SF_6 (kinetic diameter:0.55nm) cannot go through the pore of AlPO-18 membrane (0.38nm) while can go through the pore of the impurity AlPO-5 (0.73nm), which may be the reason of high gas permeances for all impure AlPO-18 membranes.
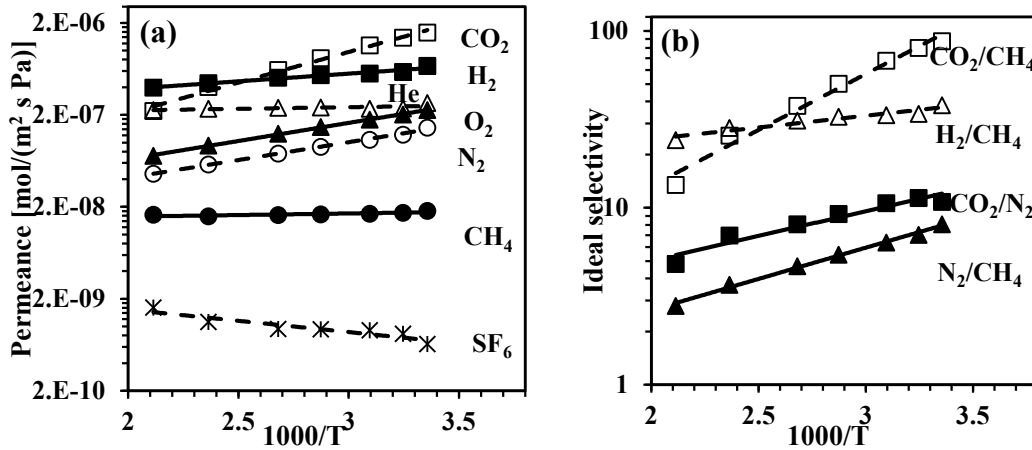
Figure 3-28 Effect of temperature on single gas permeance (a) and ideal selectivity (b) of AlPO-18 membrane (DIPEA-15) by gel composition of $1Al_2O_3:1P_2O_5:1.0DIPEA: 120H_2O$.

As same as previous, membrane DIPEA-15 was also used to investigate the effect of temperature for the gas permeation properties. From Figure 3-28a, single gas permeances of H_2, CO_2, O_2, N_2 four gases decreased with increasing temperature from 298K to 473K, and single gas permeances of He and CH_4 are essentially independent of temperature. However, single gas permeance of SF_6 increased with increasing temperature, indicated the activated diffusion happens, and some defects formed in the membrane [6], which resulted in the reduction of the CO_2/CH_4, H_2/CH_4, CO_2/N_2, N_2/CH_4 ideal selectivity (Figure 3-28b).
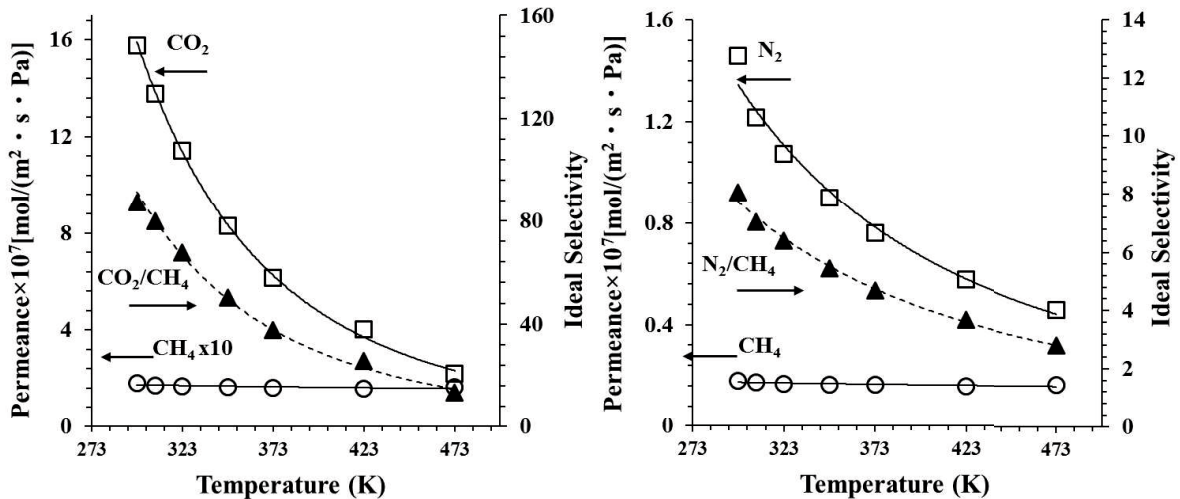
Figure 3-29 Temperature dependence on **AlPO-18** membrane (DIPEA-15) for CO_2/CH_4 (left) and N_2/CH_4 (right) separation under vacuum method. Pressure drop was 0.11MPa.

Figure 3-29 is single gas permeation properties of CO_2/CH_4 and N_2/CH_4

separations as a function of temperature for AlPO-18 membrane (DIPEA-15). CO_2 single gas permeance decreased from 15.8 x 10^{-7} mol/(m^2 s Pa) to 2.20 x 10^{-7} mol/(m^2 s Pa) and the CO_2/CH_4 ideal selectivity decreased from 87.4 to 13.4 by increasing temperature from 298K to 473K. N_2 single gas permeance decreased from 1.46 x 10^{-7} mol/(m^2 s Pa) to 0.46 x 10^{-7} mol/(m^2 s Pa) along with N_2/CH_4 decreased from 8.08 to 2.79. The lower single gas permeance may due to the thick selective layer(~12μm) as shown in Figure 3-26b.
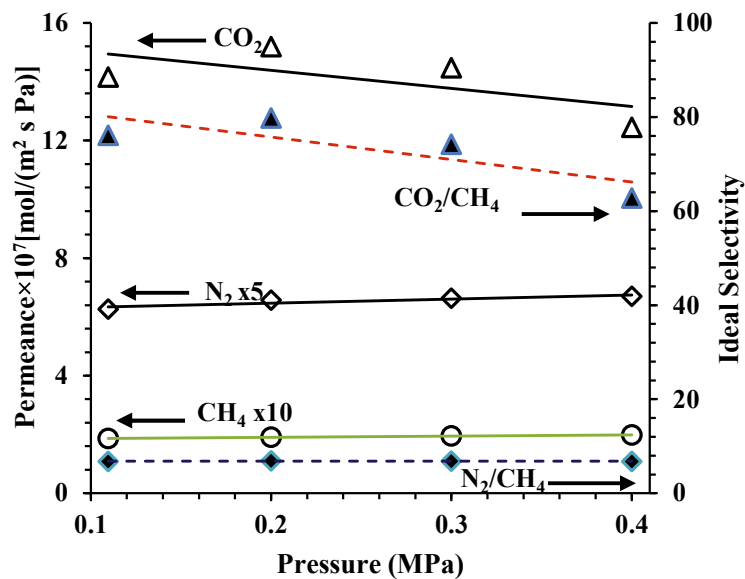
Figure 3-30 Pressure dependence on **AlPO-18** membrane (DIPEA-15) for CO_2/CH_4 and N_2/CH_4 separation under vacuum method. Temperature was 308K.

Figure 3-30 shows single gas permeances of CO_2, N_2 and CH_4 through membrane DIPEA-15 as a function of pressure. CO_2 single gas permeance decreased, the CO_2 permeance decreased when increasing pressure from 0.2MPa to 0.4MPa, and has a slight maximum at a feed pressure of 200 kPa, whereas both the N_2 and CH_4 permeance increases slightly with pressure., the N_2 single gas permeance increased to 1.34 x10^{-7} mol/(m^2 s Pa), and the CO_2 single gas permeance decreased to 1.25 x10^{-6} mol/(m^2 s Pa) at 0.4MPa. While, both the CO_2/CH_4 and N_2/CH_4 ideal selectivity decreased with pressure range from 0.2MPa to 0.4MPa, and have a highest perm-selectivity at 0.2MPa, the CO_2/CH_4 and N_2/CH_4 perm-selectivity dropped to 62.8 and 6.76 at 0.4MPa, respectively.

3.3.3.4 Comparison
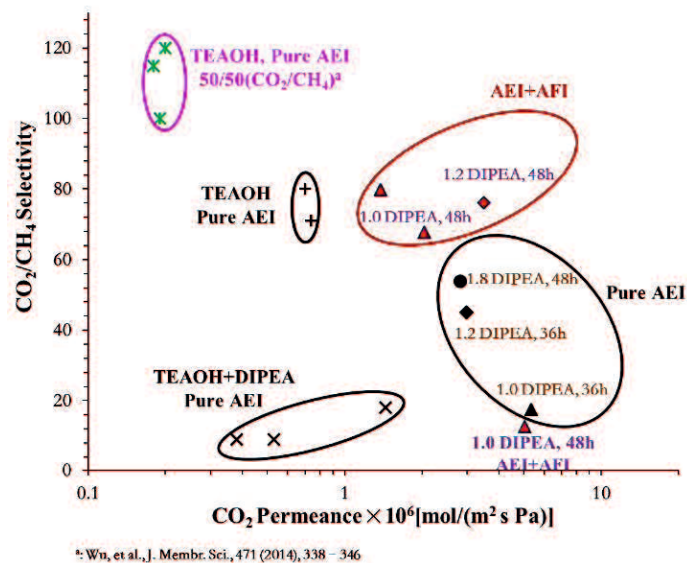
Figure 3-31 P_{CO2} vs $\alpha_{CO2/CH4}$ of AlPO-18 membranes under different synthesis conditions.

The CO_2, CH_4 gas permeation properties of the AlPO-18 membranes prepared with combined TEAOH and DIPEA templates, single TEAOH template and single DIPEA template were plotted in Figure 3-31. Highest CO_2 single gas permeance is 53.4 x10^{-7} mol/(m^2 s Pa) of the membrane prepared with DIPEA, and the highest CO_2/CH_4 perm-selectivity membrane were obtained by the single TEAOH template.

Table 3-10 and Table 3-11 compared the N_2/CH_4 and CO_2/CH_4 separations for the membranes prepared in this study with other inorganic membranes reported in the literatures. Within these materials, our membranes displayed moderate N_2/CH_4 permeation properties, while, for CO_2/CH_4 separation, our membranes displayed the highest CO_2 permeance with the moderate selectivity, especially for the combined AEI and AFI membranes, indicated a protentional application for natural gas purification.

Table 3-10 Comparison of N_2/CH_4 separations through the inorganic membranes.

Material	Thickness (μm)	N_2/CH_4 selectivity	N_2 Permeance [10^{-7}mol/(m^2 s Pa)]	Test conditions	Reference
SAPO-34	1.8-2.2	7.4-8.6	5.79-8.68	Feed pressure: 223kPa, ΔP=138kPa;296K	[12]
SAPO-34	3.0-4.2	6.5-7.4	2.95-4.35	Feed pressure: 223kPa, ΔP=138kPa;296K	[13]
SAPO-34	2.3	5.7-11.3	0.94-4.02	Feed pressure: 275kPa, ΔP=174kPa;295K	[11]
SAPO-34	6.2	8	1.67	Feed pressure: 223kPa, ΔP=138kPa;296K	[1]
SAPO-34	2.0-3.0	5-7	1.00	Feed pressure: 350kPa, 293K	[5]
SSZ-13	7.8	13	0.22	Feed pressure: 270kPa, 293K	[5]
Carbon molecular sieve[1]	70±15	7.7	~0.0003	Feed pressure: 448kPa, 308K	[15]
AlPO-18	2.4	3.0-4.6	4.54-10.3	Feed pressure: 223kPa, ΔP=138kPa;296K	[14]
AP-2[1] (Pure AEI)	-	6.89	0.62	Feed pressure: 110kPa, ΔP=110kPa;298K	This study
DIPEA-5[1] (Pure AEI)	4.0	4.07	2.18	Feed pressure: 110kPa, ΔP=110kPa;298K	This study
DIPEA-10[1] (AEI+AFI)	4.0	6.05	2.82	Feed pressure: 110kPa, ΔP=110kPa;298K	This study

Table 3-11 Comparison of CO_2/CH_4 separations through the inorganic membranes.

Material	CO_2/CH_4 selectivity	CO_2 Permeance [10^{-7} mol/(m^2 s Pa)]	Test conditions	Reference
T	400	0.046	Feed pressure: 100kPa, ΔP=100kPa;308K	[2]
DDR	200	3.00	Feed pressure: 200kPa, ΔP=100kPa;298K (with sweep gas)	[3]
ZIF-8	4~7	240	Feed pressure: 139.5kPa, ΔP=40kPa;295K	[10]
SAPO-34	171	18.0	Feed pressure: 222kPa, ΔP=138kPa;295K	[4]
Si-CHA[1]	54	17.0	ΔP=100kPa;313K	[6]
SSZ-13[1]	56	8.60	ΔP=100kPa;313K	[6]
SAPO-17	53	11.0	Feed pressure: 303kPa, ΔP=200kPa;298K	[7]
AlPO-17	25	5.23	Feed pressure: 303kPa, ΔP=200kPa;298K	[7]
AlPO-18	220	6.50	Feed pressure: 303kPa, ΔP=200kPa;298K	[8]
AlPO-18	120	2.0	Feed pressure: 200kPa, ΔP=100kPa;298K (with sweep gas)	[9]
AlPO-18	60	0.66	ΔP=138kPa;295K	[17]
a-3[1] (Pure AEI)	13.7	18.04	Feed pressure: 110kPa, ΔP=110kPa;308K	This study
AP-2[1] (Pure AEI)	91.7	8.64	Feed pressure: 110kPa, ΔP=110kPa;298K	This study
DIPEA-5[1] (Pure AEI)	60.2	32.2	Feed pressure: 110kPa, ΔP=110kPa;298K	This study
DIPEA-10[1] (AEI+AFI)	89.6	41.7	Feed pressure: 110kPa, ΔP=110kPa;298K	This study

[1]: single gas test.

3.4 Conclusions

AlPO-18 membranes were prepared by using combined TEAOH and DIPEA templates, single TEAOH template and single DIPEA template, respectively. Pure AlPO-18 membranes with different gas permeation properties can be obtained through these three routes. Through combined TEAOH and DIPEA templates, the as-synthesized pure AlPO-18 membranes displayed moderate CO_2 single gas permeance with lowest CO_2/CH_4 ideal selectivity. Through single TEAOH template, the obtained AlPO-18 membranes displayed highest CO_2/CH_4 selectivity however lowest CO_2 gas permeance, meanwhile, those AlPO-18 membranes show bad reproducibility. Through single DIPEA template, both pure and impure AlPO-18 membranes were formed by changing the n(DIPEA), synthesis temperature and synthesis time. The membrane with single DIPEA template displayed highest CO_2 single gas permeance with moderate CO_2/CH_4 ideal selectivity.

Gas permeation properties of both pure and impure AlPO-18 membranes were affected by measuring conditions of temperature and pressure. CO_2, N_2 single gas permeances decreased dramatically by increasing temperature, while CH_4 single gas permeance was almost independent of temperature. Pressure also dramatically decreased CO_2 single gas permeance however slightly increased both N_2 and CH_4 single gas permeances.

References

[1]   S. Li, Z. Zong, S.J. Zhou, Y. Huang, Z. Song, X. Feng, R. Zhou, H.S. Meyer, M. Yu, M.A. Carreon, SAPO-34 Membranes for N_2/CH_4 separation: Preparation, characterization, separation performance and economic evaluation, Journal of Membrane Science. 487 (2015) 141-151.

[2]   Y. Cui, H. Kita, K. I. Okamoto, Preparation and gas separation performance of zeolite T membrane, Journal of Materials Chemistry. 14 (2004) 924-932.

[3]   S. Himeno, T. Tomita, K. Suzuki, K. Nakayama, K. Yajima, S. Yoshida, Synthesis and Permeation Properties of a DDR-Type Zeolite Membrane for Separation of CO_2/CH_4 Gaseous Mixtures, Industrial and Engineering Chemistry Research. 46 (2007) 6989-6997.

[4]   M.A. Carreon, S. Li, J.L. Falconer, R.D. Noble, Alumina-Supported SAPO-34 Membranes for CO_2/CH_4 Separation, Journal of the American Chemical Society. 130 (2008) 5412-5413.

[5]   T. Wu, M.C. Diaz, Y. Zheng, R. Zhou, H.H. Funke, J.L. Falconer, R.D. Noble, Influence of propane on CO_2/CH_4 and N_2/CH_4 separations in CHA zeolite membranes, Journal of Membrane Science. 473 (2015) 201-209.

[6]   K. Kida, Y. Maeta, K. Yogo, Preparation and gas permeation properties on pure silica CHA-type zeolite membranes, Journal of Membrane Science. 522 (2017) 363-370.

[7]   S. Zhong, N. Bu, R. Zhou, W. Jin, M. Yu, S. Li, Aluminophosphate-17 and silicoaluminophosphate-17 membranes for CO_2 separations, Journal of Membrane Science. 520 (2016) 507-514.

[8]   B. Wang, N. Hu, H. Wang, Y. Zheng, R. Zhou, Improved AlPO-18 membranes for light gas separation, Journal of Materials Chemistry A. 3 (2015) 12205-12212.

[9]   T. Wu, B. Wang, Z. Lu, R. Zhou, X. Chen, Alumina-supported AlPO-18 membranes for CO_2/CH_4 separation, Journal of Membrane Science. 471 (2014) 338-346.

[10]   S.R. Venna, M.A. Carreon, Highly Permeable Zeolite Imidazolate Framework-8

Membranes for CO_2/CH_4 Separation, Journal of the American Chemical Society. 132 (2010) 76-78.

[11]   Y. Huang, L. Wang, Z. Song, S. Li, M. Yu, Growth of High-Quality, Thickness-Reduced Zeolite Membranes towards N_2/CH_4 Separation Using High-Aspect-Ratio Seeds, Angewandte Chemie International Edition. 54 (2015) 10843-10847.

[12]   Z. Zong, M.A. Carreon, Thin SAPO-34 membranes synthesized in stainless steel autoclaves for N_2/CH_4 separation, Journal of Membrane Science. 524 (2017) 117-123.

[13]   Z. Zong, X. Feng, Y. Huang, Z. Song, R. Zhou, S.J. Zhou, M.A. Carreon, M. Yu, S. Li, Highly permeable N_2/CH_4 separation SAPO-34 membranes synthesized by diluted gels and increased crystallization temperature, Microporous and Mesoporous Materials. 224 (2016) 36-42.

[14]   Z. Zong, S.K. Elsaidi, P.K. Thallapally, M.A. Carreon, Highly Permeable AlPO-18 Membranes for N_2/CH_4 Separation, Industrial and Engineering Chemistry Research. 56 (2017) 4113-4118.

[15]   X. Ning, W.J. Koros, Carbon molecular sieve membranes derived from Matrimid® polyimide for nitrogen/methane separation, Carbon. 66 (2014) 511-522.

[16]   L.M. Robeson, The upper bound revisited, Journal of Membrane Science. 320 (2008) 390-400.

[17]   M.L. Carreon, S. Li, M.A. Carreon, A.J. Hill, S.J. Pas, S.T. Mudie, E. Van Wagner, B.D. Freeman, D.J. Cookson, AlPO-18 membranes for CO_2/CH_4 separation, Chemical Communications. 48 (2012) 2310-2312.

[18]   K. Tanaka, H. Kita, K. Okamoto, A. Nakamura, Y. Kusuki, Gas Permeability and Permselectivity in Homo- and Copolyimides from 3,3′,4,4′-Biphenyltetracarboxylic Dianhydride and 3,3′- and 4,4′-Diaminodiphenylsulfones, Polymer Journal. 22 (1990) 381-385.

[19]   L. Marchese, J. Chen, J.M. Thomas, S. Coluccia, A. Zecchina, Bronsted, Lewis, and Redox Centers on CoAPO-18 Catalysts. 1. Vibrational Modes of Adsorbed Water, The Journal of Physical Chemistry. 98 (1994) 13350-13356.

[20] H. van Heyden, G. Munz, L. Schnabel, F. Schmidt, S. Mintova, T. Bein, Kinetics of water adsorption in microporous aluminophosphate layers for regenerative heat exchangers, Applied Thermal Engineering. 29 (2009) 1514-1522.

[21] A.M. Avila, H.H. Funke, Y. Zhang, J.L. Falconer, R.D. Noble, Concentration polarization in SAPO-34 membranes at high pressures, Journal of Membrane Science. 335 (2009) 32-36.

[22] G. He, Y. Mi, P. Lock Yue, G. Chen, Theoretical study on concentration polarization in gas separation membrane processes, Journal of Membrane Science. 153 (1999) 243-258.

[23] H. van Heyden, S. Mintova, T. Bein, AlPO-18 nanocrystals synthesized under microwave irradiation, Journal of Materials Chemistry. 16 (2006) 514-518.

[24] M. Vilaseca, S. Mintova, V. Valtchev, T.H. Metzger, T. Bein, Synthesis of colloidal AlPO4-18 crystals and their use for supported film growth, Journal of Materials Chemistry. 13 (2003) 1526-1528.

[25] M. Vilaseca, S. Mintova, K. Karaghiosoff, T.H. Metzger, T. Bein, AlPO4-18 synthesized from colloidal precursors and its use for the preparation of thin films, Applied Surface Science. 226 (2004) 1-6.

[26] L. Tosheva, E.-P. Ng, S. Mintova, M. Hölzl, T.H. Metzger, A.M. Doyle, $AlPO_4$-18 Seed Layers and Films by Secondary Growth, Chemistry of Materials. 20 (2008) 5721-5726.

[27] J.C. Poshusta, V.A. Tuan, J.L. Falconer, R.D. Noble, Synthesis and Permeation Properties of SAPO-34 Tubular Membranes, Industrial and Engineering Chemistry Research. 37 (1998) 3924-3929.

[28] S. Li, J.G. Martinek, J.L. Falconer, R.D. Noble, T.Q. Gardner, High-Pressure CO_2/CH_4 Separation Using SAPO-34 Membranes, Industrial and Engineering Chemistry Research. 44 (2005) 3220-3228.

[29] S. Li, J.L. Falconer, R.D. Noble, Improved SAPO-34 Membranes for CO_2/CH_4 Separations, Advanced Materials. 18 (2006) 2601-2603.

[30] Y. Hasegawa, C.Abe, T. Ikeda, K. Sato, Influence of change in the unit cell parameters on permeation properties of AEI-type zeolite membrane, Journal of

Membrane Science. 499 (2016) 538-543.

[31] R.A. Rakoczy, S. Ernst, M. Hartmann, Y. Traa, J. Weitkamp, Synthesis of large molecular sieve crystals with the AFI (AlPO4-5) topology, Catalysis Today. 49 (1999) 261-266.

[32] Y. Zheng, N. Hu, H. Wang, N. Bu, F. Zhang, R. Zhou, Preparation of steam-stable high-silica CHA (SSZ-13) membranes for CO_2/CH_4 and C_2H_4/C_2H_6 separation, Journal of Membrane Science. 475 (2015) 303-310.

Chapter 4 Preparation and Gas Permeation Properties of CHA Zeolite Membranes

4.1 Introduction

Natural gas processing requires that impurities such as CO_2 or N_2 be removed to obtain higher purity CH_4, since both N_2 and CO_2 decrease the heating value and CO_2 is corrosive in the presence of moisture. Carbon dioxide can be removed with amine scrubbers or polymer membranes, but at the high pressures typical of natural gas wells, operation of scrubbers is expensive and most polymer membranes plasticize and lose selectivity. Nitrogen is typically separated from natural gas by cryogenic distillation, which is an expensive and energy-intensive process. Recent developments for these separations include adsorbents such as carbon molecular sieves [1] and ion-exchanged clinoptilolite zeolite [2–4] for pressure swing adsorption [5]. Polymer membranes such as cellulose acetate have been used for CO_2 removal, but they are not sufficiently selective for N_2/CH_4 separations, and their fluxes are low.

Several zeolite membranes have been reported to separate CO_2/CH_4 mixtures, including T [6,7], DDR [8,9], MFI [10–13], Y [14–16], AlPO-18 [17], SSZ-13 [18], and SAPO-34 [19–21]. The SAPO-34 membranes had the highest permeances ($> 10^{-6}$ mol/(m^2 s Pa)), and their CO_2/CH_4 selectivities were as high as 100 at 4.6-MPa feed pressure. The SAPO-34 zeolite has the CHA structure, which is a 3-D pore system with ellipsoidal cages (0.67 nm x 1.0 nm) that are accessible via eight-membered ring windows (0.38-nm diameter). The pores in SAPO-34 are essentially the same size as the kinetic diameter of CH_4. Larger hydrocarbons such as propane and n-butane, which had kinetic diameters of 0.43 nm, also adsorb in SAPO-34, because these molecules have cross sections similar to methane and their chains are sufficiently flexible that they can enter the SAPO-34 pores [22]. Another zeolite with the CHA structure is SSZ-13, but it does not contain phosphorous, and it has a high Si/Al ratio. In the first report of SSZ-13 membranes for CO_2/CH_4 separations, the selectivity was only about 11 at a

permeance of ~2.0×10^{-7} mol/(m^2 s Pa) at 298 K and a feed pressure of 223 kPa [18]. These membranes were hydrothermally synthesized on the inside surface of porous stainless-steel tubes with 44% porosity and 4-μm diameter pores. Recently, SSZ-13 membranes prepared by secondary growth on the outside of porous mullite tubes were reported to have CO_2/CH_4 separation selectivities exceeding 200 [23], and this type membrane was used in the current study.

The separation of N_2/CH_4 mixtures using membranes has received less attention because the kinetic diameters of N_2 and CH_4 differ by less than 5% (0.364 nm for N_2, 0.38 nm for CH_4), and thus separation by size is difficult. In addition, both gases adsorb weakly, and thus adsorption-based selectivity is also low. Polymer membranes have low fluxes for these gases, and selectivities for CH_4 over N_2 in rubbery polymers is only around 5. Likewise, N_2/CH_4 selectivities for glassy polymer membranes are typically less than 3 [5]. Silica membranes have shown potential for removing N_2 with N_2/CH_4 selectivities exceeding 10, based on single-gas permeances [5], but to our knowledge N_2/CH_4 mixture permeances for these membranes have not been reported. Ion-exchanged ETS-4 membranes [24] were selective for N_2, with N_2/CH_4 selectivities of 5.4 at 308 K, but N_2 permeances were only ~10^{-8} mol/(m^2 s Pa). The N_2/CH_4 ideal selectivity of DDR3 membranes exceeded 25 at ambient temperature, but the measurements were carried out with a sweep gas on the permeate side, and mixture permeances were not reported [25].

In addition to CH_4, CO_2, and N_2, natural gas contains higher hydrocarbons (mainly ethane, propane, and n-butane), and these can affect membrane separations, even if their concentrations are only a few percent. Both propane and n-butane have been reported to slowly decrease permeances and selectivities over several days during CO_2/CH_4 separations on SAPO-34 membranes [26]. The original permeances and selectivities were recovered when the higher hydrocarbons were removed from the CO_2/CH_4feed. However, these membranes had permeances that were only about 10-20% of permeances reported for SAPO-34 membranes prepared more recently (different precursors were used to prepare these membranes), and thus the effect of these hydrocarbons on separations may be different [20].

In this paper, the effect of propane on CO_2/CH_4 and N_2/CH_4 separations was studied for both SAPO-34 and SSZ-13 membranes. The permeances were an order of magnitude higher for SAPO-34 membranes than for SSZ-13 membranes, probably because the SAPO-34 membranes were grown on the inside of porous alumina tubes with 100-nm pores, whereas the SSZ-13 membranes were grown on the outside of porous mullite tubes with 1.3-m pores [23]. The best SSZ-13 membrane had higher selectivities for CO_2/CH_4 separations (280 at 350 kPa feed pressure, 205 at 1.73-MPa feed pressure) and N_2/CH_4 separations (12 at 350-kPa feed pressure, 9 at 1.73-MPa feed pressure). The membranes had low concentrations of defects, and CO_2/i-butane separation selectivities greater than 500,000 were measured for one SAPO-34 membrane. Propane significantly decreased the N_2 permeance in both types of membranes, and it decreased the CO_2 permeance to a lesser extent in SAPO-34 membranes, likely because propane's heat of adsorption is similar to that of CO_2. The selectivities were much less affected by propane. For higher feed pressures, propane initially increased the CO_2 permeance and decreased the CH_4 permeance in SSZ-13 membranes, so that selectivities increased significantly. All permeances decreased over days in the presence of propane so that steady state was not achieved, and SAPO-34 membranes were affected more than SSZ-13 membranes; the effects were reversible in all cases.

4.2 Experimental

4.2.1 SAPO-34 membranes

Two SAPO-34 membranes were prepared as described previously [20] by secondary growth on the inside of seeded, porous Al_2O_3 tubes (1-cm O.D.). The SAPO-34 seed crystals were synthesized by microwave heating at 453 K for 7 h from a gel with the composition of 1 Al_2O_3: 1 P_2O_5: 0.6 SiO_2: 2TEAOH: 75 H_2O, where TEAOH is tetraethylammonium hydroxide. The SAPO-34 membrane synthesis was carried out at 493 K for 6 h using a gel composition of 0.85 Al_2O_3: 1 P_2O_5: 0.3 SiO_2: 2TEAOH: 155 H_2O. The template was removed from the membranes by calcination under vacuum

at 723 K for 6 h with heating and cooling rates of 1 K/min.

4.2.2 SSZ-13 seeds synthesis

The SSZ-13 seed crystals were synthesized using a procedure similar to that described by Yuen and Zones [27]. The molar composition of the gel was 1.0 SiO_2: 0.10 Na_2O: 0.025 Al_2O_3: 0.40 TMAdaOH: 44 H_2O, where TMAdaOH is N, N, N, trimethtyl-1-adamantammonium hydroxide. The gel was prepared by mixing NaOH, $Al(OH)_3$ and DI water and stirring the mixture at room temperature for 1 h to form a homogenous aluminate solution. Then water and template were slowly added to the solution over 15 min, and the solution was stirred for 1 h without heating. Finally, colloidal silica (Ludox TM-40, Sigma-Aldrich) was added to the solution, which was stirred for an additional 1 h, and the mixtures were aged overnight at room temperature while being stirred. The gel was transferred to a Teflon-lined autoclave and held in an oven at 433 K for 96 h. After synthesis, the SSZ-13 crystals were recovered by centrifugation, and they were washed three times in DI water and dried overnight at 373 K. The template was removed from the crystals in air at 823 K for 10 h with heating and cooling rates of 10 K/min.

4.2.3 SSZ-13 membranes

Six SSZ-13 membranes were prepared on the outside of porous mullite tubes (NIKKATO Company, 12-mm O.D., 1.3-µm average pore size) by secondary growth. Ten-cm long tubes were polished using 800# sandpaper and washed several times with boiling DI water for 30 min and dried overnight at 373 K. The outer surface of the tubes was coated with SSZ-13 crystals by rub-coating with a 10% seed/water slurry, and then placed in an autoclave containing 270 g of synthesis gel. The gel had a molar composition of 1.0 SiO_2: 0.1 Na_2O: 0.025 Al_2O_3: 0.05 TMAdaOH: 0.05 TEAOH: 80 H_2O. All the chemicals were purchased from Sigma-Aldrich. The gel was prepared by dissolving NaOH, $Al(OH)_3$, TMAdaOH (25%) and TEAOH (35%) in DI water and then adding colloidal silica (Ludox TM-40). The solution was stirred for 48 h at 333 K to obtain a uniform gel.

Hydrothermal synthesis was carried out in an oven at 443 K for 48 h. The resulting

membranes were washed under running tap water for 15 min, soaked in deionized water overnight, and then dried overnight at 373 K. The membranes were calcined in air at 753 K for 6 h with heating and cooling rates of 0.5 K/min. The calcined membranes were stored at 373 K prior to separation measurements.

4.2.4 Characterization

The crystal structures of SSZ-13 and SAPO-34 powders collected from the bottom of the autoclaves after membrane synthesis were confirmed by XRD (Scintag PAD-V XRD instrument with Cu Kα radiation). The crystal size and shape were determined by SEM (JEOL JSM-6400).

4.2.5 Gas permeation and separation measurements

Single-gas fluxes and mixture separations were measured in two flow systems described previously [28]. The feed flow rates were adjusted with electronic mass flow controllers. The feed pressure was either 270 kPa, 350 kPa or 1.73 MPa, and was controlled with back pressure regulators. The permeate pressure was maintained at 84 kPa (ambient pressure in Boulder, CO). No sweep gas was used. Fluxes were measured with bubble flow meters, and compositions were measured by a GC (HP 5890 or SRI 8610C) with a Hayesep D column and a TCD and a FID. An automated sample loop collected samples from the feed and permeate streams. The tubular membranes were sealed in a stainless-steel module with silicone or Viton O-rings. The module for the SSZ-13 membranes with the zeolite layer on the outside of the tube used two O-rings at each end. Because the O-rings were in direct contact with the SSZ-13 layer, the seals were probably not as good as the seals on the smooth glazing of the SAPO-34 membranes, which required only one O-ring at each end. Thus, extremely high selectivities were probably not attainable with the SSZ-13 membranes.

Teflon inserts were used to minimize concentration polarization in the module for the SAPO-34 membranes [28], but this could not be done for the SSZ-13 membranes, and thus concentration polarization decreased SSZ-13 selectivities when they were high and/or when separations were done at high pressures. Research grade CH_4, CO_2, and

N$_2$ were used. Either research grade propane was used, or instrument-grade propane was purified with activated carbon, Al$_2$O$_3$, and KMnO$_4$ to remove higher hydrocarbons, moisture, and unsaturated species. Propane (1, 5, or 9%) was added to the binary feed gases by either adding pure propane (for measurements at 270 and 350 kPa) or by feeding a mixture of propane with CO$_2$ or N$_2$ at the higher pressures.

Log-mean partial pressure differences were used to calculate permeances. Most of the separations were carried out at room temperature using equimolar mixtures of CO$_2$/CH$_4$ and N$_2$/CH$_4$, but CO$_2$/CH$_4$ separation was also carried out for a SSZ-13 membrane at temperatures from 298 to 473K. A dead-end system without sweep gas was used for single-gas flux measurements.

4.3 Results and discussion

4.3.1 Separations in SAPO-34 membranes

Selectivities and permeances for the SAPO-34 membranes were reported previously [20,21,29,30]. At room temperature and 275-kPa feed pressure, the CO$_2$/CH$_4$ separation selectivities were ~100 and the CO$_2$ permeances were ~1.5x10^{-6} mol/(m^2 s Pa). At room temperature and 4.6 MPa feed pressure, the CO$_2$/CH$_4$ separation selectivities remained near 100 for the best membranes, but the CO$_2$ permeances dropped to ~5x10^{-7} mol/(m^2 s Pa) because CO$_2$ approached saturation loading in the SAPO-34 pores at the high pressures. These membranes were also selective for N$_2$/CH$_4$ separations at room temperature, and the N$_2$/CH$_4$ selectivity was 5-7 for a feed pressure of 350 kPa. The N$_2$ permeance was ~1x10^{-7} mol/(m^2 s Pa), which is significantly lower than the CO$_2$ permeance because the larger N$_2$ has a lower diffusivity than CO$_2$, and N$_2$ also has a lower loading because it has a significantly lower heat of adsorption [19,31,32].

Carbon dioxide/i-butane separation selectivities were measured on similar membranes to identify the fraction of flow through defects larger than 0.50 nm. As reported previously, the CO$_2$/ibutane selectivities were 15,000-20,000 for an 80/20 CO$_2$/i-butane feed when silicone O-rings were used [21] and the feed pressure was 275

kPa. For another membrane, the CO_2/i-butane selectivities were about 20,000 with silicone O-rings, but CO_2/i-butane selectivities exceeded 500,000 when Viton O-rings were used. Apparently, i-butane dissolves in and diffuses through the silicone O-rings, and because the i-butane permeances through the membranes were so low, the permeance through the silicone O-rings dominated. These are much higher gas-phase separation selectivities than have been reported previously for zeolite membranes, and they demonstrate that SAPO-34 membranes can be prepared with extremely low concentrations of defects. Selectivities of 500,000 cannot be measured accurately because of the difficulty of sealing the membranes in the module and because concentration polarization cannot be eliminated for such selectivities.

4.3.2 Separations in SSZ-13 membranes

As shown in Table 4-1, the separation selectivities for both CO_2/CH_4 and N_2/CH_4 mixtures were higher for the six SSZ-13 membranes. The best membranes (SZ-1 and SZ-5) had a CO_2/CH_4 selectivity of about 280 at a feed pressure of 270 kPa. However, their CO_2 permeances ($1.8-2.1 \times 10^{-7}$ mol/(m^2 s Pa)) were only about 10% of SAPO-34 membranes permeances, most likely because the SSZ-13 layers were grown on the outside of supports with large pores (1.3 μm), whereas the SAPO-34 layers were on the inside of supports with much smaller pores (0.1 μm). As a result, SSZ-13 zeolite grew inside the support pores and formed a thicker separation layer (Figure 4-1). The CO_2 permeances are reproducible (Table 4-1), but the CH_4 permeances show more variation, likely because these small permeances are more sensitive to O-ring sealing and small defects.
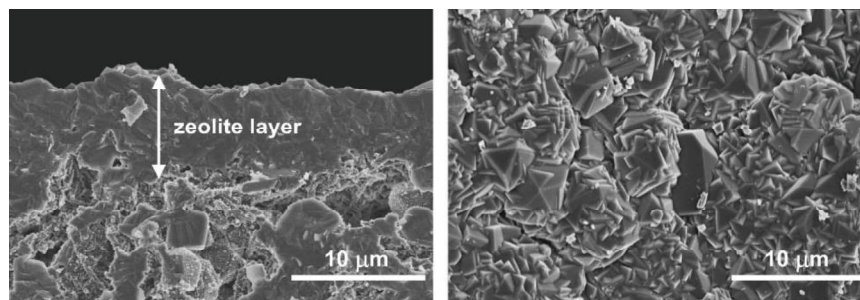
Figure 4-1 Scanning electron micrograph of a) cross section and b) top view of a SSZ-13 membrane on a porous tubular mullite support.

Table 4-1 Single-gas and mixture permeances and CO_2/CH_4 selectivities at 270-kPa feed pressure and 298 K for SSZ-13 membranes.

Membrane	Single-gas permeance [mol/(m² s Pa)]		Ideal selectivity	Mixtures permeance [mol/(m² s Pa)]		Separation selectivity
	$CO_2 \times 10^7$	$CH_4 \times 10^9$	CO_2/CH_4	$CO_2 \times 10^7$	$CH_4 \times 10^9$	CO_2/CH_4
SZ-1	2.2	1.4	156	2.1	0.77	280
SZ-2	2.2	3.4	66	2.6	2.7	95
SZ-3	2.1	2.0	110	2.2	1.4	155
SZ-4	2.0	2.2	92	2	1.6	125
SZ-5	1.8	1.2	152	1.8	0.63	276
SZ-6	2.1	2.5	85	2.1	1.6	136
Average	2.1±0.14	2.1±0.7	110±34	2.1±0.24	1.5±0.7	178±73

As shown in Table 4-1, the CO_2 single-gas permeances were close to their mixture permeances for the SSZ-13 membranes. However, the CH_4 mixture permeances were 21 to 47% lower than their single-gas permeances, and thus the mixture selectivities were on average 60% higher than the ideal selectivities, apparently because CO_2 preferentially adsorbs in the SSZ-13 pores because of its higher heat of adsorption.

The CO_2/i-butane separation selectivity was > 20,000 for SSZ-13 membrane SZ-1 and about 2,800 for membrane SZ-5, indicating that the concentration of defects larger than 0.50 nm was low for SSZ-13 membranes. These selectivities are for a feed pressure of 270 kPa and a 90% CO_2/10% ibutane feed and are probably lower limits because the O-rings are not expected to seal as well on the zeolite layer as on a smooth glazed layer. Moreover, because the SSZ-13 layer was on the outside of the support, concentration polarization could not be minimized as it was for the SAPO-34 membranes, where a Teflon support was inserted inside the tube [28]. At these high selectivities, concentration polarization is expected to be significant. The i-butane permeances were similar in mixtures with N_2 or CO_2, but because N_2 permeates slower than CO_2, the N_2/i-butane selectivity was only 1,400 for membrane SZ-1.

As shown in Table 4-1, the two membranes (SZ-1 and SZ-5) had similar CO_2/CH_4 separation selectivities at 270-kPa feed pressure, indicating that the CH_4 flux through defects that permeated ibutane did not contribute significantly to the total CH_4 flux. As the pressure increased, the CO_2/CH_4 separation selectivity for both membranes

decreased significantly (Figure 4-2) as the CO_2 permeance decreased and the CH_4 permeance increased. These measurements were carried out at a feed flow rate of 0.6 SLPM (standard L/min). The CO_2/CH_4 separation selectivities were 70 (SZ-1) and 73 (SZ-5) at 1.73-MPa feed pressure. These permeances were significantly affected by concentration polarization at high pressure [28], however, so that when the feed flow rate was increased from 0.6 to 4.0 SLPM for membrane SZ-1 at 1.73 MPa, the CO_2/CH_4 separation selectivity increased from 70 to 205. Thus, the selectivity was only 25% lower at the high feed pressure at high flow rates. The CO_2/CH_4 selectivity of membrane SZ-5, which had more defects based on its i-butane flux, increased to 122 when the feed flow rate increased to 4 SLPM. Thus, the CO_2/CH_4 selectivity at high pressure correlates with the defect concentration, as measured by the CO_2/i-butane selectivity. Indeed, defects are expected to have a bigger influence on selectivity at higher pressures.
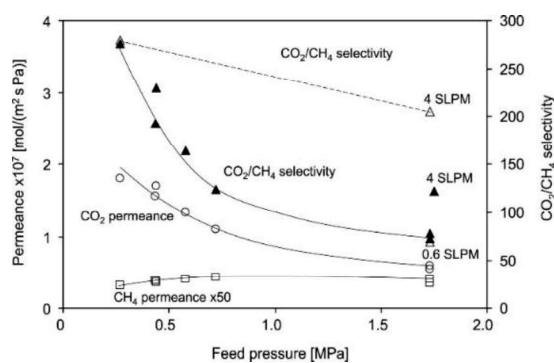
Figure 4-2 CO_2 and CH_4 permeances and CO_2/CH_4 separation selectivities for SSZ-13 membrane SZ-5 as a function of feed pressure at 293 K and CO_2/CH_4 selectivities of SSZ-13 membrane SZ-1 (open triangles). The feed flow rate was 0.6 SLPM except where noted.

The CO_2 permeance and the CO_2/CH_4 selectivity also decreased as the temperature increased for SSZ-13 membrane SZ-1 (Figure 4-3); the selectivity was 91 at 373 K and 35 at 473 K. These trends are similar to those reported previously for SAPO-34 membranes [19], but the selectivities are higher.
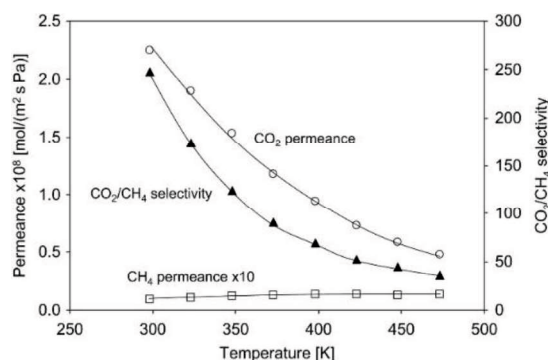
Figure 4-3 Carbon dioxide and CH_4 permeances and CO_2/CH_4 separation selectivities for SSZ-13 membrane SZ-1 as a function of temperature at 270-kPa feed pressure.

Table 4-2 Single-gas and mixture permeances and selectivities at 298 K for N_2 and CH_4 for SSZ-13 membranes at 270-kPa feed pressure.

Membrane	Single-gas permeance		Ideal selectivity	Mixtures permeance [mol/(m² s Pa)]		Separation selectivity
	$N_2 \times 10^8$	$CH_4 \times 10^9$	N_2/CH_4	$N_2 \times 10^8$	$CH_4 \times 10^9$	N_2/CH_4
SZ-1	2.2	1.4	16	1.8	1.4	13
SZ-2	1.1	3.4	3	1.3	2.9	4
SZ-3	2.3	2.0	12	2.3	2.4	9
SZ-4	2.1	2.2	10	2.0	2.3	9
SZ-5	1.6	1.2	13	1.2	1.1	11
SZ-6	2.5	2.5	10	2.4	2.9	8
Average	2±0.5	2.1±0.73	10.8±4	1.83±0.46	2.2±0.7	9±2.8

As observed for the SAPO-34 membranes, the N_2 permeances through the SSZ-13 membranes (1.8×10^{-8} mol/(m² s Pa) for membrane SZ-1 at 270-kPa feed pressure) were much lower than the CO_2 permeances for the same reasons. Thus, the N_2/CH_4 separation selectivities, which were 9-13 at 270 kPa for the best membranes (Table 4-2), were lower than the CO_2/CH_4 separation selectivities [33]. These selectivities are higher than the N_2/CH_4 selectivities for SAPO-34 membranes; those values did not exceed 7. The N_2/CH_4 ideal selectivities for the best membranes (SZ-1 and SZ-5) were about 20% higher than their mixture selectivities because CH_4 decreased the N_2 permeance, but N_2 did not affect the CH_4 permeance. At a feed pressure of 1.73 MPa, the N_2/CH_4 separation selectivity for SSZ-13 membrane SZ-1 was about 9 (Figure 4-4). Both the N_2 and CH_4 permeances increased with N2 feed concentration, but N_2 increased more than CH_4, probably because at higher N_2 loadings [33], CH_4 had less

effect on N_2 permeation.
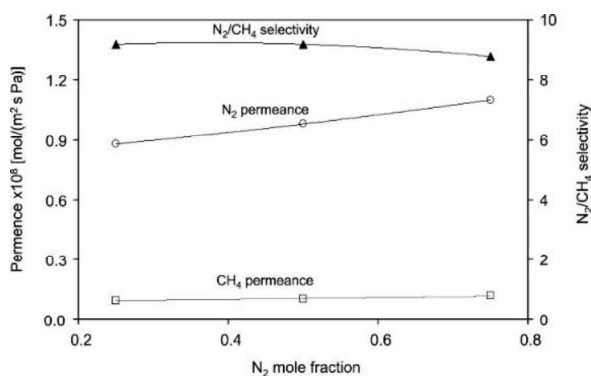
Figure 4-4: Nitrogen and CH_4 permeances and N_2/CH_4 separation selectivity at 293 K for SSZ-13 membrane SZ-1 as a function of N_2 mole fraction in the feed at a 1.73-MPa feed pressure.

4.3.3 Effect of propane on CO_2/CH_4 separations in SAPO-34 membranes

As shown in Figure 4-5, when 5% propane was added to the CO_2/CH_4 feed at 350-kPa pressure, the CO_2 permeance for SAPO-34 membrane SA-1 dropped by 14% immediately, and then it continued to decrease so that after 6 h, the CO_2 permeance had dropped 40%. The CO_2/CH_4 selectivity increased slightly when 5% propane was added to the feed, and even though the CO_2 permeance decreased with time, the CO_2/CH_4 selectivity remained constant at about 82. The propane permeance reached steady state almost immediately, and the initial CO_2/propane selectivity was 550; the CO_2/propane selectivity decreased with time as the CO_2 permeance decreased. The decrease in CO_2 permeance with time is probably due to propane slowly adsorbing in SAPO-34 pores [34]. The propane diffusivity is low in SAPO-34 pores, so it requires a long time to reach a steady-state loading, particularly in the presence of CO_2. Because the propane permeance was constant, most of the propane must permeate through defects, and the loading in the defects reached steady state quickly. The contribution of propane diffusion through the SAPO-34 pores to the propane flux was insignificant. When propane was removed from the feed, the membrane recovered its original permeances slowly, and the initial CO_2 permeance was only obtained in a reasonable time by heating the membrane to 473 K.
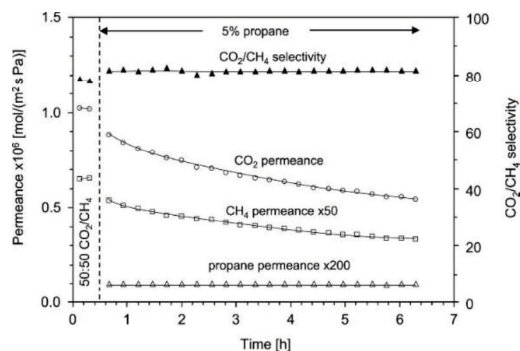
Figure 4-5 Carbon dioxide and CH4 permeances and CO_2/CH_4 separation selectivity at room temperature and 350-kPa feed pressure for SAPO-34 membrane SA-1 when 5% propane was added to the feed.

The slow decrease in CO_2 permeance in the presence of propane could be due to adsorption of a low-concentration impurity (unsaturated hydrocarbon, moisture) in the SAPO-34 pores, but only ethane was detected by GC in significant concentrations in the propane feed. Moreover, the decrease in CO_2 permeance was the same for both instrument-grade and research-grade propane. In addition, a purifier containing $KMnO_4$-impregnated Al_2O_3 beads, which should remove unsaturated hydrocarbon such as propylene, did not significantly change the permeation behavior. Thus, the slow decrease in CO_2 permeance with time was probably not the result of an impurity, but was due to slow adsorption of propane in the SAPO-34 pores.

4.3.4 Effect of ethane on CO_2/CH_4 separations in SAPO-34 membranes

When 5% ethane was added to a CO_2/CH_4 feed to SAPO-34 membrane SA-2 at a pressure of 350 kPa, the CO_2 and CH_4 permeances initially dropped, as shown in Figure 4-6. After few minutes, permeances increased to steady-state values that were about 14% lower than their original values and they remained stable for 3 h. This is in contrast to propane addition (Figure 4-5), which decreased CO_2 permeances by 35% over 3 h. When ethane was added, the CO_2 permeance decreased more than the CH_4 permeances so that the CO_2/CH_4 selectivity was 6% lower. Ethane has a lower heat of adsorption than propane in SAPO-34 [34], and thus affects the permeances less than propane. Ethane is also smaller than propane and thus should interfere less with the diffusion of other gases in the zeolite channels. Because the heat of adsorption of ethane is low, the

86

CO_2 permeances recovered about 97 % of their original values within a few minutes after ethane was removed from the feed, as shown in Figure 4-6.
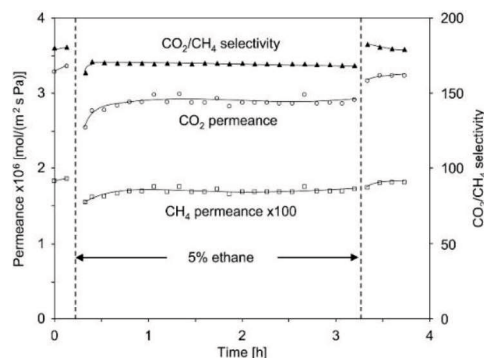
Figure 4-6 Carbon dioxide and CH_4 permeances and CO_2/CH_4 separation selectivity for SAPO-34 membrane SA-2 when 5% ethane was added to the feed at 350-kPa feed pressure.

4.3.5 Effect of propane on CO_2/CH_4 separations in SSZ-13 membranes

Propane affected CO_2/CH_4 separation significantly less in SSZ-13 membranes than in SAPO- 34 membranes. As shown in Figure 4-7 for a feed pressure of 350 kPa, the CO_2 permeance through SSZ-13 membrane SZ-1 initially dropped by 3% when 5% propane was added to the feed, and then it slowly decreased a total of ~13% over 2 days. The CH_4 permeance decreased 23% over the same time period, so the CO_2/CH_4 selectivity increased 13% when propane was added, and then it stabilized at ~250 for the next 2 days. The CO_2/propane selectivity was ~3,300 after two days. For membrane SZ- 5, the CO_2/propane selectivity was 1,600 with a CO_2 permeance of 1.6×10^{-7} mol/(m^2 s Pa) at 270-kPa feed pressure. The propane permeance was similar in mixtures with N_2 or CO_2, suggesting that the essentially all propane permeation is through defects, and thus propane permeance reached steady state quickly. Otherwise, the propane flux through SSZ-13 pores should be lower in mixtures with CO_2 because CO_2 competes better for adsorption sites. Propane adsorbs in the SSZ-13 pores [35,36] and decreases CO_2 and CH_4 permeances. Propane permeance through the SSZ-13 pores was apparently insignificant compared to its flux through the defects. When propane was removed from the feed, about 95% of the original CO_2 and CH_4 permeances and the CO_2/CH_4 selectivity were recovered in 6 h, and permeances slowly approached the initial values over about 2 days.
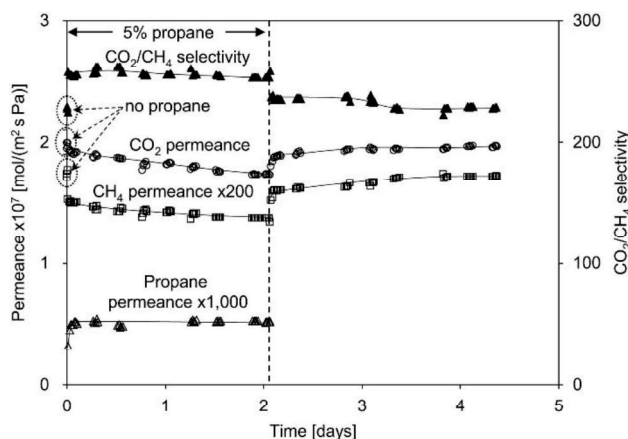
Figure 4-7 Carbon dioxide, methane, and propane permeances and CO_2/CH_4 separation selectivity at 293 K for SSZ-13 membrane SZ-1 in the presence of 5% propane at 350-kPa feed pressure.

In contrast to the behavior at a feed pressure of 350 kPa, adding propane to the CO_2/CH_4 feed at 1.73 MPa increased both selectivity and CO_2 permeance, as shown in Figure 4-8 for membrane SZ-5. Adding 5% propane initially increased the CO_2 permeance by ~10%; the CO_2 permeances then slowly decreased, but was still higher than its original value even after 4 days. In contrast to the CO_2 permeance, the CH_4 permeance slightly decreased when propane was added to the feed, and thus propane increased the CO_2/CH_4 selectivity by 15%. When propane was removed from the feed, the CO_2 permeance relatively quickly returned to its original value.
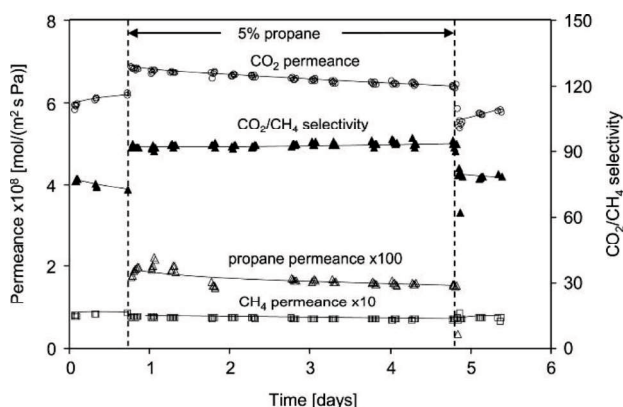
Figure 4-8 Carbon dioxide, methane, and propane permeances and CO_2/CH_4 separation selectivity at 293 K for SSZ-13 membrane SZ-5 in the presence of 5% propane at 1.73 MPa feed pressure.

Although the CO_2 permeance increased when propane was added, it was still lower

than the single-gas CO_2 permeance at 1.73-MPa feed pressure (7.7×10^{-8} mol/(m^2 s Pa)). The CH_4 mixture permeance was about 15% lower than its single-gas permeance (1×10^{-9} mol/(m^2 s Pa)), and it dropped an additional 15% in the presence of propane. The CO_2/CH_4 ideal selectivity at 1.73 MPa was 77, which is similar to the mixture selectivity without propane. However, the ideal selectivity was measured at twice the partial pressures of CO_2 and CH_4 in of the mixture, and the ideal selectivity is expected to be higher at lower pressures, where the CO_2 loading is further from saturation. The lower CO_2 permeance in the presence of CH_4 at 1.73 MPa probably results from concentration polarization since these measurements were made at a feed flow rate of 0.6 SLPM. When the flow rate at 1.73 MPa increased to 2 SLPM for CO_2/CH_4 mixtures, the selectivity increased by about 30%, and the CO_2 flux increased by ~20%. Similar flow-rate dependence has been observed for CO_2/CH_4 mixtures with SAPO-34 membranes at high pressure [28]. In contrast, the CO_2/CH_4 mixture selectivity for the SSZ- 13 membrane at low pressure (Table 4-1) was 80% higher than its ideal selectivity because preferential adsorption of CO_2 decreased the CH_4 permeance. As shown in Figure 4-9, propane affects CO_2 permeance and CO_2/CH_4 selectivity more as the feed pressure increases, but the decrease in CH_4 permeance is less sensitive to the pressure.
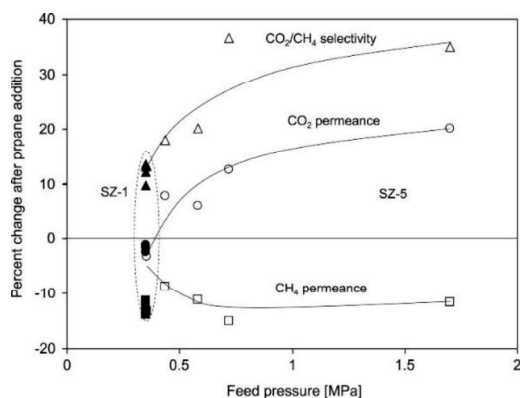
Figure 4-9 Percentage change in CO_2 and CH_4 permeances and CO_2/CH_4 separation selectivity after adding 5% propane to feed as a function of feed pressure (open symbols, SSZ-13 membrane SZ-5; closed symbols, SSZ-13 membrane SZ-1).

When a higher propane concentration (9%) was added to a CO_2/CH_4 feed at 1.73 MPa for SSZ- 13 membrane SZ-1, the CO_2 permeance increased more (16%), as shown in Figure 4-10, and then the CO_2 permeance decreased by 5% over the next 24 h. Thus,

the CO_2 permeance was still greater than its original value after 24 h. Similar to the behavior for 5% propane, the CH_4 permeance rapidly decreased by 20% when 9% propane was added to the feed, and then it slowly dropped over the next 24 h. Because CO_2 permeance increased and CH_4 permeance decreased, the CO_2/CH_4 selectivity increased by 40%, from 68 to 96, when 9% propane was added. The selectivity increased by another 6% over the next 24 h because the CH_4 permeance decreased faster than the CO_2 permeance. As observed for other separations, the propane permeance stabilized after the first measurement. The CO_2/propane selectivity was between 2,070 and 2,200.
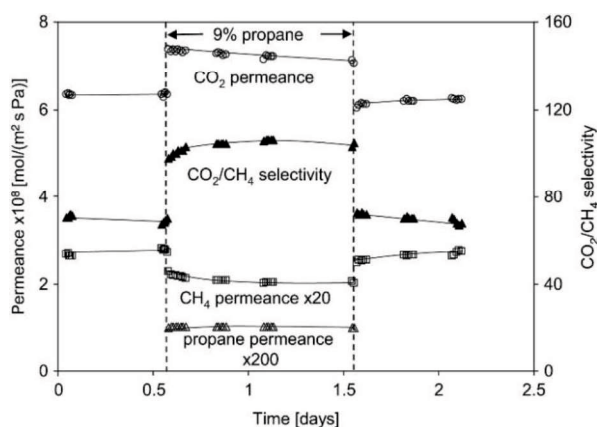
Figure 4-10 Carbon dioxide, CH_4, and propane permeances and CO_2/CH_4 separation selectivity at 293 K for SSZ-13 membrane SZ-1 in the presence of 9% propane at 1.73-MPa feed pressure.

The CO_2 permeance for a 95% CO_2/5% propane mixture decreased linearly with increased temperature, as shown in Figure 4-11, but the propane permeance remained nearly constant. As a result, the CO_2/propane selectivity decreased from about 5,500 at 295 K to 830 at 423K. Each data point in Figure 4-8 was obtained after a 1-h equilibration time, and fluxes changed less than 3% in 1 h. The temperature independence of the propane permeance also indicates that propane permeates through defects and the amount permeating through SSZ-13 pores is insignificant. The propane loading in the SSZ-13 pores decreases as temperature increases, as does the CO_2 loading. However, the activation energy for propane diffusivity in SSZ-13 pores is expected to be much larger than that for CO_2 or CH_4 since propane is so close in size to the SSZ-13 pores. Thus, the propane permeance in SSZ-13 pores might be expected

to increase with temperature; we cannot explain its temperature independence.

Propane may affect permeation more in SAPO-34 than SSZ-13 membranes because the heat of adsorption of propane is higher in SAPO-34 (24.6 kJ/mol) than in SSZ-13 (19.4 kJ/mol), whereas the heat of adsorption of CO_2 is similar in the two zeolites (SAPO-34, 25.5 kJ/mol; SSZ-13, 24 kJ/mol) [36,37]. Thus, CO_2 should better compete with propane for adsorption sites in SSZ-13 pores than in SAPO-34 pores.
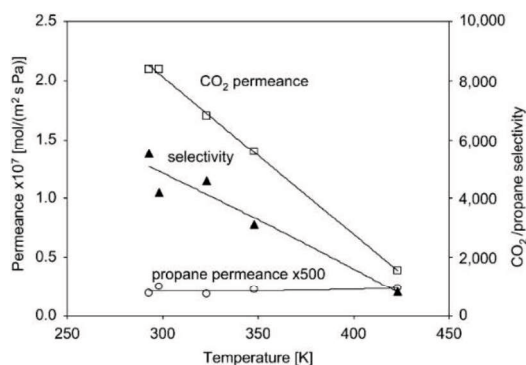
Figure 4-11 Carbon dioxide and propane permeances and CO_2/propane separation selectivity of a 95% CO_2/5% propane mixture for SSZ-13 membrane SZ-1 as a function of temperature at 350-kPa feed pressure.

Propane might increase the CO_2 permeance and decrease the CH_4 permeance at high pressure by deforming the 8-member ring windows in SSZ-13 from a circular to an elongated shape, similar to what Sastre et al. [38] observed with molecular dynamics when propane adsorbed in AFX and AEI zeolites. These zeolites also have 8-membrane ring windows. For the AFX zeolites, propane diffusivities decreased by 60-70% at 300 K as the propane loading increased, likely because one dimension of the windows narrowed as more propane adsorbed. The AEI zeolites only showed slight changes in diffusivity, even though the model also predicted significant distortions of their pore openings.

Adsorbate-induced distortion of the flexible zeolite structure and changes in diffusivities were observed previously for p-xylene in silicalite-1 zeolite. Ortho- and m-xylene did not adsorb in freshly prepared silicalite-1, but reached 50% loading in ~7 h after the sample was exposed to an adsorption/desorption cycle of para-xylene that apparently caused slight but permanent changes in the pore structure, even after all p-xylene was removed [39].

Nicolas et al. [40] reported that the CO_2/N_2 separation selectivity increased for an MFI membrane when propane was added; propane decreased the CO_2 permeance by about 60% but decreased the N_2 permeance more, so that the CO_2/N_2 selectivity increased from 3 to 5.5. As the temperature increased, the CO_2 and N_2 permeances increased and the selectivity decreased, likely because propane desorbed. They concluded that the selectivity increased because N_2 adsorption decreased more than CO_2 adsorption because CO_2 likely interacts more strongly with adsorbed propane.

4.3.6 Effect of propane on N_2/CH_4 separations in SSZ-13 membranes

In contrast to its effect on CO_2 permeances, propane decreased the N_2 permeance at all pressures studied, and in almost all cases it also decreased the N_2/CH_4 selectivity. Steady state was not reached in any of the N_2/CH_4 separation measurements in the presence of propane. When 5% propane was added to a N_2/CH_4 feed, N_2 permeance initially dropped by about 10%, and then continuously decreased so that the N_2 permeance was 44% lower after 7 days (Figure 4-12). The CH_4 permeance also decreased when propane was added, and after an initial decrease of 20%, the CH_4 permeance decreased proportionally less than the N_2 permeance so that the selectivity continuously decreased with time (from 13 to 11 over 7 days). The propane permeance stabilized over 24 h at a value 25% higher than in a mixture with CO_2 and CH_4 (Fig.4-7). Because CO_2 adsorbs more strongly than N_2, it competes better with propane for adsorption sites in the SSZ-13 pores. Thus, in the presence of CO_2, not much propane permeated through SSZ-13 pores, and the propane flux through defects stabilized quickly. For mixtures with N_2, some propane probably permeates through SSZ-13 pores and this permeation is slow so the propane permeation could take longer to stabilize. The additional permeation of propane through SSZ-13 pores in the presence of N_2 means that the total propane permeance is higher than in the presence of CO_2.
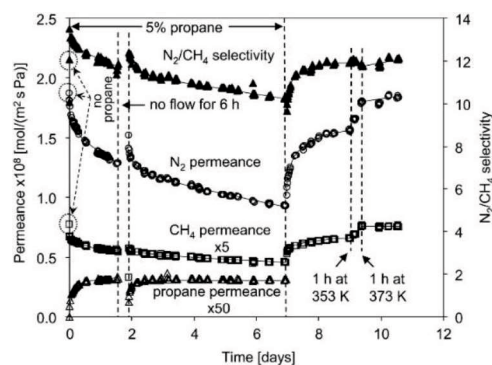
Figure 4-12 Nitrogen, methane, and propane permeances and N_2/CH_4 separation selectivity at 293 K in the presence of 5% propane for SSZ-13 membrane SZ-1 at 350-kPa feed pressure.

At 270 kPa, the N_2/propane separation selectivity was 254 for membrane SZ-1 and 100 for membrane SZ-5. The N_2 permeance slowly recovered when propane was removed from the feed, so that after 2 days, only 83% of the initial N_2 permeance was restored. Heating the membrane to 373 K for 1 h recovered the initial permeances, showing that the behavior was reversible.

In a separate experiment, when 5% propane was added to a N_2/CH_4 feed, N_2 and CH_4 permeances continuously decreased by 17% and 10%, respectively, over 1 day, and the N_2/CH_4 selectivity decreased by 8% (Figure 4-13). The propane permeances had not stabilized in 1 day. As shown in Figure 4-14 when propane was removed from the feed, the N_2 permeance increased to its initial value in 1 day and the propane GC peak for the permeate decreased in a similar time scale. Thus suggests that these propane peaks are mostly due to desorption from the SSZ-13 pores, and this propane hinders N_2 permeation.
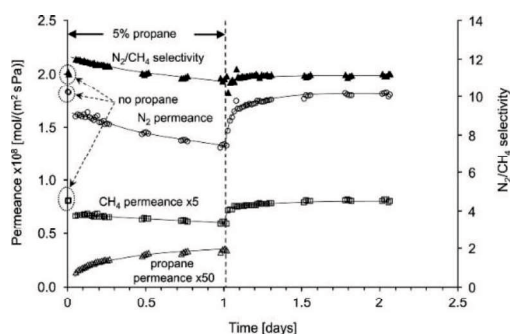
Figure 4-13 Nitrogen, methane, and propane permeances and N_2/CH_4 separation selectivity at 293 K for SSZ-13 membrane SZ-1 in the presence of 5% propane at 350-kPa feed pressure.
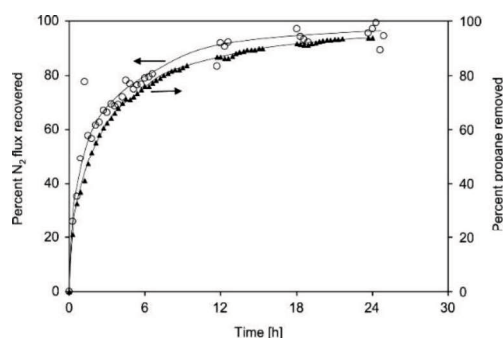
Figure 4-14 Percent of N_2 flux recovered (from Figure 4-13) and percent decrease in the propane concentration in the permeate after removing 5% propane from the feed for SSZ-13 membrane SZ-1 at 293 K and 350-kPa feed pressure.

At 1.73-MPa feed pressure, the behavior for N_2/CH_4 mixtures in the presence of propane was similar to that observed for the lower-pressure feed. As shown in Figure 4-15, adding 5% propane to the feed decreased the N_2 permeance by 36% and the CH_4 permeance by 6.5% after 2 days, so the selectivity decreased from 8 to 6. When the temperature was increased to 332 K, the permeance initially increased, but then decreased over 20 h. When propane was removed from the feed at 293 K, the N_2 permeance slowly recovered, but 90% of the original N_2 permeance was attained after 1 h when the temperature was increased to 373 K hour. Even 1% propane decreased the N_2 permeance by about 25% after 2 days of continuous flow at 1.73-MPa feed pressure, but selectivity was less affected, and permeances recovered slowly when propane was removed from the feed.
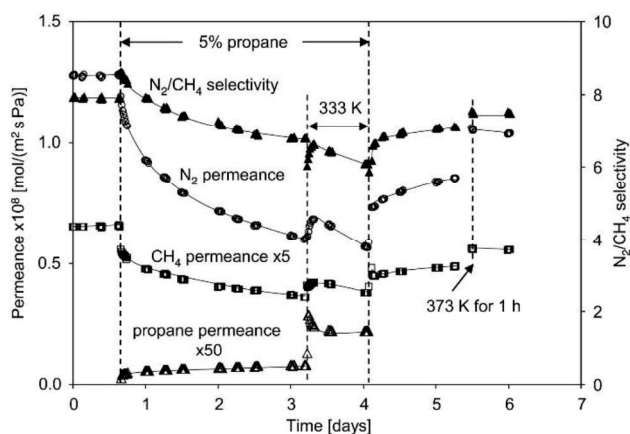
Figure 4-15 Permeances and N_2/CH_4 separation selectivity at 293 K for SSZ-13 membrane SZ-1 in the presence of 5% propane for 1.73-MPa feed pressure.

94

4.3.7 Implications for membrane applications

Both SAPO-34 and SSZ-13 zeolite membranes have low defect concentrations (based on CO_2/i-butane selectivities), and they have potential for CO_2/CH_4 and N_2/CH_4 separations at high pressures. The SSZ-13 membranes have higher CO_2/CH_4 and N_2/CH_4 selectivities but lower permeances than SAPO-34 membranes, which are prepared on supports with smaller pores and thus are thinner. Using a smaller-pore support to prepare SSZ-13 membranes would also likely yield higher permeances. In addition, SSZ-13 membranes are less affected by propane than SAPO-34 membranes, and thus they may have more potential for applications. The typical propane and n-butane concentrations in natural gas would have to be decreased for effective use of SAPO-34 membranes for either CO_2/CH_4 or N_2/CH_4 separation. The SSZ-13 membranes are more suitable for N_2/CH_4 separations, but removing propane is probably necessary for their use on a large scale. Moreover, at high pressure, propane improves CO_2/CH_4 separations, but some type of periodic regeneration, such as raising the temperature, would be necessary to limit how much the permeance decreased long term.

4.4 Conclusions

SSZ-13 and SAPO-34 membranes can be prepared with few defects larger than 0.5 nm, as indicated by the high CO_2/i-butane separation selectivities (> 500,000 for SAPO-34, 20,000 for SSZ-13). These high selectivities are likely lower limits because of concentration polarization and possible O-ring sealing problems. SSZ-13 membranes separate N_2/CH_4 mixtures with higher selectivities of 9-13 at low pressure. The highest N_2/CH_4 selectivity for SAPO-34 membranes was 7. SSZ-13 membranes separate CO_2/CH_4 mixtures with higher selectivities (> 200 at high pressure) than SAPO-34 membranes, but their permeances are only ~10% of the SAPO-34 membrane permeances because the SSZ-13 membranes are thicker. Propane continuously decreases CO_2 and N_2 permeances for both SSZ-13 and SAPO-34 membranes at low pressures, but permeances decreased ten times faster for SAPO-34 membranes. Propane only changed selectivities slightly but steady state was not reached even after seven

days. At high pressures, CO_2 permeances and CO_2/CH_4 selectivities initially increased for SSZ-13 membrane, and then CO_2 permeances decreased a few percent per day. For 9% propane in the feed, the CO_2/CH_4 selectivity initially increased 40%. Propane decreases N_2 permeance more than CO_2 permeance because CO_2 competes better for adsorption sites than N_2 in the zeolite pores because of its higher heat of adsorption. Propane adsorbs in SSZ-13 and SAPO-34 pores, but essentially all its permeance is through defects.

References

[1] M.W. Ackley, R.T. Yang, Kinetic separation by pressure swing adsorption: Method of characteristics model, AIChE Journal. 36 (1990) 1229-1238.

[2] M.W. Ackley, R.T. Yang, Diffusion in ion-exchanged clinoptilolites, AIChE Journal. 37 (1991) 1645-1656.

[3] A. Jayaraman, R.T. Yang, D. Chinn, C.L. Munson, Tailored clinoptilolites for nitrogen/methane separation, Industrial and Engineering Chemistry Research. 44 (2005) 5184-5192.

[4] E. Kouvelos, K. Kesore, T. Steriotis, H. Grigoropoulou, D. Bouloubasi, N. Theophilou, S. Tzintzos, N. Kanelopoulos, High pressure N_2/CH_4 adsorption measurements in clinoptilolites, Microporous and Mesoporous Materials. 99 (2007) 106-111.

[5] T.E. Rufford, S. Smart, G.C.Y. Watson, B.F. Graham, J. Boxall, J.C. Diniz da Costa, E.F. May, The removal of CO_2 and N_2 from natural gas: A review of conventional and emerging process technologies, Journal of Petroleum Science and Engineering. 94-95 (2012) 123-154.

[6] Y. Cui, H. Kita, K. I. Okamoto, Preparation and gas separation performance of zeolite T membrane, Journal of Materials Chemistry. 14 (2004) 924-932.

[7] S.M. Mirfendereski, T. Mazaheri, M. Sadrzadeh, T. Mohammadi, CO_2 and CH_4 permeation through T-type zeolite membranes: Effect of synthesis parameters and feed pressure, Separation and Purification Technology. 61 (2008) 317-323.

[8] T. Tomita, K. Nakayama, H. Sakai, Gas separation characteristics of DDR type zeolite membrane, Microporous and Mesoporous Materials. 68 (2004) 71-75.

[9] S. Himeno, T. Tomita, K. Suzuki, K. Nakayama, K. Yajima, S. Yoshida, Synthesis and permeation properties of a DDR-type zeolite membrane for separation of CO_2/CH_4 gaseous mixtures, Industrial and Engineering Chemistry Research. 46 (2007) 6989-6997.

[10] M.P. Bernal, J. Coronas, M. Menendez, J. Santamaria, Separation of CO_2/N_2 mixtures using MFI-type zeolite membranes, AIChE Journal. 50 (2004) 127–135.

[11] C.H. Nicolas, J. Sublet, Y. Schuurman, M. Pera-Titus, Role of adsorption and diffusion pathways on the CO_2/N_2 separation performance of nanocomposite B-MFI-alumina membranes, Chemical Engineering Science. 66 (2011) 6057-6068.

[12] J.C. Poshusta, R.D. Noble, J.L. Falconer, Temperature and pressure effects on CO_2 and CH_4 permeation through MFI zeolite membranes, Journal of Membrane Science. 160 (1999) 115-125.

[13] L. Sandström, E. Sjöberg, J. Hedlund, Very high flux MFI membrane for CO_2 separation, Journal of Membrane Science. 380 (2011) 232-240.

[14] X. Gu, J. Dong, T.M. Nenoff, Synthesis of defect-free FAU-type zeolite membranes and separation for dry and moist CO_2/N_2 mixtures, Industrial and Engineering Chemistry Research. 44 (2005) 937-944.

[15] J.C. White, P.K. Dutta, K. Shqau, H. Verweij, Synthesis of ultrathin zeolite Y membranes and their application for separation of carbon dioxide and nitrogen gases, Langmuir. 26 (2010) 10287-10293.

[16] Y. Hasegawa, T. Tanaka, K. Watanabe, B.H. Jeong, K. Kusakabe, S. Morooka, Separation of CO_2-CH_4 and CO_2-N_2 systems using ion-exchanged fau-type zeolite membranes with different Si/Al ratios, Korean Journal of Chemical Engineering. 19 (2002) 309-313.

[17] M.L. Carreon, S. Li, M.A. Carreon, AlPO-18 membranes for CO_2/CH_4 separation, Chemical Communications. 48 (2012) 2310-2312.

[18] H. Kalipcilar, T.C. Bowen, R.D. Noble, J.L. Falconer, Synthesis and Separation Performance of SSZ-13 Zeolite Membranes on Tubular Supports, Chemistry of Materials. 14 (2002) 3458-3464.

[19] S Li, J. L. Falconer, Richard D. Noble, SAPO-34 membranes for CO_2/CH_4 separation, Journal of Membrane Science. 241 (2004) 121-135.

[20] R. Zhou, E.W. Ping, H.H. Funke, J.L. Falconer, R.D. Noble, Improving SAPO-34 membrane synthesis, Journal of Membrane Science. 444 (2013) 384-393.

[21] H.H. Funke, M.Z. Chen, A.N. Prakash, J.L. Falconer, R.D. Noble, Separating molecules by size in SAPO-34 membranes, Journal of Membrane Science. 456 (2014) 185-191.

[22] K. Agarwal, M. John, S. Pai, B.L. Newalkar, R. Bhargava, N.V. Choudary, SAPO-34 assisted C_3 separation: Modeling and simulation, Microporous and Mesoporous Materials. 132 (2010) 311-318.

[23] Y. Zheng, N. Hu, H. Wang, N. Bu, F. Zhang, R. Zhou, Preparation of steam-stable high-silica CHA (SSZ-13) membranes for CO_2/CH_4 and C_2H_4/C_2H_6 separation, Journal of Membrane Science. 475 (2015) 303-310.

[24] G. Guan, K. Kusakabe, S. Morooka, Synthesis and permeation properties of ion-exchanged ETS-4 tubular membranes, Microporous and Mesoporous Materials. 50 (2001) 109-120.

[25] J. van den Bergh, W. Zhu, J. Gascon, J.A. Moulijn, F. Kapteijn, Separation and permeation characteristics of a DD3R zeolite membrane, Journal of Membrane Science. 316 (2008) 35-45.

[26] S. Li, G. Alvarado, R.D. Noble, J.L. Falconer, Effects of impurities on CO_2/CH_4 separations through SAPO-34 membranes, Journal of Membrane Science. 251 (2005) 59-66.

[27] E. Harry Robson and Karl Petter Lillerud, Eds., Verified synthesis of zeolitic materials, Elsevier, Amsterdam, P.121, 2001.

[28] A.M. Avila, H.H. Funke, Y. Zhang, J.L. Falconer, R.D. Noble, Concentration polarization in SAPO-34 membranes at high pressures, Journal of Membrane Science. 335 (2009) 32-36.

[29] J.C. Poshusta, V.A. Tuan, E.A. Pape, R.D. Noble, J.L. Falconer, Separation of light gas mixtures using SAPO-34 membranes, AIChE Journal. 46 (2000) 779-789.

[30] S. Li, J.L. Falconer, R.D. Noble, R. Krishna, Modeling permeation of CO_2/CH_4, CO_2/N_2, and N_2/CH_4 mixtures across SAPO-34 membrane with the Maxwell-Stefan equations, Industrial and Engineering Chemistry Research. 46 (2007) 3904-3911.

[31] M.E. Rivera-Ramos, A.J. Hernández-Maldonado, Adsorption of N_2 and CH_4 by ion-exchanged silicoaluminophosphate nanoporous sorbents: Interaction with monovalent, divalent, and trivalent cations, Industrial and Engineering Chemistry Research. 46 (2007) 4991-5002.

[32] M.E. Rivera-Ramos, G.J. Ruiz-Mercado, A.J. Hernández-Maldonado, Separation

of CO$_2$ from light gas mixtures using ion-exchanged silicoaluminophosphate nanoporous sorbents, Industrial and Engineering Chemistry Research. 47 (2008) 5602-5610.

[33] J. Tang, Y. Zhou, W. Su, X. L. Liu, Y. Sun, Synthesis of zeolite SSZ-13 for N$_2$ and CO$_2$ separation, Adsorption Science and Technology. 31 (2013) 549–558.

[34] J.F.M. Denayer, L.I. Devriese, S. Couck, J. Martens, R. Singh, P.A. Webley, G.V. Baron, Cage and window effects in the adsorption of n-alkanes on chabazite and SAPO-34, The Journal of Physical Chemistry C. 112 (2008) 16593-16599.

[35] D. Olson, Light hydrocarbon separation using 8-member ring zeolites, US Patent 6488741, 2002.

[36] H.H. Funke, M.Z. Chen, A.N. Prakash, J.L. Falconer, R.D. Noble, Separating molecules by size in SAPO-34 membranes, Journal of Membrane Science. 456 (2014) 185-191.

[37] J.Y. Kim, J. Kim, S.T. Yang, W.S. Ahn, Mesoporous SAPO-34 with amine-grafting for CO$_2$ capture, Fuel 108 (2013) 515–520.

[38] G. Sastre, Computational study of diffusion of propane in small pore acidic zeotypes AFX and AEI, Catalysis Today 226 (2014) 25-36.

[39] H. Karslı, A. Çulfa, H. Yücel, Sorption properties of silicalite-1 of pure silica form: The influence of sorption history on sorption kinetics of critically sized molecules, Zeolites 12 (1992) 728-732.

[40] C. Nicolas, M. Pera-Titus, Nanocomposite MFI-alumina hollow fiber membranes: Influence of NOx and propane on CO$_2$/N$_2$ separation properties, Industrial and Engineering Chemistry Research. 51 (2012) 10451-10461.

Chapter 5 Preparation and Gas Permeation Properties of PESU-based Mixed Matrix Membranes with CHA and AEI Zeolite Particles

5.1 Introduction

Membrane based gas separation processes have drawn an increasing attention for gas separation application [1–4] due to its energy cost saving, ease operating and low environmental impact. Polymer membranes [5–8], are attractive for air, H_2 and CO_2 separation because of its good mechanical strength, low operating cost and high flexibility, while, the trade-off between permeability and selectivity limited the further improvement for industrial gas separation. In comparison, inorganic membranes [9–13] exhibited both high permeability and selectivity for gas separation, but the poor reproducibility of inorganic membrane lead to problems for gas separation in industrial-scale. Therefore, the Mixed Matrix Membranes (MMMs), which was comprised by imbedding inorganic fillers into a polymeric matrix, as one of the alternative candidate to overcome those limitations between polymer and inorganic membranes in gas separation, acquired a lot of intensive researches in recent years [14–19]. Zornoza *et al.*[20] prepared the 6FDA polyimide based MMMs with Grignard functionalized mesoporous silica. Those membranes displayed the H_2/CH_4 separation selectivity of 21.8 with H_2 permeability of 794 Barrer, CO_2/N_2 separation selectivity of 24.4 with CO_2 permeability of 1214 Barrer, CO_2/CH_4 separation selectivity of 31.5 with CO_2 permeability of 1245 Barrer, and O_2/N_2 separation selectivity of 4.3 with O_2 permeability of 178 Barrer. These results indeed prove the gas permeation properties of the inorganic filler filled MMMs were improved compared with the pure polymer. MMMs as a hybrid material, which was not simply combined the processability of polymer and the superior permeability and selectivity of inorganic fillers [21]. In fact the performance of the MMMs was varied by many factors such as the suitable combination of the filler and the polymer matrix, the properties of the filler and the

interface between the polymer and the filler [14]. Thus, for making successful mixed matrix membrane, one of the key challenging is to choose the proper matrix and filler to meet the suitable combination, meanwhile, for a good polymer matrix, it should meet the demand with a commercially acceptable performance and still have a good flexible when membrane formation [22,23]. Polyethersulfone (PESU) [24] with a good glass transition temperature Tg (~215°C), good mechanical property, thermal, hydrolytic stability and good oxidative [25], as well as the low cost, shows a widely study in these years [26–28]. At the same time, CHA type and AEI type zeolite with the unique pore size ~0.38nm, good thermal and hydrothermal stability along with the different adsorption properties for different gases which showed excellent gas separation performances [29–33]. Both SAPO-34 zeolite and SSZ-13 zeolite have the chabazite structure. SAPO-34 zeolite was a Si-substituted aluminophosphates crystalline materials built of equimolar AlO_4^- and PO_4^+ tetrahedral units together with SiO_4 unit, while SSZ-13 zeolite was built without PO_4^+ tetrahedral units and showed high Si/Al ratio [34,35]. The difference in SAPO-34 and SSZ-13 structure may display different gas permeation properties in gas separation process.

In this work, both AEI type AlPO-18 and CHA type SAPO-34, SSZ-13 zeolites with different crystal sizes were prepared to fill in the PESU polymer for making mixed matrix membranes, and compared the different gas permeation proprieties of MMMs with different sizes zeolites. In the other hand, we also compared gas permeation of the MMMs with loading the same CHA structure zeolites (SAPO-34 and SSZ-13) with different crystals compositions.

5.2 Experimental

5.2.1 Zeolite synthesis

5.2.1.1 CHA type zeolites

Three SAPO-34 zeolites were made by using different gel compositions as described in Table 5-1, and details of the synthesis procedures were described in

Chapter 2. The synthesis details of SSZ-13 crystal also described in Chapter 2.

Table 5-1. Synthesis conditions of SAPO-34 zeolites.

Zeolite	Gel composition	Syn. Cond.
SAPO-34-1	$1Al_2O_3:2P_2O_5:0.6SiO_2:4TEAOH:75H_2O$	453K, 4h
SAPO-34-2	$1Al_2O_3:1P_2O_5:0.6SiO_2:1.5TEAOH:0.5DIPEA:75H_2O$	473K, 12h
SAPO-34-3	$1Al_2O_3:1P_2O_5:0.6SiO_2:1.5TEAOH:0.5DIPEA:75H_2O$ (Added 0.2% SAPO-34-2)	473K, 12h

5.2.1.2 AEI type zeolites

Three AlPO-18 zeolites were made by using different gel compositions as described in Table 5-2, details of the synthesis procedures were also described in Chapter 2

Table 5-2 Synthesis conditions of SAPO-34 zeolites.

Zeolite	Gel composition	Syn. Cond.
AlPO-18-1	$1Al_2O_3:3.16P_2O_5:6.32TEAOH:186H_2O$	423K, 20h
AlPO-18-2	$1Al_2O_3:1P_2O5:1.8TEAOH:60H_2O:2IPA$	423K, 20h
AlPO-18-3	$1Al_2O_3:1P_2O5:1.8TEAOH:60H_2O$	423K, 20h

5.2.2 Membrane preparation

5.2.2.1 Neat PESU membrane fabrication

The neat PESU membrane was produced by adding 15 wt.% commercially polyethersulfone (PESU, BASF Chemical CO., Germany) into N-Methyl-2-pyrrolidone (NMP) solution (99.13%, Wako) at 80°C and stirred for 4h to dissolve it, then stirred at R.T overnight, then put into ultrasonic machine for more 4h before being cast onto glass board with the glass rod of 50-70μm thickness. The casted films were then dried for 2 h at 80°C under vacuum to remove most solvent, and finally heated the films at 200°C under vacuum for 20 h until the membrane became hard.

5.2.2.2 Mixed matrix membrane fabrication

PESU based mixed matrix membranes (MMMs) were fabricated by loading 20-30 wt.% SAPO-34, SSZ-13 and AlPO-18 zeolites into PESU. The zeolites were dried in a

vacuum oven at 200°C for 24h to remove all the moisture and adsorbed stuff. Afterwards, the particles were dispersed in N-Methyl-2-pyrrolidone (NMP) solution (99.13%, Wako) stirred for 1h and ultrasonicated for 4h to get fully dispersion. Next, added the PESU (BASF Chemical CO., Germany) into the resulting dispersion at 80°C to dissolve it and stirred for another 4h, then the resulting polymer/zeolites mixtures were mixed together at R.T for 12h and ultrasonicated for more 4h before being cast onto glass board with the glass rod of 50-70μm thickness. The casted films were then dried for 2 h at 80°C under vacuum to remove most solvent, and finally heated the films at 200°C under vacuum for 20 h until the membrane became hard.

5.2.3 Characterization

The morphology of as-synthesized zeolites and the compatibility of these mixed matrix membrane that between the zeolite filler and PESU matrix were determined by a field emission scanning electron microscope (FE-SEM, JEOL JSM 6335F) at an acceleration voltage of 5KV. The crystallinity of the neat PESU membrane and PESU based mixed matrix membranes along with the as-synthesized crystals phase were identified by X-ray diffraction (XRD, SHIMADZU XRD-6100) using a Shimadzu XD-3 diffractometer with Cu-Ka radiation at a scanning range of 2θ =5~45° and a scanning rate of 4°/min.

5.2.4 Gas permeation

Single gas permeation of He, H_2, CO_2, O_2, N_2, CH_4 six gases were measured by means of vacuum method with a fixed volume pressure gauge [36] using a time-lag method [37]. The membranes were performed at 35°C with a feed pressure of 0.3MPa using an apparatus as described by Cui et al [10] and illustrated in Figure 5-1. Before permeation measurement, membranes were degassed in the gas permeation apparatus system under vacuum at 353K for 3h. Area of membranes were fixed to 18.86cm^2. The solution-diffusion theory was used to describe the mixed matrix membrane permeation, For a particular penetrant i, the permeability coefficient (P_i) was calculated from the penetrant diffusion coefficient (D_i) and the solubility coefficient (S_i), the permeability

coefficient (P_i) was represented in Barrer (1 Barrer $=10^{-10}$ [cm^3(STP) cm]/(cm^2 s cmHg)), which was defined as follow:

$P_i = D_i \cdot S_i$

The permeability coefficient P_i and the time-lag θ were directly measured by the time-lag method under vacuum, while the diffusion coefficient D_i was estimated by the time-lag θ and the thickness of the film (l):

$D_i = l^2/(6\theta)$

Meanwhile, the permselectivity (α_{AB}) of the mixed matrix membrane, as to say, the ability of separating specie A form specie B, was calculated as follow:

$\alpha_{AB} = P_A/P_B$

As the permeability coefficient P_i describe in Eq. (1), so the permselectivity (α_{AB}) can be written as:

$\alpha_{AB} = (D_A/D_B)/(S_A/S_B) = \alpha^D_{AB} \, \alpha^S_{AB}$

Therefore, the diffusion coefficient (D_i) and the solubility coefficient (S_i) altogether determined the quality of the MMMs.
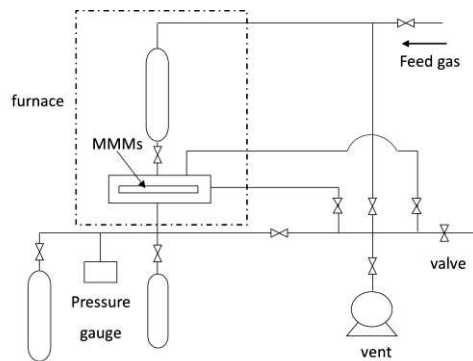
Figure 5-1 Schematic diagram of gas permeation apparatus with vacuum method.

5.3 Results and discussion

A plenty of researches on the gas separation through mixed matrix membranes already concluded that the gas separation performance of MMMs was not only affected by the simple properties of the filler and the polymer itself, but the quite good combination of the polymer and the filler [14,38,39]. And the MMMs with loading sub-

micron range zeolite would enhance the interface contact between polymer and the filler and provide more interfacial area [39]. For this purpose, we systematically investigated the gas permeation properties of PESU-SP-34 MMMs, PESU-SSZ-13 MMMs and PESU-AP-18 MMMs.

5.3.1 Zeolite characterization

The properties of adopted, SAPO-34, SSZ-13 and AlPO-18 zeolites are shown in Table 5-3. The corresponding morphologies of the SAPO-34, AlPO-18 and SSZ-13 zeolites were characterized by SEM as shown in Figure 5-2 and Figure 5-3, respectively.

Table 5-3 Properties of CHA type and AEI type zeolites.

Zeolite	Synthesis condition	Crystal shape	Size (nm)
SAPO-34 zeolite			
SAPO-34-1	453K, 4h	spherical	~100
SAPO-34-2	473K, 12h	spherical + cubic	~100-500
SAPO-34-3	473K, 12h	spherical	~200
SSZ-13 zeolite			
SSZ-13	423K, 6d	cubic	~400
AlPO-18 zeolite			
AlPO-18-1	423K, 20h	Sheet-like	300
AlPO-18-2	423K, 20h	-	300-500
AlPO-18-3	423K, 20h	Sheet-like	500-700
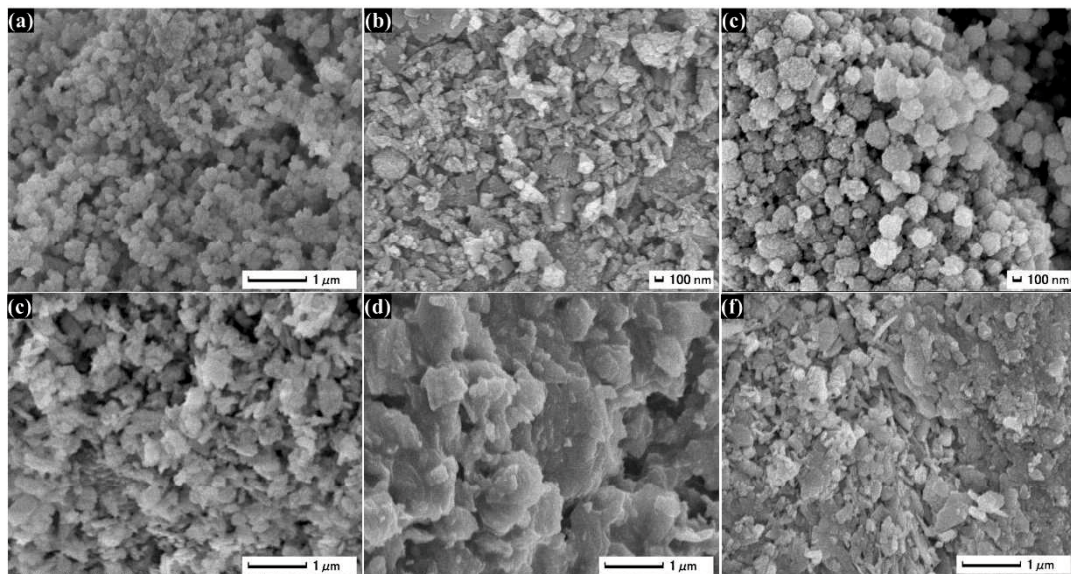
Figure 5-2 The SEM images of SAPO-34 zeolites (a) SAPO-34-1, (b) SAPO-34-2, (c) SAPO-34-2, and AlPO-18 zeolites (d) AlPO-18-1, (e) AlPO-18-2, (f) AlPO-18-3.

Three SAPO-34 zeolites with the crystals sizes range from 100nm to 500nm and three AlPO-18 zeolites with the crystals sizes range from 300nm to 700nm were confirmed from Figure 5-2. Meanwhile, cubic SSZ-13 zeolite with crystals size of ~400nm is confirmed by SEM as shown in Figure 5-3.
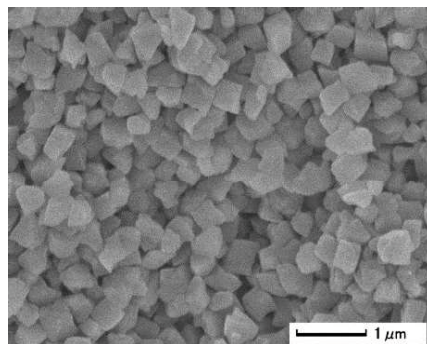
Figure 5-3 The SEM image of SSZ-13 zeolite.

5.3.2 Membrane characterization

Mixed matrix membranes (MMMs) obtained with loading 40 wt.% SAPO-34, SSZ-13 and AlPO-18 zeolites turned to rigidification and were broken before or during test. Then the effective PESU-SP-34 (-SSZ-13 and -AlPO-18) mixed matrix membranes only with adding 20 wt.% and 30 wt.% SAPO-34 (SSZ-13 and AlPO-18). The corresponding XRD patterns of fabricated MMMs were displayed in Figure 5-4, as shown in Figure 5-4, the neat PESU membrane with a broad peak of 2θ ranges from 15° to 22.5° due to the amorphous structure, and the amorphous peak become weaker after loading both CHA-type SAPO-34, SSZ-13 and AEI-type AlPO-18 zeolites. But even after increasing SAPO-34 and SSZ-13 zeolites up to 30 wt.% (Figure 5-4a) and loading AlPO-18 zeolites up to 40 wt.% (Figure 5-4b), the peak of the neat PESU membrane was still existed. And these SAPO-34 filled MMMs show much weaker zeolite peaks compared with the zeolite itself (as seen in Chapter 2), and the XRD patterns with loading 20 wt.% and 30 wt.% showed almost similar zeolite peak intensity for loading with SAPO-34 crystals, which may be result from the aggregation and may result in the similar gas separation performance for the MMMs with different zeolite loadings. And compared with the SSZ-13 zeolite based Mixed Matrix Membrane, the MMMs showed the highest zeolite peak intensity among these MMMs and the

intensities are increased when increasing the loading from 20 wt.% to 30 wt.%. This may be result from the different physical properties [18] of the silicoaluminophosphates type and aluminosilicate type CHA zeolites, which at last resulted in the different compatibility among these mixed matrix membranes. For loading AlPO-18 zeolites, the intensities of the crystals are also increased.
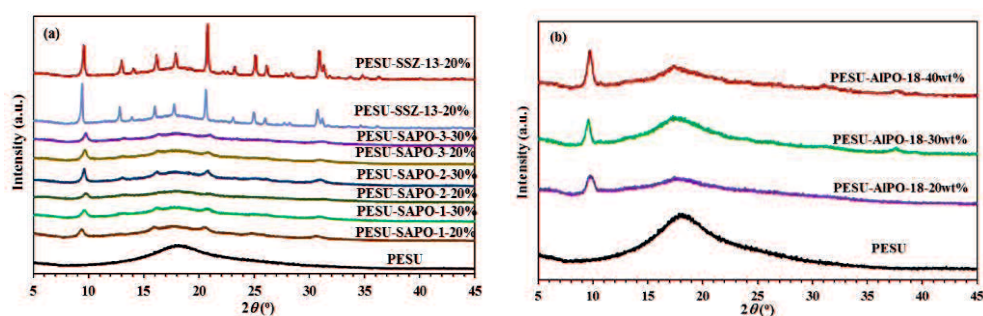
Figure 5-4 The XRD patterns of PESU-based Mixed Matrix Membranes (MMMs). (a) PESU-CHA MMMs, (b)PESU-AEI MMMs.

5.3.3 Gas permeation properties of Mixed Matrix Membranes (MMMs)

Loading with different zeolites will lead to differences among the MMMs because of the different behavior [40] among the SAPO-34, SSZ-13 and AlPO-18 zeolites.

5.3.3.1 Gas permeation properties of CHA zeolites filled mixed matrix membranes

The single gas permeability of PESU/SAPO-34 (SSZ-13) mixed matrix membranes were summarized in Table 5-4 and plotted in Figure 5-5. The single gas permeability of all these 6 gases increased after loading both all three SAPO-34 and SSZ-13 zeolites into the PESU polymer. From the Figure 5-5, it's obvious to notice that the single gas permeability followed the order of H_2 (2.89 Å) > CO_2 (3.3 Å) > O_2 (3.46 Å) > N_2 (3.64 Å) > CH_4 (3.8 Å) of all these MMMs except for PESU-SP-1. For the MMMs with loading smaller and homogeneous nano-sized SAPO-34-1, these 6 gases single gas permeability increased ~2 times (Table 5-4) compared with the pure PESU membrane. The average of H_2 permeability increased ~136% and CO_2 permeability increased ~113%, while the average of N_2 permeability increased ~600% and CH_4 permeability increased more than 700%. The CH_4 single gas permeability was a little

higher than the N_2 single gas permeability. It may account for the interface void defects from the incompatibility between the filler and the polymer matrix. lead the CH_4 molecular go through the non-selective and less resistant by-pass without going through the pores with the zeolites [14]. And for the heterogeneous SAPO-34-2 zeolite filled MMMs, as with the bigger and different size ranges zeolite filled into the PESU polymer, the PESU-SP-2 MMMs showed the highest single gas permeability among all this SAPO-34 filled mixed matrix membranes except for PESU-SP-1. For the PESU-SP-3 membranes, which showed the lowest single gas permeability among all these CHA-type zeolites filled mixed matrix membranes, but still increased the H_2 single gas permeability from 14 barrer to 18 barrer and CO_2 single gas permeability from 6.8 barrer to 8.2 barrer with 20 wt.% loading.

Table 5-4 Single gas permeability of PESU/CHA MMMs.

Membrane	Permeability [Barrer]					
	He	H_2	CO_2	O_2	N_2	CH_4
PESU-SP-1 (20 wt.%)	38	39	17	4.0	1.7	2.0
PESU-SP-1 (20 wt.%)-2	25	27	12	2.7	1.1	1.2
PESU-SP-2 (20 wt.%)	25	26	13	2.3	0.39	0.33
PESU-SP-2 (30 wt.%)	34	37	20	3.6	0.64	0.54
PESU-SP-3 (20 wt.%)	19	18	8.2	1.6	0.24	0.19
PESU-SP-3 (30 wt.%)	21	20	8.9	1.6	0.26	0.19
PESU-SSZ-13 (20 wt.%)	26	27	13	2.2	0.35	0.30
PESU-SSZ-13 (30 wt.%)	33	34	16	2.7	0.47	0.41
PESU	13	14	6.8	1.2	0.20	0.18
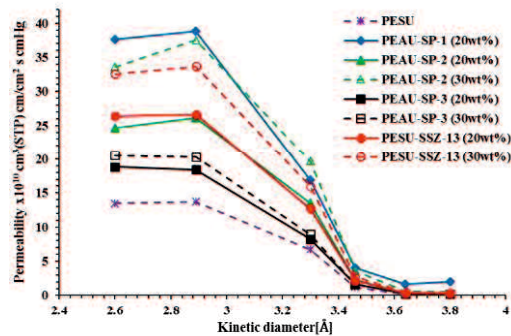
Figure 5-5 The Single gas permeability of PESU/SAPO-34 (SSZ-13) Mixed Matrix Membranes as a function of gas kinetic diameter.

Table 5-5 shows the ideal selectivity of all these SAPO-34 (SSZ-13) filled mixed

matrix membranes, for SAPO-34-1 filled MMMs, since it displayed the highest single gas permeability of all six gases among all these MMMs, while it showed much lower ideal selectivity for all gases, even lower than the neat PESU polymer. The bad incompatibility that increased the single gas permeability and decreased the ideal selectivity. The MMM with loading heterogeneous SAPO-34-2 increased both H_2 and CO_2 single gas permeability and improved ideal selectivity of H_2/CH_4 and CO_2/CH_4, and filling the homogeneous SAPO-34-3 into the PESU polymer showed the highest ideal selectivity of H_2/CH_4 and CO_2/CH_4 but a little lower single gas permeability for H_2 and CO_2. And with SSZ-13 zeolite, with 20 wt.% loading, it shows similar ideal selectivity as with SAPO-34-3 zeolite but with better single gas permeability. Meanwhile, for both SAPO-34 and SSZ-13 zeolites filled membranes, it's obvious to notice single gas permeabilities of the measured 6 gases increased as increasing the zeolite loading from 20 wt.% to 30 wt.%. And compared with the two types CHA structure filled mixed matrix membranes, the SSZ-13 filled MMMs shows a little higher single gas permeability and maintains the ideal selectivity. At the same time, we also can learn that loading zeolite into PESU can improve the single gas permeability from the Figure 5-6.

Table 5-5 The ideal selectivity of PESU/CHA MMMs.

Membrane	Ideal selectivity α[-]					
	H_2/N_2	H_2/CH_4	CO_2/CH_4	O_2/N_2	CO_2/N_2	H_2/O_2
PESU-SP-1 (20 wt.%)	23	20	8.5	2.4	10	10
PESU-SP-1 (20 wt.%)-2	25	22	9.3	2.6	11	9.9
PESU-SP-2 (20 wt.%)	67	78	40	5.9	34	11
PESU-SP-2 (30 wt.%)	59	70	37	5.6	31	10
PESU-SP-3 (20 wt.%)	77	95	43	6.8	35	11
PESU-SP-3 (30 wt.%)	78	110	48	6.3	34	12
PESU-SSZ-13 (20 wt.%)	77	88	42	6.2	37	12
PESU-SSZ-13 (30 wt.%)	72	82	39	5.8	34	12
PESU	69	77	38	6.2	34	11

Figure 5-6 shows the gas permeability of MMMs compared with neat PESU membrane. It's obvious loading zeolite into PESU polymer increased all the single gas permeability. Both the permeability and ideal selectivity were increased for loading

both SAPO-34-3 and SSZ-13 zeolites from 20 wt.% to 30 wt.%. And it's obvious that the MMMs with loading SAPO-34-1dramatically decreased the ideal selectivity since it improves the gas permeability, this may result from defects that formed in the PESU-SP-1 MMMs.
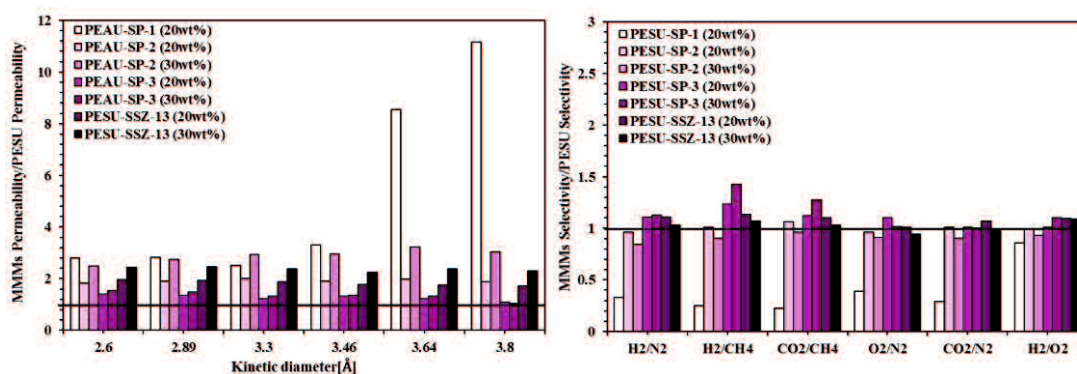
Figure 5-6 Permeability(left) and selectivity (right) of mixed matrix membranes compared with neat PESU membrane.

As the connection between polymer and the filler strongly affected the gas permeation properties, in order to confirm the differences between these MMMs, the cross sectional of these dense films SEM images with 20 wt.% zeolites loading were shown in Figure 5-7. For the SAPO-34 zeolites filled MMMs, the images of Figure 5-7a and Figure 5-7b, corresponding to the smallest SAPO-34-1 filled membrane, it's clearly to notice the big agglomeration among these SAPO-34-1 zeolites which formed a big void at the interface, finally strongly affect the gas permeation properties. The SEM images of PESU-SP-2 were shown in Figure 5-7c and Figure 5-7d, because of the heterogeneous particle distribution and the agglomeration in some degree [41], here we still can see some voids between the interfaces. For PESU-SP-3 (Figure 5-7e and Figure 5-7f), because of the small enough crystals size of SAPO-34-3 particles, since it still aggregates, however the aggregated crystals almost inserted into the polymer, which shows good gas permeation properties, and compared with this three SAPO-34 filled MMMs, as the better compatibility as shown in Figure 5-7g and Figure 5-7h for PESU-SSZ-13 MMMs, which also leads to good gas permeation properties.

Meanwhile, cross sectional of these dense MMMs films SEM images with 30 wt.% zeolites loading were shown in Figure 5-8. Compared with 20 wt.%, for the MMMs with loaded SAPO-34-1 and SAPO-34-2, the agglomeration become more sever, lead

to more defects such as more voids [14,39], which in verse, decreased the ideal selectivity and improved the permeability. By filling 30 wt.% SAPO-34-3 zeolites into the PESU polymer, due to the homogeneous crystals size, the crystals can insert into the polymer evenly, which improved both gas permeability and selectivity. While for the MMMs loaded with SSZ-13 crystals, since the crystals can distribute well, due to the bigger crystal sizes, it may improve the gas permeability while reduce the selectivity.
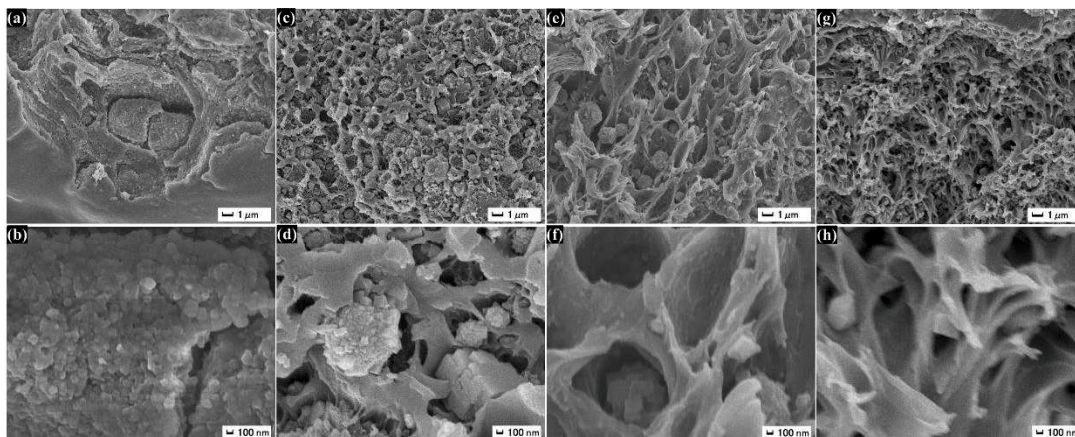
Figure 5-7 SEM images of Mixed matrix membranes with loading 20 wt.% zeolites, (a) and (b): PESU-SP-1; (c) and (d): PESU-SP-2; (e) and (f): PESU-SP-3, (g) and (h): PESU-SSZ-13.
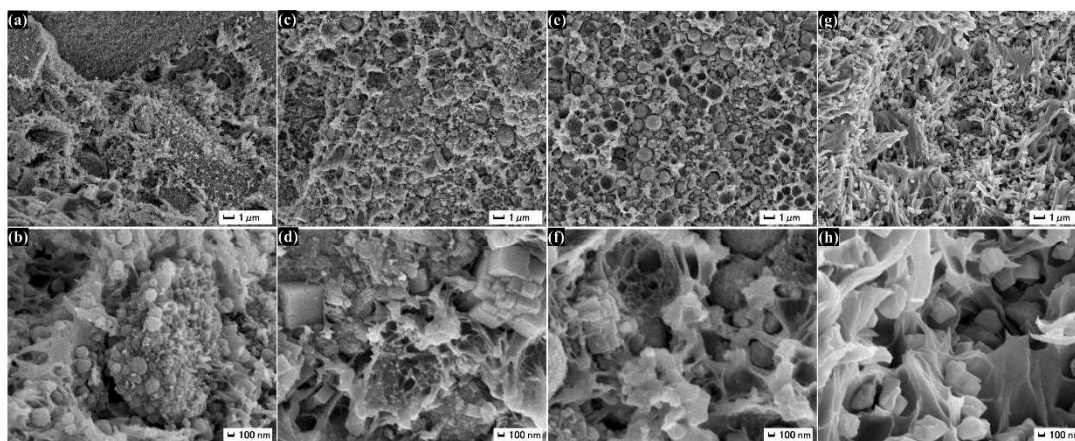
Figure 5-8 SEM images of Mixed matrix membranes with loading 30 wt.% zeolites, (a) and (b): PESU-SP-1; (c) and (d): PESU-SP-2; (e) and (f): PESU-SP-3, (g) and (h): PESU-SSZ-13.

Meanwhile, we also compared the difference of these MMMs in permeability, solubility and diffusion coefficient, which summarized in Table 5-6 and Table 5-7, respectively. It's clearly to see the MMMs loaded with SAPO-34 crystals show similar gas solubility for PESU-SP-2 MMMs and PESU-SP-3 MMMs. For PESU-SP-1 MMMs, the gas solubilities were lower and diffuse so quick (Table 5-6) may result from the bad

connection between the polymer and the crystals (Figure 5-7a and b). Since the degree of the compatibility is severe for PESU-SP-2 MMMs, it shows higher diffusion than PESU-SP-3 MMMs. For SSZ-13 loaded PESU-SSZ-13 MMMs, here we showed the same phenomenon as Luo *et al.*[42] description, the membrane shows much higher (~2 times) gas solubility than the same structure SAPO-34 in Table 5-6, while the PESU-SSZ-13 membranes also displayed higher gas diffusion performance, which at last performed the similar ideal selectivity with PESU-SP-34 membranes.

Table 5-6 The correlation of Permeability, Solubility and Diffusion of PESU/CHA MMMs.

Membrane	Permeability (P) $[10^{-10}cm^3(STP)\ cm/(cm^2\ s\ cmHg)]$				Solubility Coefficient (S) $[10^{-3}cm^3(STP)/(cm^3\ cmHg)]$				Gas diffusion Coefficient (D) $[10^{-7}(cm^2/sec)]$			
	CO_2	O_2	N_2	CH_4	CO_2	O_2	N_2	CH_4	CO_2	O_2	N_2	CH_4
PESU-SP-1 (20wt%)	16.9	4.04	1.69	1.99	60.3	3.38	2.22	3.33	0.280	1.20	0.774	0.597
PESU-SP-1 (20wt%)	11.7	2.73	1.06	1.25	92.9	5.34	3.51	2.50	0.125	0.511	0.302	0.500
PESU-SP-2 (20wt%)	13.5	2.32	0.391	0.335	167	10.3	9.37	32.2	0.0805	0.225	0.0418	0.0106
PESU-SP-2 (30wt%)	19.7	3.60	0.638	0.539	197	12.0	10.8	33.4	0.100	0.301	0.0593	0.0162
PESU-SP-3 (20wt%)	8.25	1.63	0.239	0.194	109	6.26	4.90	15.4	0.0758	0.260	0.0488	0.0126
PESU-SP-3 (30wt%)	8.92	1.64	0.260	0.185	163	10.0	7.96	22.9	0.0549	0.163	0.0327	0.0081
PESU-SSZ-13 (20wt%)	12.7	2.16	0.347	0.304	325	17.6	21.1	54.0	0.0390	0.123	0.0165	0.0056
PESU-SSZ-13 (30wt%)	16.0	2.75	0.471	0.409	378	20.2	28.3	58.8	0.0422	0.136	0.0167	0.0070
PESU	6.75	1.22	0.198	0.178	69.5	3.99	2.44	9.35	0.0970	0.305	0.0810	0.0190

The addition of SAPO-34 and SSZ-13 into the PESU can enhance the diffusion selectivity (Table 5-7), while have a different effect on the solubility selectivity, in a word, gas selectivity of MMMs can be improve by increasing solubility selectivity.

Table 5-7 The ideal selectivity of Permeability, Solubility and Diffusion coefficient for PESU/CHA MMMs.

Membrane	CO_2/CH_4			CO_2/N_2			O_2/N_2		
	α_P	α_S	α_D	α_P	α_S	α_D	α_P	α_S	α_D
PESU-SP-1 (20 wt%)	8.49	18.1	0.47	10.0	27.16	0.36	2.39	1.52	1.55
PESU-SP-2 (20 wt%)	40.3	5.19	7.57	34.4	17.87	1.93	5.94	1.10	5.39
PESU-SP-2 (30 wt%)	36.6	5.91	6.19	30.9	18.34	1.69	5.64	1.11	5.07
PESU-SP-3 (20 wt%)	42.6	7.08	6.02	34.5	22.23	1.55	6.81	1.28	5.32
PESU-SP-3 (30 wt%)	48.2	7.11	6.77	34.3	20.42	1.68	6.29	1.26	4.98
PESU-SSZ-13 (20 wt%)	41.7	6.02	6.93	36.6	15.44	2.36	6.23	0.83	7.46
PESU-SSZ-13 (30 wt%)	39.0	6.43	6.00	33.9	13.39	2.53	5.84	0.72	8.13
PESU	37.9	7.43	5.11	34.2	28.49	1.20	6.17	1.63	3.77

5.3.3.2 Gas permeation properties of AEI zeolites filled mixed matrix membranes

The single gas permeability of PESU/AlPO-18 mixed matrix membranes were summarized in Table 5-8 and plotted in Figure 5-9, the single gas permeability was followed the order of $H_2 > CO_2 > O_2 > N_2 > CH_4$ on all these AlPO-18 zeolites filled MMMs, indicating the effect of molecular sieve among those MMMs.

Table 5-8 Single gas permeability of PESU/AEI MMMs.

Membrane	Permeability [Barrer]					
	He	H_2	CO_2	O_2	N_2	CH_4
PESU-AP-1-20 wt.%	28	29	13	2.5	0.73	0.73
PESU-AP-2-20 wt.%-1	25	24	11	1.8	0.26	0.27
PESU-AP-2-20 wt.%-2	33	34	16	2.8	0.51	0.47
PESU-AP-2-20 wt.%-3	18	19	10	1.7	0.29	0.27
PESU-AP-3-20 wt.%	18	17	8.3	1.4	0.24	0.21
PESU-AP-3-30 wt.%	16	16	7.2	1.3	0.22	0.17
PESU	13	14	6.8	1.2	0.20	0.18

It is easily found the gas permeability of those MMMs were dramatically improved by incorporating AlPO-18 zeolites. Permeability was increased by filling smaller crystals. In the case of PESU-AP-3-20 wt.%, gas permeability of H_2 and CO_2 were increased from 14 to 17 barrer and 6.8 to 8.3 barrer compared with pure PESU membrane, respectively. Further incorporating 30 wt.% AlPO-18-3, gas permeability of H_2 and CO_2 were decreased to 16 barrer and 7.2 barrer. For PESU-AP-2-20 wt.%, the H_2 and CO_2 gas permeability enhanced a lot with H_2 increased from 13 to 34 barrer and CO_2 increased from 6.8 to 16 barrer, respectively.
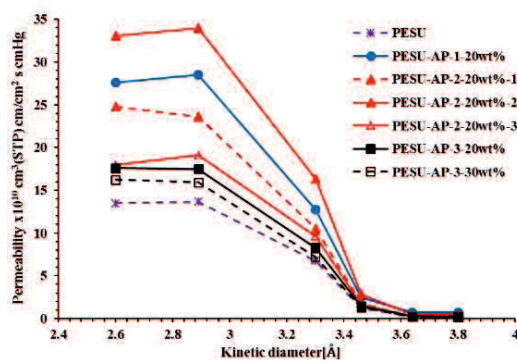
Figure 5-9 The Single gas permeability of PESU/AlPO-18 mixed matrix membranes as a function of gas kinetic diameter.

Table 5-9 The ideal selectivity of PESU/AEI MMMs.

Membrane	Ideal selectivity α [-]					
	H_2/N_2	H_2/CH_4	CO_2/CH_4	O_2/N_2	CO_2/N_2	H_2/O_2
PESU-AP-1-20 wt.%	39	39	17	3.4	17	11
PESU-AP-2-20 wt.%-1	91	89	40	6.8	40	13
PESU-AP-2-20 wt.%-2	67	73	35	5.5	32	12
PESU-AP-2-20 wt.%-3	67	70	35	5.8	34	12
PESU-AP-3-20 wt.%	74	83	39	6.1	35	12
PESU-AP-3-30 wt.%	74	92	42	6.1	34	12
PESU	69	77	38	6.2	34	11

The ideal selectivities of AlPO-18 filled MMMs were illustrated in Table 5-9. Similar as the MMMs filled with SAPO-34 zeolites, by incorporating smaller size crystals, due to more defects formed, since improved the gas permeability while the ideal selectivity was reduced. In the case of PESU-AP-3 MMMs, since the permeability of H_2 and CO_2 decreased by the filler loading increased from 20 wt.% to 30 wt.%, the ideal selectivities of H_2/CH_4 and CO_2/CH_4 were increased from 83 to 92 and 39 to 42 by the filler loading increased from 20 wt.% to 30 wt.%.
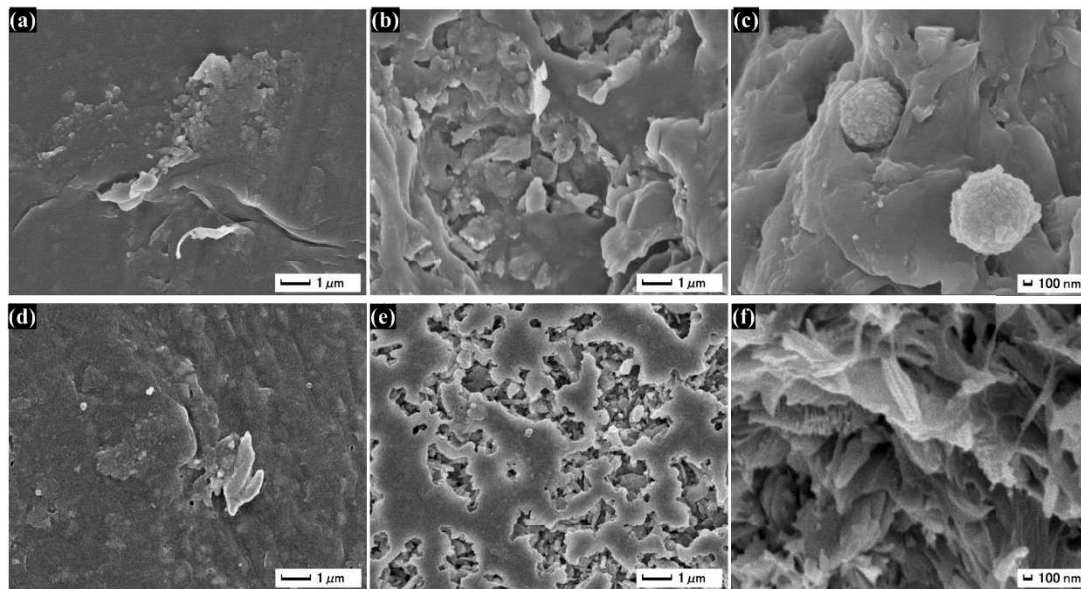
Figure 5-10 SEM images of mixed matrix membranes with loading 20 wt.% AlPO-18 zeolites; surface from air side (a), surface from glass side (b) cross sectional (c) of PESU-AP-1; surface from air side (d), surface from glass side (e) cross sectional (f) of PESU-AP-3.

The SEM images of AlPO-18 loaded MMMs are shown in Figure 5-10. For PESU-

AP-1 MMMs with filling the smallest crystals size AlPO-18-1 zeolites, crystals become agglomeration in the PESU that result in the void defects [14]. and for the PESU-AP-3 MMMs, only few zeolites were found from the cross-sectional as shown in Figure 5-10f, many crystals were found from the surface, it may due to the bad compatibility [38] between AlPO-18 and PESU, thus did not change a lot for gas permeability.
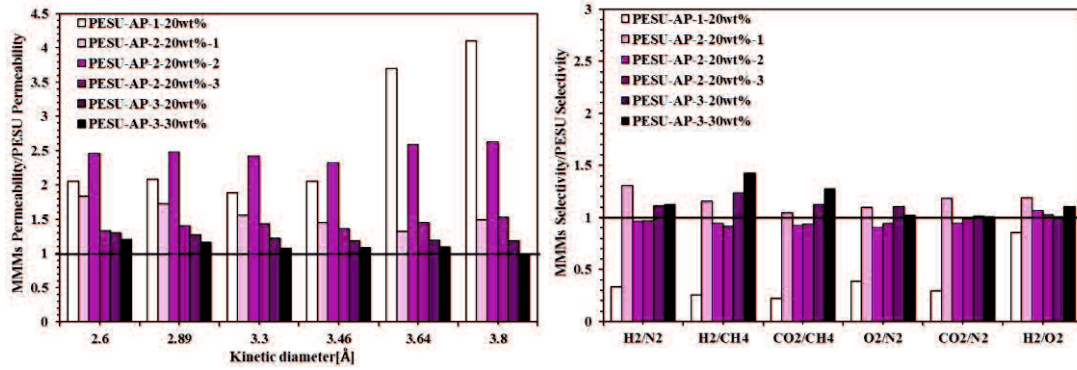
Figure 5-11 Permeability(left) and selectivity (right) of mixed matrix membranes compared with neat PESU membrane.

Figure 5-11 shows the gas permeability of AlPO-18 zeolites loaded MMMs compared with neat PESU membrane, it's easily seen loading zeolite into PESU polymer increased all the single gas permeability, loaded with smallest AlPO-18 zeolites into PESU polymer, gas permeability was largely enhanced while decreased all the ideal selectivity. The PESU-AP-2 MMMs by incorporating AlPO-18-2 shows both high gas permeability and ideal selectivity.

5.4 Conclusions

Three AlPO-18 zeolites with different crystals sizes under 1μm, three SAPO-34 crystals with different crystals sizes under 500nm and one SSZ-13 with ~400nm crystal size were used as filler for fabricating PESU-based mixed matrix membranes (MMMs). CHA type zeolites SAPO-34 and SSZ-13 showed more effective over AEI type AlPO-18 to fabricate PESU-based MMMs for gas separation. Compared with the smallest SAPO-34-1 crystals and the inhomogeneous SAPO-34-2, the MMMs by incorporating homogeneous SAPO-34-3 with the crystal size of ~200nm and SSZ-13 with the crystal size ~400nm showed a continuous interface with less defects.

The MMMs using 30 wt.% SAPO-34-3 showed an increase of ~42.8% in H_2 single gas permeability and 30.8% in CO_2 single gas permeability, which result in the ideal selectivity of a 42.8% increase for H_2/CH_4 and 26.3% increase for CO_2/CH_4. And the MMMs using 20 wt.% SSZ-13 with the crystal size ~400nm showed an increase of ~92.8% in H_2 single gas permeability and 91.2% in CO_2 single gas permeability, which result in a 14.2% increase for H_2/CH_4 ideal selectivity and 10.5% for CO_2/CH_4 ideal selectivity. In all, we can conclude that SAPO-34 as the filler showed higher ideal selectivity and SSZ-13 as the filler displayed higher single gas permeability.

References

[1]   R.W. Baker, B.T. Low, Gas separation membrane materials: A perspective, Macromolecules. 47 (2014) 6999-7013.

[2]   A. Brunetti, P. Bernardo, E. Drioli, G. Barbieri, Membrane Engineering: Progress and Potentialities in Gas Separations, John Wiley & Sons, Ltd, (2010) 279-312.

[3]   P. Bernardo, E. Drioli, G. Golemme, Membrane gas separation: A review/state of the art, Industrial and Engineering Chemistry Research. 48 (2009) 4638-4663.

[4]   R.W. Baker, Future Directions of Membrane Gas Separation Technology, Industrial and Engineering Chemistry Research. 41 (2002) 1393-1411.

[5]   L.M. Robeson, Z.P. Smith, B.D. Freeman, D.R. Paul, contributions of diffusion and solubility selectivity to the upper bound analysis for glassy gas separation membranes, Journal of Membrane Science. 453 (2014) 71-83.

[6]   Y. Yampolskii, Polymeric Gas Separation Membranes, Macromolecules. 45 (2012) 3298-3311.

[7]   L.M. Robeson, Correlation of separation factor versus permeability for polymeric membranes, Journal of Membrane Science. 62 (1991) 165-185.

[8]   L. Vinet, A. Zhedanov, A "missing" family of classical orthogonal polynomials, Macromolecules. 44 (2011) 085201.

[9]   H. Li, Z. Song, X. Zhang, Y. Huang, S. Li, Y. Mao, H.J. Ploehn, Y. Bao, M. Yu, Ultrathin, Molecular-Sieving Graphene Oxide Membranes for Selective Hydrogen Separation, Science. 342 (2013) 95-98.

[10]   Y. Cui, H. Kita, K. Okamoto, Preparation and gas separation properties of zeolite T membrane, Chemical Communications. 0 (2003) 2154-2155.

[11]   R.M. de Vos, H. Verweij, High-Selectivity, High-Flux Silica Membranes for Gas Separation, Science. 279 (1998) 1710-1711.

[12]   S.R. Venna, M.A. Carreon, Highly Permeable Zeolite Imidazolate Framework-8 Membranes for CO_2/CH_4 Separation, Journal of the American Chemical Society. 132 (2010) 76-78.

[13] S Li, J. L.Falconer, Richard D.Noble, SAPO-34 membranes for CO_2/CH_4 separation, Journal of Membrane Science. 241 (2004) 121-135.

[14] T.S. Chung, L.Y. Jiang, Y. Li, S. Kulprathipanja, Mixed matrix membranes (MMMs) comprising organic polymers with dispersed inorganic fillers for gas separation, Progress in Polymer Science. 32 (2007) 483-507.

[15] C. Zhang, Y. Dai, J.R. Johnson, O. Karvan, W.J. Koros, High performance ZIF-8/6FDA-DAM mixed matrix membrane for propylene/propane separations, Journal of Membrane Science. 389 (2012) 34-42.

[16] B. Zornoza, C. Tellez, J. Coronas, J. Gascon, F. Kapteijn, Metal organic framework based mixed matrix membranes: An increasingly important field of research with a large application potential, Microporous and Mesoporous Materials. 166 (2013) 67-78.

[17] G. Dong, H. Li, V. Chen, Challenges and opportunities for mixed-matrix membranes for gas separation, Journal of Materials Chemistry A. 1 (2013) 4610-4630.

[18] Z. V. Singh, M.G. Cowan, W.M. McDanel, Y. Luo, R. Zhou, D.L. Gin, R.D. Noble, Determination and optimization of factors affecting CO_2/CH_4 separation performance in poly(ionic liquid)-ionic liquid-zeolite mixed-matrix membranes, Journal of Membrane Science. 509 (2016) 149-155.

[19] L. Diestel, N. Wang, A. Schulz, F. Steinbach, J. Caro, Matrimid-Based Mixed Matrix Membranes: Interpretation and Correlation of Experimental Findings for Zeolitic Imidazolate Frameworks as Fillers in H_2/CO_2 Separation, Industrial and Engineering Chemistry Research. 54 (2015) 1103-1112.

[20] B. Zornoza, C. Téllez, J. Coronas, O. Esekhile, W.J. Koros, Mixed matrix membranes based on 6FDA polyimide with silica and zeolite microsphere dispersed phases, AIChE Journal. 61 (2015) 4481-4490.

[21] V. Martin-Gil, A. López, P. Hrabanek, R. Mallada, I.F.J. Vankelecom, V. Fila, Study of different titanosilicate (TS-1 and ETS-10) as fillers for Mixed Matrix Membranes for CO_2/CH_4 gas separation applications, Journal of Membrane Science. 523 (2017) 24–35.

[22] R. Mahajan, R. Burns, M. Schaeffer, W.J. Koros, Challenges in forming successful mixed matrix membranes with rigid polymeric materials, Journal of Aplied Polymer Science. 86 (2002) 881-890.

[23] R.Mahajan, W.J. Koros, Factors Controlling Successful Formation of Mixed-Matrix Gas Separation Materials, Industrial and Engineering Chemistry Research. 39 (2000) 2692-2696.

[24] L.S. Ferreira, J.O. Trierweiler, Modeling and simulation of the polymeric nanocapsule formation process, IFAC Proceedings Volumes. 42 (2009) 405-410.

[25] C. Zhao, J. Xue, F. Ran, S. Sun, Modification of polyethersulfone membranes - A review of methods, Progress in Materials Science. 58 (2013) 76-150.

[26] Y. Li, T. Chung, C. Cao, S. Kulprathipanja, The effects of polymer chain rigidification, zeolite pore size and pore blockage on polyethersulfone (PES)-zeolite A mixed matrix membranes, Journal of Membrane Science. 260 (2005) 45-55.

[27] J. Ahn, W.J. Chung, I. Pinnau, M.D. Guiver, Polysulfone/silica nanoparticle mixed-matrix membranes for gas separation, Journal of Membrane Science. 314 (2008) 123-133.

[28] Y. Li, H.M. Guan, T.S. Chung, S. Kulprathipanja, Effects of novel silane modification of zeolite surface on polymer chain rigidification and partial pore blockage in polyethersulfone (PES)-zeolite A mixed matrix membranes, Journal of Membrane Science. 275 (2006) 17-28.

[29] T. Wu, M.C. Diaz, Y. Zheng, R. Zhou, H.H. Funke, J.L. Falconer, R.D. Noble, Influence of propane on CO_2/CH_4 and N_2/CH_4 separations in CHA zeolite membranes, Journal of Membrane Science. 473 (2015) 201-209.

[30] R. Zhou, E.W. Ping, H.H. Funke, J.L. Falconer, R.D. Noble, Improving SAPO-34 membrane synthesis, Journal of Membrane Science. 444 (2013) 384-393.

[31] Y. Zheng, N. Hu, H. Wang, N. Bu, F. Zhang, R. Zhou, Preparation of steam-stable high-silica CHA (SSZ-13) membranes for CO_2/CH_4 and C_2H_4/C_2H_6 separation, Journal of Membrane Science. 475 (2015) 303-310.

[32] H. Kalipcilar, T.C. Bowen, R.D. Noble, J.L. Falconer, Synthesis and Separation

Performance of SSZ-13 Zeolite Membranes on Tubular Supports, Chemistry of Materials. 14 (2002) 3458-3464.

[33] B. Wang, N. Hu, H. Wang, Y. Zheng, R. Zhou, Improved AlPO-18 membranes for light gas separation, Journal of Materials Chemistry A. 3 (2015) 12205-12212.

[34] Stacey I. Zones, Zeolite SSZ-13 and Its Method of Preparation, U S Patent. (1985) 4,544,538.

[35] S. Ashtekar, S.V. V. Chilukuri, D.K. Chakrabarty, Small-Pore Molecular Sieves SAPO-34 and SAPO-44 with Chabazite Structure: A Study of Silicon Incorporation, The Journal of Physical Chemistry. 98 (1994) 4878-4883.

[36] K. Tanaka, M. Okano, H. Toshino, H. Kita, K.I. Okamoto, Effect of methyl substituents on permeability and permselectivity of gases in polyimides prepared from methyl-substituted phenylenediamines, Journal of Polymer Science Part B: Polymer Physics. 30 (1992) 907–914.

[37] K. Tanaka, H. Kita, K. Okamoto, A. Nakamura, Y. Kusuki, The Effect of Morphology on Gas Permeability and Permselectivity in Polyimide Based on 3,3′,4,4′-Biphenyltetracarboxylic Dianhydride and 4,4′-Oxydianiline, Polymer Journal. 21 (1989) 127-135.

[38] P.S. Goh, A.F. Ismail, S.M. Sanip, B.C. Ng, M. Aziz, Recent advances of inorganic fillers in mixed matrix membrane for gas separation, Separation and Purification Technology. 81 (2011) 243-264.

[39] M.A. Aroon, A.F. Ismail, T. Matsuura, M.M. Montazer-Rahmati, Performance studies of mixed matrix membranes for gas separation: A review, Separation and Purification Technology. 75 (2010) 229-242.

[40] V. Martin-Gil, A. López, P. Hrabanek, R. Mallada, I.F.J. Vankelecom, V. Fila, Study of different titanosilicate (TS-1 and ETS-10) as fillers for Mixed Matrix Membranes for CO_2/CH_4 gas separation applications, Journal of Membrane Science. 523 (2017) 24–35.

[41] M.J.C. Ordoñez, K.J. Balkus, J.P. Ferraris, I.H. Musselman, Molecular sieving realized with ZIF-8/Matrimid® mixed-matrix membranes, Journal of Membrane Science. 361 (2010) 28–37.

[42] Y. Luo, H.H. Funke, J.L. Falconer, R.D. Noble, Adsorption of CO_2, CH_4, C_3H_8, and H_2O in SSZ-13, SAPO-34, and T-Type Zeolites, Industrial and Engineering Chemistry Research. 55 (2016) 9749-9757.

Chapter 6 Preparation and Gas Permeation Properties of 6FDA-based Mixed Matrix Membranes with CHA Zeolite Particles

6.1 Introduction

Mixed Matrix Membranes (MMMs) were firstly discovered by UOP and attracted insensitively investigation in recently [1–7]. The emerged technology that combined the inorganic moieties and polymers, is considered to be a promising approach to overcome the so-called Robeson upper bound limit of the permeability and selectivity [8]. While, the big challenge in Mixed Matrix Membranes (MMMs) is still exist with the defects such as the nonselective interfacial voids [9–12], polymer chain rigidification [13–16] and pore blockage [14,16]. In one way, the appropriate choose of polymer matrix and the inorganic fillers is a reasonably way to obtain the defect-free and successful Mixed Matrix Membranes (MMMs).

The polyimides, general with good thermal, chemical stability and good mechanical properties, are suitable for gas separation application [17–19], especially for the polyimide with 2,2-bis(3,4-dicarboxyphenyl) hexafluoropropane dianhydride (6FDA) based membrane. A lot of studies have been reported that 6FDA-based membranes displayed attractive gas transportation properties [3,6,7,20]. Introduction of -$C(CF_3)_2$- group in 6FDA dianhydrides can restrict the torsional motion of neighboring phenyl rings and the packing properties of the chains, which can increase the gas permeability and selectivity [6,19,21]. The 6FDA based polymer membranes are mainly studies with containing s series of diamine moieties, meanwhile, it has been also reported the diamine moieties such as 2,4,6-trimethyl-1,3-phenylene-diamine (TrMPD) exhibited high permeability and selectivity for gas separation [19].

In this work, 6FDA-TrMPD (PI) polymer was firstly prepared by polymerization process, and then used for the polymer matrix, and three CHA type SAPO-34 zeolites with different sizes were used as filler for making 6FDA-TrMPD based self-supported mixed matrix membranes (MMMs). Gas permeation properties of the as-synthesized

MMMs were investigated, meanwhile, gas permeation properties were also studies by milling method for making MMMs.

6.2 Experimental

6.2.1 Chemicals

The structures of monomers 4,4′-(hexafluoroisopropylidene) diphthalic anhydride (6FDA) and 2.4.6-trimethyl-1,3-phenylene-diamine (TrMPD) were shown in Figure 6-1. The 6FDA monomer was obtained from TCI Co. and TrMPD monomer was supplied by Sigma-Aldrich, respectively. N-methyl-2-pyrrolidinone (NMP) of analytical grade, Acetic anhydride (>99.5%), triethylamine (99%), were purchased from Wako without further purification.
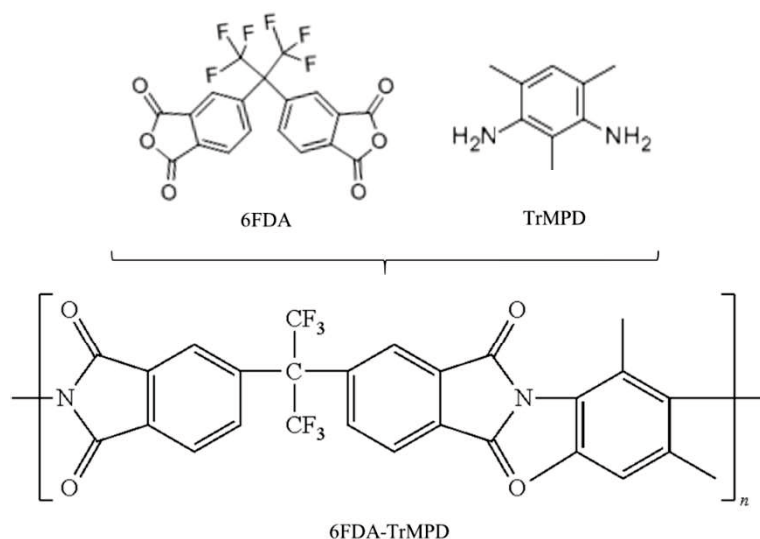
Figure 6-1 Chemical structures of the monomers and the polyimide.

6.2.2 SAPO-34 zeolites

The properties of SAPO-34 zeolites with different crystals sizes adopted as filler for preparing the MMMs were described in Table 6-1, details of the synthesis procedures were described in Chapter 2.

Table 6-1. Synthesis conditions of SAPO-34 zeolites.

Zeolite	Gel composition	Aged time(h)	Syn. Conditions
SAPO-34-1 (1)	$1Al_2O_3:1P_2O_5:0.6SiO_2:1.5TEAOH^1:0.5DIPEA:75H_2O$	12	473K, 12h
SAPO-34-2 (2)	$1Al_2O_3:1P_2O_5:0.6SiO_2:1.5TEAOH:0.5DIPEA:75H_2O$	12	473K, 12h
SAPO-34-3 (3)	$1Al_2O_3:1P_2O_5:0.6SiO_2:1.5TEAOH:0.5DIPEA:75H_2O$ Added 0.2% SAPO-34-1	12	473K, 12h

1: TEAOH from TCI Co.

6.2.3 Synthesis of 6FDA-TrMPD polyimide

The monomers of 6FDA and TrMPD were firstly purified by vacuum sublimation. The sublimation schematic was shown in Figure 6-2. Then polymerization was performed, the preparation of 6FDA-TrMPD is carried out in two stages: first the polyamide acid was produced by mixing the purified monomers 6FDA and TrMPD in an anhydrous medium within the NMP solution under the inert N_2 atmosphere; then chemically imidization was performed by adding the mixture of acetic anhydride and triethylamine into the solution. The resulting solution was stirred at R.T. for 1h, following stirred for 2h under 50°C, then precipitated the as-synthesized polyimide in ethanol, washed for 3 times, finally, dried the polyimide in a vacuum oven at 100°C for 24h. The structure of the obtained 6FDA-TrMPD was shown in Figure 6-1.
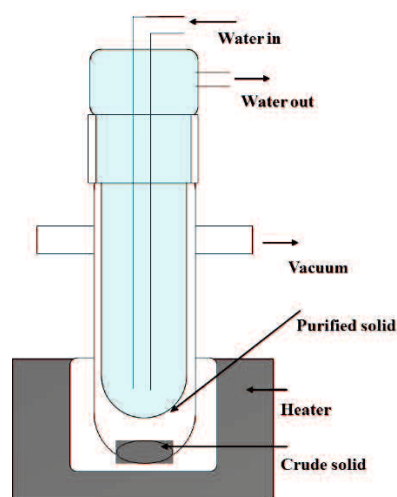
Figure 6-2 Schematic diagram of Sublimation.

6.2.4 Membrane fabrication

The pure self-supported 6FDA-TrMPD membrane was prepared by adding the 6FDA-TrMPD into NMP (6FDA-TrMPD: NMP=15.wt %: 85.wt %) solution and stirred until fully dissolve. Then remove the bubble from the casting solution, and casted the solution onto glass board with the glass rod of 50-70μm thickness, and slowly evaporated abundant NMP solvent at 80°C for 2 h, and finally heated the films at 200°C under vacuum for 20 h until the membrane became hard.

The self-supported 6FDA-TrMPD/SAPO-34 mixed matrix membranes (MMMs) were fabricated by adding 20-40 wt.% SAPO-34 zeolites into the polymer matrix. The SAPO-34 zeolites were dried in a vacuum oven at 200°C for 24h to remove all the moisture and adsorbed stuff before usage. Afterwards, the SAPO-34 particles were dispersed in NMP solution, then the resulting solution were stirred for 1h and sonicated for 4h at R.T. to get fully dispersion. Next, added the as-synthesized 6FDA-TrMPD into the resulting dispersion at 80°C to dissolve it and stirred for another 4h, then the resulting polymer mixtures were mixed together at R.T. for 12h and sonicated for more 4h. Bubble should be removed from the casting solution before being cast onto glass board with the glass rod of 50-70μm thickness. The casted films were then dried for 2 h at 80°C under vacuum to remove most NMP solvent, and finally heated the films at 200°C under vacuum for 20 h until the membrane became hard.

6.2.5 Characterization

The morphology and the compatibility of these mixed matrix membrane that between the zeolite filler and 6FDA-TrMPD matrix were determined by a field emission scanning electron microscope (FE-SEM, JEOL JSM 6335F) at an acceleration voltage of 5KV. The crystallinity of the neat 6FDA-TrMPD membrane and 6FDA-TrMPD based mixed matrix membranes were identified by X-ray diffraction (XRD, SHIMADZU XRD-6100) using a Shimadzu XD-3 diffractometer with Cu-Ka radiation at a scanning range of $2\theta=5\sim45°$ and a scanning rate of 4°/min.

6.2.6 Gas permeation

Single gas permeations of He, H_2, CO_2, O_2, N_2, CH_4 six gases were measured by means of vacuum method with a fixed volume pressure gauge [22] using a time-lag method [23]. The membranes were performed at 35°C with a feed pressure of 0.3MPa. Setup details were described in Chapter 4. Before permeation measurement, membranes were degassed in the gas permeation apparatus system under vacuum at 353K for 3h. Area of membranes were fixed to 18.86cm^2. The permeability coefficient P_i and the time-lag θ were directly measured through time-lag method under vacuum, while the diffusion coefficient D_i was estimated by the time-lag θ and the thickness of the film (l):

$D_i = l^2/(6\theta)$

The solubility coefficient was caculated through the permeability coefficient and diffusion coefficient:

$P_i = D_i \cdot S_i$

6.3 Results and discussion

6.3.1 Properties of SAPO-34 zeolites

The properties of SAPO-34 zeolites used here are shown in Table 6-2, the corresponding morphologies of the three SAPO-34 zeolites were characterized by SEM and showed in Figure 6-3.

Table 6-2. Properties of CHA type zeolites.

Zeolite	Synthesis condition	Crystal shape	Size (nm)
SAPO-34-1 (1)	473K, 12h	Cubic	>1000
SAPO-34-2 (2)	473K, 12h	spherical + cubic	~100-500
SAPO-34-3 (3)	473K, 12h	spherical	~200

As shown in Figure 6-3, SAPO-34-1 zeolites prepared with TEAOH from TCI. Co. have a crystals size more than 1μm aggregated by the ~500nm crystals, SAPO-34-2 zeolites have a wide crystals size ranges from 100nm to 500nm, SAPO-34-3 zeolites have a homogeneous crystals size of ~200nm.
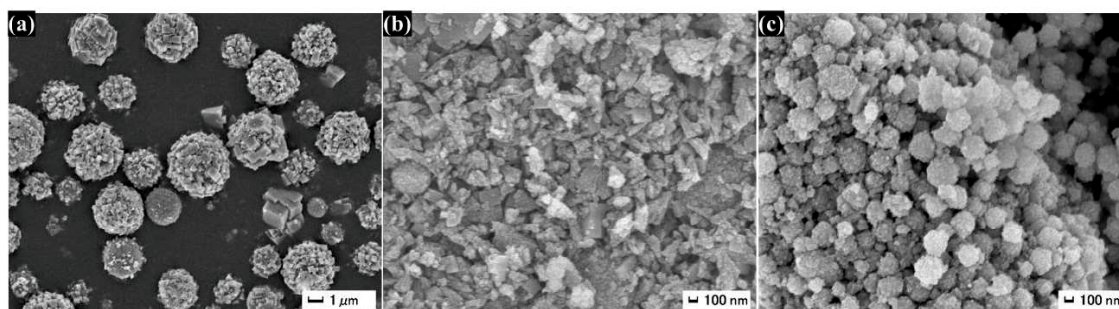
Figure 6-3 SEM images of SAPO-34 zeolites (a) SAPO-34-1, (b) SAPO-34-2, (c) SAPO-34-3.

6.3.2 Characterization of mixed matrix membranes (MMMs).
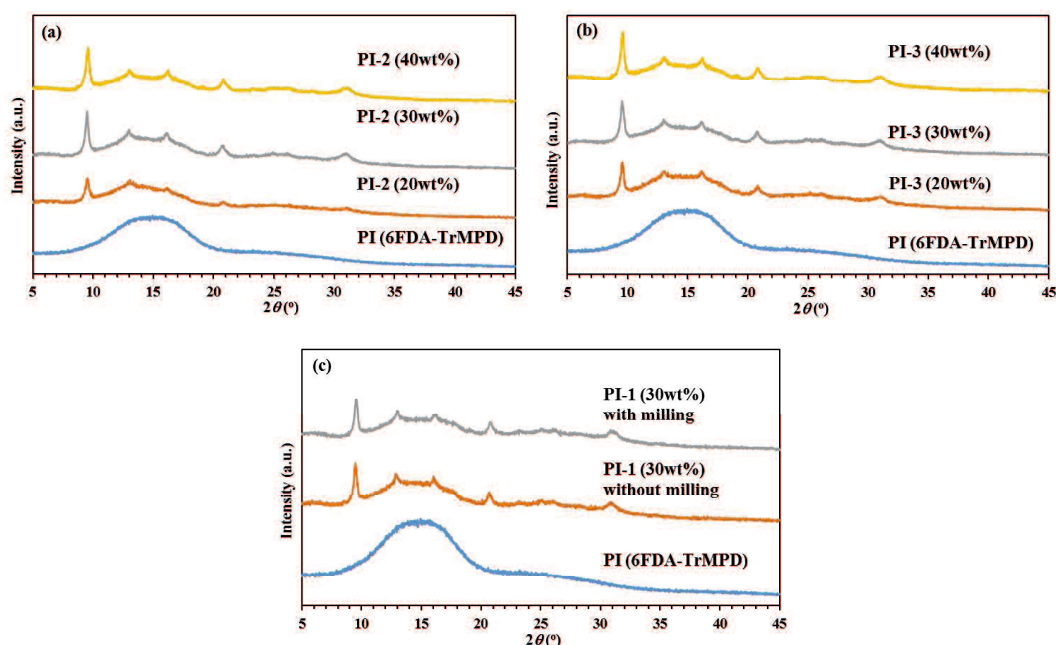
Figure 6-4 XRD patterns of 6FDA-TrMPD (PI) and 6FDA-TrMPD (PI) based MMMs with different concentration by filling different SAPO-34 zeolites (a) SAPO-34-2, (b) SAPO-34-3, (c) SAPO-34-1.

Two zeolites SAPO-34-2 and SAPO-34-3 were filled in 6FDA-TrMPD (PI) with the loading of 20 wt.%, 30 wt.%, and 40 wt.% respectively, the corresponding XRD patterns were shown in Figure 6-4, The neat PI polymer has a broad peak with the 2θ ranges from 10° to 20° due to its amorphous property. The amorphous peak become weaker after loading both three SAPO-34 zeolites. And the intensity of the amorphous peak decreased as increasing the filler loading from 20 wt.% to 40 wt.%, even after increasing SAPO-34 zeolites up to 40 wt.% (Figure 6-4a and b) the peak of the neat PI

membrane was still existed. However, the intensity of the SAPO-34 crystals within MMMs increased after enhancing the loadings, but this SAPO-34 filled MMMs show much weaker zeolite peaks compared with the zeolite itself (as seen in Chapter 2). In the case of SAPO-34-1 filled PI-1 MMMs, the MMMs show similar intensity, indicating the milling method wouldn't change the incorporating degree.

Cross-sectional SEM images of SAPO-34-2 filled mixed matrix membrane with the loading of 20 wt.%, 30 wt.%, and 40 wt.% were shown in Figure 6-5. The SAPO-34 crystals can distribute into the PI membrane, while, due to the heterogeneous crystals sizes, the distribution was not so evenly, and agglomeration similar as MFI zeolites [24] was occurred during the formation of mixed matrix membrane due to the strong van der Waals attractions between the SAPO-34 particles, which will affect the separation performance of membrane. As increased the loading of the SAPO-34-2 zeolite, the degree of the agglomeration increased to some degree. With the poor connection of zeolite and polymer, the incompatibility between zeolite and 6FDA-TrMPD (PI) polymer result in the sieve-in-a-cage morphology [15,25] which may affect the gas permeability properties of these membranes.
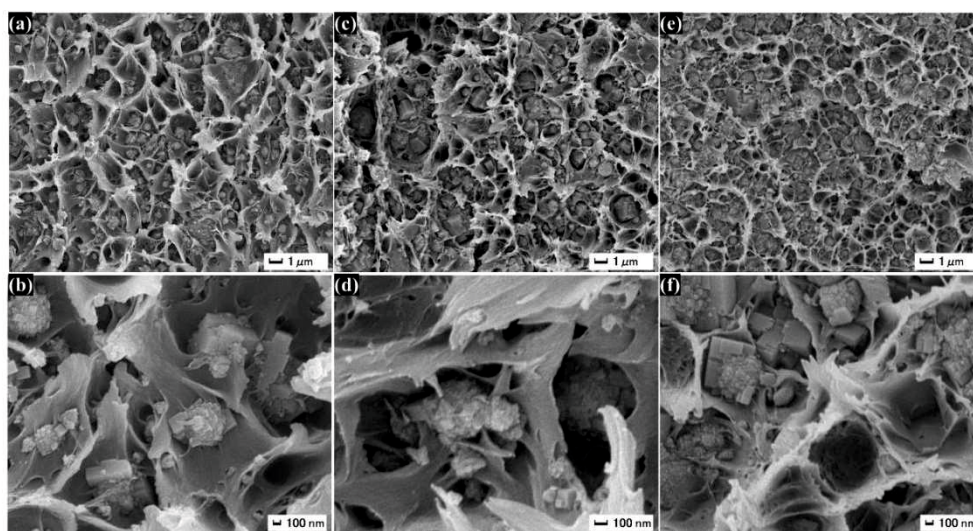
Figure 6-5 SEM images of mixed matrix membranes, (a)and (b): PI-2(20 wt.%); (c)and (d): PI-2(30 wt.%); (e)and (f): PI-2(40 wt.%).

Considerate the incompatibility between zeolite and polymer, milling method was adopting to release this situation. SAPO-34-1 with the biggest crystal size more than 1 μm was used to investigate the effect of the milling method during the preparation of

6FDA-TrMPD based self-supported mixed matrix membrane. Figure 6-6 and Figure 6-7 show the SEM images of 6FDA-TrMPD (PI) based mixed matrix membranes loaded with 30% SAPO-34-1 zeolite without milling and with milling method. The milling method were performed by adding the mill ball into the casting solution and milled together with~100r/min for 12h before casting.
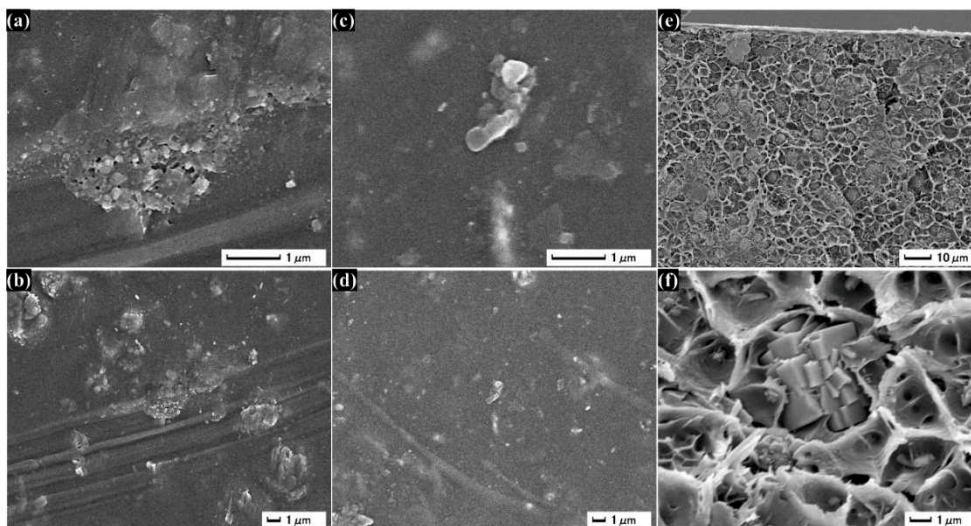
Figure 6-6 SEM images of Mixed matrix membrane PI-1 (30 wt.%) without milling, (a)and (b): surface from glass side; (c)and (d): surface from air side; (e)and (f): cross sectional.
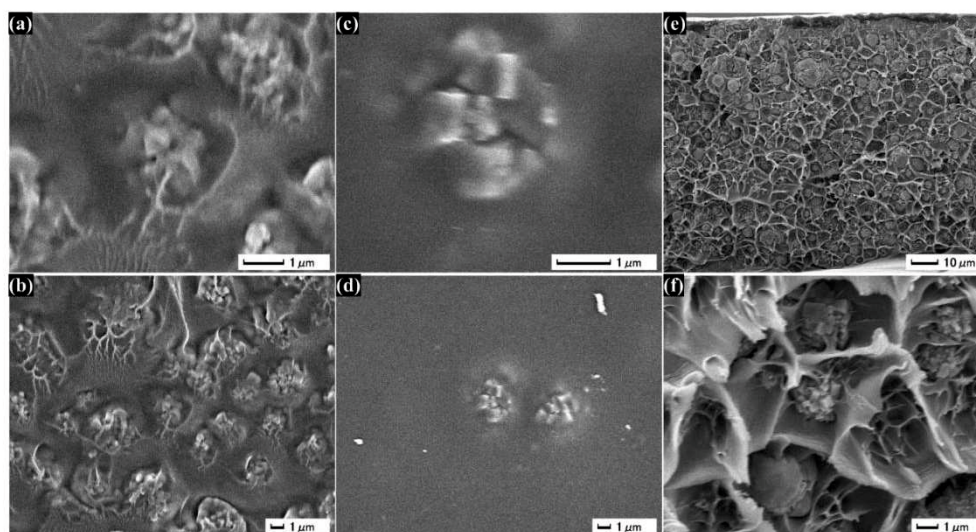
Figure 6-7 SEM images of Mixed matrix membrane PI-1 (30 wt.%) with milling, (a)and (b): surface from glass side; (c)and (d): surface from air side; (e)and (f): cross sectional.

The agglomeration was still existed in both milling (Figure 6-7e and f) and without-milling (Figure 6-6e and f) MMMs. In the case of PI-1 (30 wt.%) without milling, the surface from both glass and air sides show similar morphology, while it is clear to see

many SAPO-34 crystals appear on the the surface from glass side of the membrane PI-1 (30 wt.%) with milling. Meanwhile, the SAPO-34 zeolites become smaller in the membrane PI-1 (30 wt.%) with milling compared with the membrane without milling, it may reduce the defect, finally affect the gas permeation properties.

6.3.3 Gas permeation properties of mixed matrix membranes (MMMs).

The single gas permeability of He, H_2, CO_2, O_2, N_2 and CH_4 six gases of the pure 6FDA-TrMPD (PI) and 6FDA-TrMPD-based mixed matrix Membrane were measured and performed under vacuum method at 35°C, 0.3MPa.

Table 6-3 Single gas permeability of PI/SAPO-34 Membranes.

Membrane	Permeability [Barrer]					
	He	H_2	CO_2	O_2	N_2	CH_4
PI-3 (20 wt.%)	721	1165	1268	292	91	70
PI-3 (30 wt.%)	864	1432	1654	376	122	91
PI-3 (40 wt.%)	1103	2013	2719	622	226	162
PI-2 (20 wt.%)	669	1041	1132	252	77	59
PI-2 (30 wt.%)	748	1233	1408	325	104	74
PI-2 (40 wt.%)	861	1437	1663	382	129	96
PI-1 (30 wt.%) w/o milling	850	1310	1318	304	92	72
PI-1 (30 wt.%) with milling	962	1493	1542	342	103	77
PI	461	687	751	158	45	38

All these membranes single gas permeations were shown in Table 6-3 and plotted in Figure 6-8. All of these gases were test for 2 times to get the exactly data, as shown in Figure 6-8. It is obvious seen that loading all of these three sizes SAPO-34 zeolites dramatically enhanced the permeability of these six gases compared with pure 6FDA-TrMPD (PI) membrane. Meanwhile, according to Table 6-3, as loading SAPO-34-3 from 20 wt.% to 40 wt.%, the CO_2 single gas permeability increased from 69%-262%, and as loading SAPO-34-2 from 20 wt.% to 40 wt.%, the CO_2 single gas permeability increased from 51%-121%, and for loading 30 wt.% SAPO-34-1 with and without milling increased the CO_2 single gas permeability by 75% and 105%, respectively. At the same time, the CO_2 single gas permeability increased 120% for 30 wt.% SAPO-34-3 loading and 87% for 30 wt.% SAPO-34-2 loading. As observed, loading homogenous SAPO-34 crystals (SAPO-34-3) into 6FDA-TrMPD (PI) increased much more CO_2

single gas permeability than filling heterogeneous zeolites. And incorporating bigger sizes and heterogeneous SAPO-34 crystals (SAPO-34-1) shows a little higher CO_2 single gas permeability than loading with heterogeneous SAPO-34-2 zeolites. In addition, compared with using milling method, after milling, the CO_2 single gas permeability also increased ~17% compared with the membrane without milling, which shows a positive effect on MMMs gas permeance.
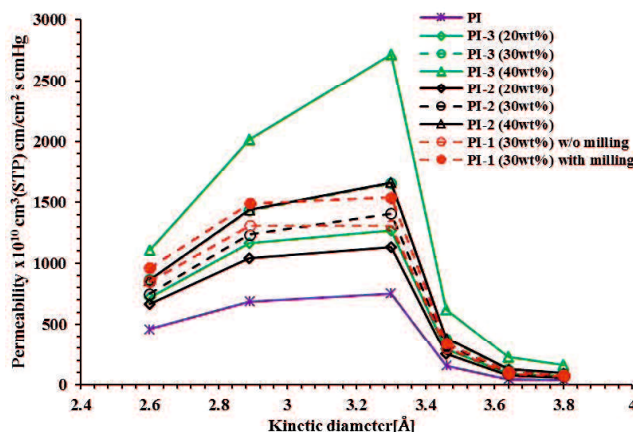
Figure 6-8 The Single gas permeability of PI/SAPO-34 mixed matrix membranes as a function of gas kinetic diameter.

Table 6-4 The ideal selectivity of PI/SAPO-34 Membranes.

Membrane	Ideal selectivity α[-]					
	H_2/N_2	H_2/CH_4	CO_2/CH_4	O_2/N_2	CO_2/N_2	H_2/O_2
PI-3 (20 wt.%)	13	17	18	3.2	14	4.0
PI-3 (30 wt.%)	12	16	18	3.1	14	3.8
PI-3 (40 wt.%)	9	12	17	2.8	12	3.2
PI-2 (20 wt.%)	14	18	19	3.3	15	4.1
PI-2 (30 wt.%)	12	17	19	3.1	14	3.8
PI-2 (40 wt.%)	11	15	17	3.0	13	3.8
PI-1 (30 wt.%) w/o milling	14	18	18	3.3	14	4.3
PI-1 (30 wt.%) with milling	14	19	20.0	3.3	15	4.4
PI	15	18	19.6	3.5	17	4.3

Since all the single gas permeability increased with loading all of these SAPO-34 zeolites, unfortunately, due to the different increment for all of the tested six gases, which in aversely decreased the ideal selectivity compared with the pure PI polymer. As shown in Table 6-4, for the CO_2/CH_4 gas pair, as loading SAPO-34-3 from 20 wt.% to 40 wt.%, the CO_2/CH_4 ideal selectivity decreased from 8%-13%, and as loading

SAPO-34-2 from 20 wt.% to 40 wt.%, the CO_2/CH_4 ideal selectivity decreased from 3%-13%, and for loading 30 wt.% SAPO-34-1 with and without milling, the CO_2/CH_4 ideal selectivity decreased 8.2% for the membrane PI-1without milling, while, the CO_2/CH_4 ideal selectivity increased by 2.0%. As observed, after milling, the membrane shows positive effect on both gas permeability and selectivity.
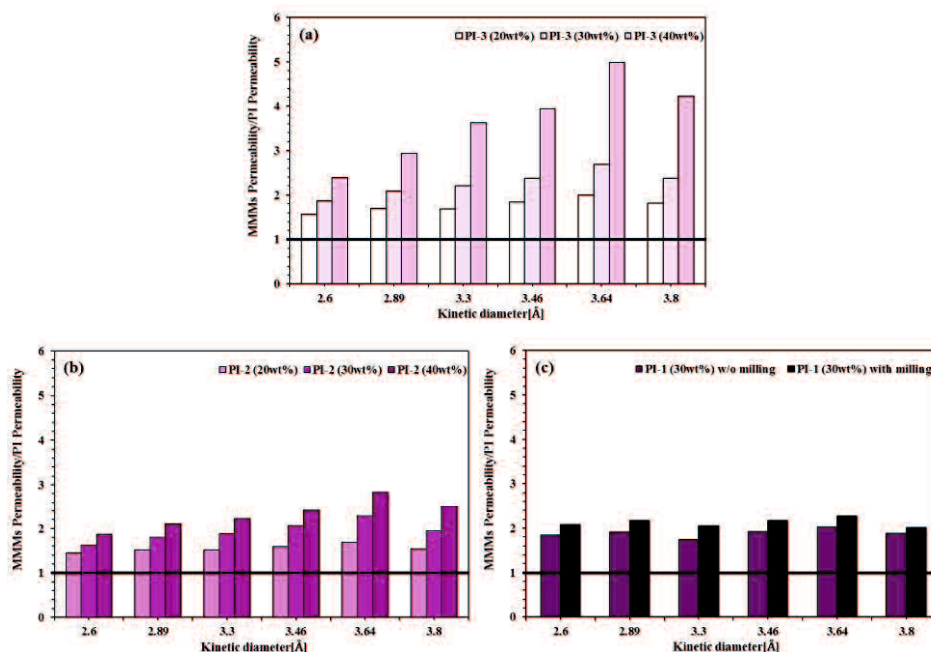
Figure 6-9 Permeability of mixed matrix membranes compared with neat PI membrane (a): PI-3 (filled with SAPO-34-3); (b): PI-2 (filled with SAPO-34-2) (c): PI-1 (filled with SAPO-34-1).

Gas permeability and the corresponding ideal selectivity of MMMs compared with neat PI membrane were shown in Figure 6-9 and Figure 6-10, respectively. It's obvious that loading zeolite into PI polymer increased all single gas permeability, in addition, for the MMMs, the less permeable gases, for instance, N_2 and CH_4, were also been improved by incorporating more zeolite into the PI polymer. Especially for the N_2, as a result, reduced the CO_2/N_2 ideal selectivity to 12 and 13 with 40 wt.% for PI-3 and PI-2, respectively. It indicates the diffusivity for MMMs affected strongly by loading the SAPO-34 zeolites.
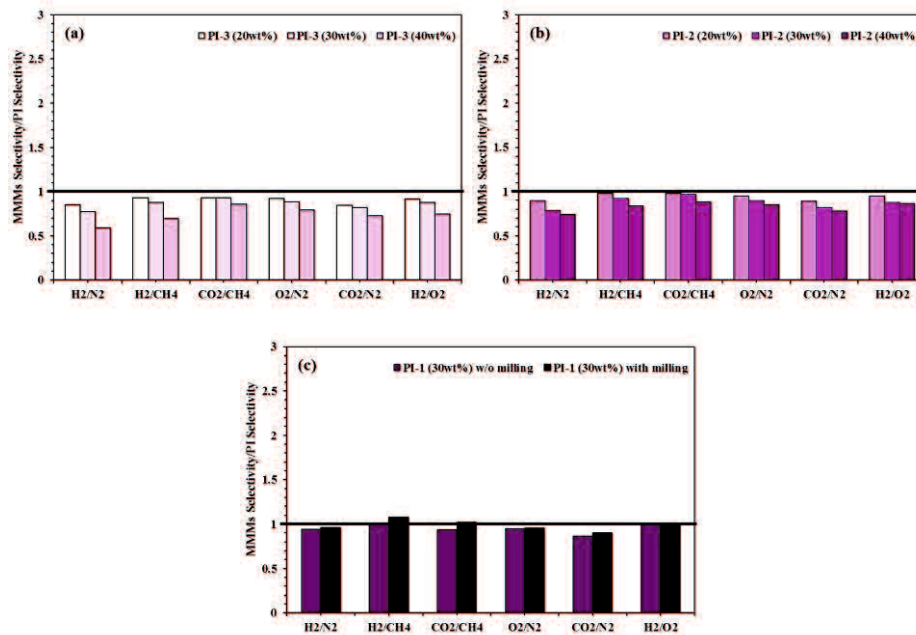
Figure 6-10 Ideal selectivity of mixed matrix membranes compared with neat PI membrane (a): PI-3 (filled with SAPO-34-3); (b): PI-2 (filled with SAPO-34-2) (c): PI-1 (filled with SAPO-34-1).

Permeability of SAPO-34 filled MMMs increased largely due to the increment with both solubility coefficient and diffusion coefficient, as seen in Table 6-5, while, as the differential with the increment for different gases, therefore, the ideal selectivity of CO_2/CH_4, CO_2/N_2 and O_2/N_2 systems were decreased as shown in Table 6-6.

Table 6-5 The correlation of Permeability, Solubility and Diffusion of PI/SAPO-34 MMMs.

Membrane	Permeability (P)				Solubility Coefficient (S)				Diffusion Coefficient (D)			
	[Barrer]				$[10^{-3}cm^3(STP)/(cm^3\ cmHg)]$				$[10^{-7}(cm^2/sec)]$			
	CO_2	O_2	N_2	CH_4	CO_2	O_2	N_2	CH_4	CO_2	O_2	N_2	CH_4
PI-3 (20 wt.%)	1268	292	91	70	314	26	27	78	4.03	11.06	3.38	0.90
PI-3 (30 wt.%)	1654	376	122	91	369	27	29	89	4.48	13.95	4.21	1.02
PI-3 (40 wt.%)	2719	622	226	162	1219	26	29	91	2.23	23.62	7.72	1.78
PI-2 (20 wt.%)	1132	252	77	59	330	26	27	82	3.43	9.69	2.85	0.72
PI-2 (30 wt.%)	1408	325	104	74	332	28	27	80	4.24	11.61	3.84	0.93
PI-2 (40 wt.%)	1663	382	129	96	369	22	29	88	4.51	17.75	4.43	1.08
PI-1 (30 wt.%) w/o milling	1310	304	92	72	405	33	35	92	3.25	9.10	2.63	0.78
PI-1 (30 wt.%) with milling	1542	342	103	77	364	28	30	84	4.24	12.41	3.48	0.91
PI	751	158	45	38	243	15	18	67	3.14	10.36	2.52	0.57

Table 6-6 The ratio of Permeability, Solubility and Diffusion coefficient of PI/SAPO-34 MMMs for CO_2/CH_4, CO_2/N_2 and O_2/N_2 systems.

Membrane	CO_2/CH_4			CO_2/N_2			O_2/N_2		
	α_P	α_S	α_D	α_P	α_S	α_D	α_P	α_S	α_D
PI-3 (20 wt.%)	18.18	4.05	4.49	13.98	11.70	1.19	3.22	0.98	3.27
PI-3 (30 wt.%)	18.19	4.15	4.39	13.54	12.71	1.06	3.08	0.93	3.31
PI-3 (40 wt.%)	16.83	13.46	1.25	12.03	41.60	0.29	2.75	0.90	3.06
PI-2 (20 wt.%)	19.18	4.03	4.77	14.76	12.27	1.20	3.29	0.97	3.40
PI-2 (30 wt.%)	18.95	4.17	4.55	13.55	12.27	1.10	3.12	1.03	3.02
PI-2 (40 wt.%)	17.37	4.17	4.16	12.92	12.68	1.02	2.97	0.74	4.01
PI-1 (30wt%) w/o milling	18.21	4.38	4.18	14.21	11.56	1.24	3.30	0.95	3.46
PI-1(30wt%)with milling	19.97	4.31	4.64	14.95	12.25	1.22	3.32	0.93	3.57
PI	19.61	3.64	5.48	16.53	13.47	1.25	3.48	0.85	4.11

For CO_2/CH_4, CO_2/N_2 and O_2/N_2 systems, the diffusion coefficient ratios were decreased after loading the SAPO-34 zeolites into the PI polymer, since the solubility ratio improved, while, as a consequence, the ideal selectivities were decreased, indicating the SAPO-34 zeolites have an important effect for diffusivity for loaded MMMs. Meanwhile, the MMMs after milling improved both CO_2 permeability and CO_2/CH_4 selectivity.

Figure 6-11 plots the relationship between gas permeability and the corresponding CO_2/CH_4, CO_2/N_2, H_2/CH_4, H_2/O_2, H_2/N_2 and O_2/N_2 systems for pure PI and SAPO-34 filled PI/SAPO-34 membranes. Both neat PI and PI based MMMs show highest CO_2 gas permeability, which is different from some reported polyimide [19,26] and polyimide based MMMs [26]. At the same time, the permeation properties were improved by largely improve the gas permeability with little reduce the selectivity.
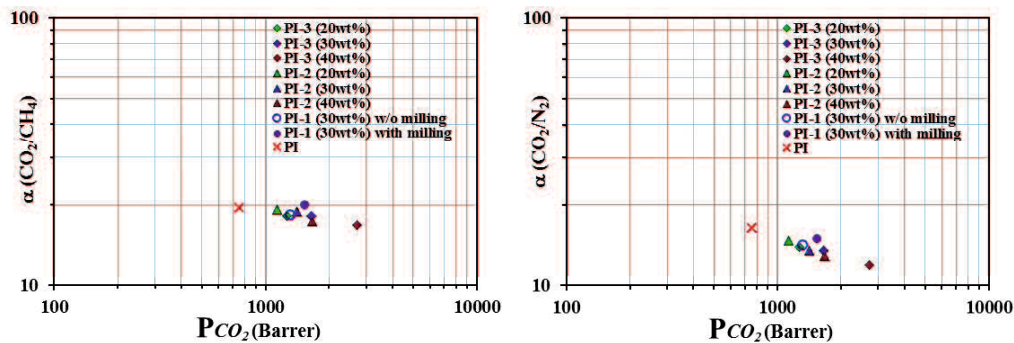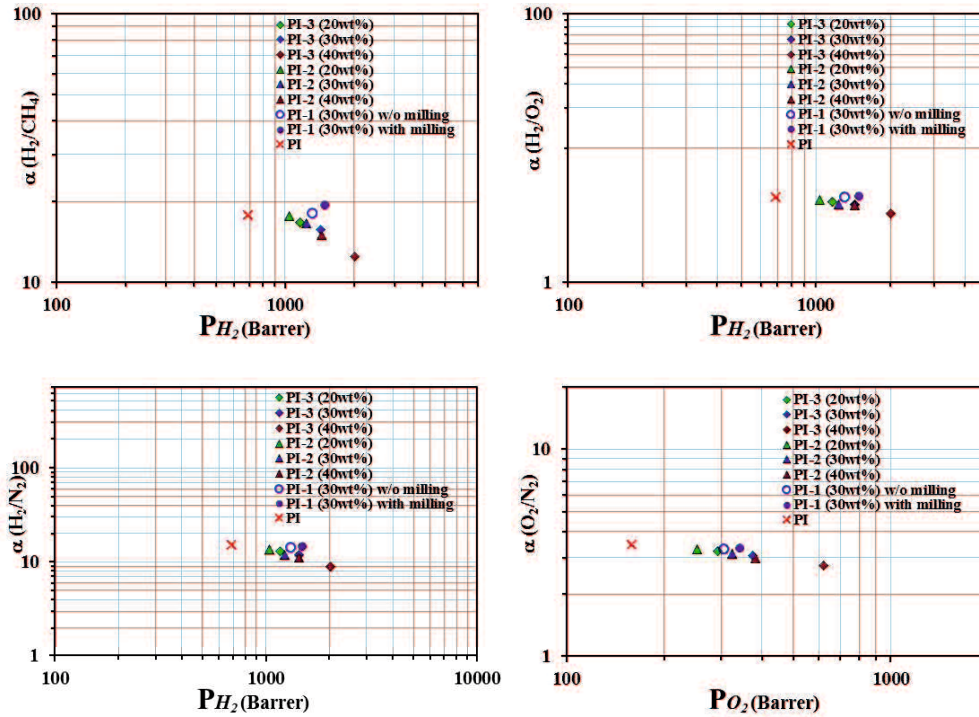
Figure 6-11 Permeability vs Selectivity of SAPO-34 loaded MMMs.

6.4 Conclusions

Three SAPO-34 crystals with different crystals sizes were used as filler for fabricating 6FDA-TrMPD (PI) based mixed matrix membranes (MMMs). Gas permeation properties were improved by incorporating three SAPO-34 zeolites into 6FDA-TrMPD (PI) polymer. Gas permeation results indicated the permeability were mainly enhanced while decreased a little of the ideal selectivity by loading SAPO-34 zeolites. Gas permeability increased as increasing the filler loading with 20 wt.%, 30 wt.% and 40 wt.%. Higher permeability can be obtained by loading homogeneous and small SAPO-34-1 for the membrane PI-3 MMMs, meanwhile, using milling method to prepare 6FDA-TrMPD (PI)/SAPO-34 MMMs can improve both CO_2 permeability and CO_2/CH_4 selectivity.

References

[1]   S. Kulprathipanja, R.W. Neuzil, N.N. Li, Separation of fluids by means of mixed-matrix membranes, US Patent 4,740,219. (1988).

[2]   C. Zhang, Y. Dai, J.R. Johnson, O. Karvan, W.J. Koros, High performance ZIF-8/6FDA-DAM mixed matrix membrane for propylene/propane separations, Journal of Membrane Science. 389 (2012) 34-42.

[3]   V. Nafisi, M.B. Hägg, Gas separation properties of ZIF-8/6FDA-durene diamine mixed matrix membrane, Separation and Purification Technology. 128 (2014) 31-38.

[4]   A. Tena, L. Fernández, M. Sánchez, L. Palacio, A.E. Lozano, A. Hernández, P. Prádanos, Mixed matrix membranes of 6FDA-6FpDA with surface functionalized γ-alumina particles. An analysis of the improvement of permselectivity for several gas pairs, Chemical Engineering Science. 65 (2010) 2227–2235.

[5]   J. Liu, T.H. Bae, W. Qiu, S. Husain, S. Nair, C.W. Jones, R.R. Chance, W.J. Koros, Butane isomer transport properties of 6FDA-DAM and MFI-6FDA-DAM mixed matrix membranes, Journal of Membrane Science. 343 (2009) 157-163.

[6]   A. Perea-Cachero, J. Sánchez-Laínez, Á. Berenguer-Murcia, D. Cazorla-Amorós, C. Téllez, J. Coronas, A new zeolitic hydroxymethylimidazolate material and its use in mixed matrix membranes based on 6FDA-DAM for gas separation, Journal of Membrane Science. 544 (2017) 88–97.

[7]   N. Jusoh, Y.F. Yeong, K.K. Lau, A. M. Shariff, Transport properties of mixed matrix membranes encompassing zeolitic imidazolate framework 8 (ZIF-8) nanofiller and 6FDA-durene polymer: Optimization of process variables for the separation of CO_2 from CH_4, Journal of Cleaner Production. 149 (2017) 80-95.

[8]   A. Galve, D. Sieffert, E. Vispe, C. Téllez, J. Coronas, C. Staudt, Copolyimide mixed matrix membranes with oriented microporous titanosilicate JDF-L1 sheet particles, Journal of Membrane Science. 370 (2011) 131-140.

[9]   F. Dorosti, M.R. Omidkhah, M.Z. Pedram, F. Moghadam, Fabrication and

characterization of polysulfone/polyimide-zeolite mixed matrix membrane for gas separation, Chemical Engineering Journal. 171 (2011) 1469-1476.

[10] H.B.T. Jeazet, C. Staudt, C. Janiak, A method for increasing permeability in O_2/N_2 separation with mixed-matrix membranes made of water-stable MIL-101 and polysulfone, Chemical Communications. 48 (2012) 2140-2142.

[11] A.L. Khan, A. Cano-Odena, B. Gutiérrez, C.Minguillón, I.F.J. Vankelecom, Hydrogen separation and purification using polysulfone acrylate-zeolite mixed matrix membranes, Journal of Membrane Science. 350 (2010) 340-346.

[12] M. Rezakazemi, A.E. Amooghin, M.M. Montazer-Rahmati, A.F. Ismail, T. Matsuura, State-of-the-art membrane based CO_2 separation using mixed matrix membranes (MMMs): An overview on current status and future directions, Progress in Polymer Science. 39 (2014) 817-861.

[13] Y. Li, H.M. Guan, T.S. Chung, S. Kulprathipanja, Effects of novel silane modification of zeolite surface on polymer chain rigidification and partial pore blockage in polyethersulfone (PES)-zeolite A mixed matrix membranes, Journal of Membrane Science. 275 (2006) 17-28.

[14] Y. Li, T.S. Chung, C. Cao, S. Kulprathipanja, The effects of polymer chain rigidification, zeolite pore size and pore blockage on polyethersulfone (PES)-zeolite A mixed matrix membranes, Journal of Membrane Science. 260 (2005) 45-55.

[15] T.S. Chung, L.Y. Jiang, Y. Li, S. Kulprathipanja, Mixed matrix membranes (MMMs) comprising organic polymers with dispersed inorganic fillers for gas separation, Progress in Polymer Science. 32 (2007) 483-507.

[16] K.M. Gheimasi, T. Mohammadi, O. Bakhtiari, Modification of ideal MMMs permeation prediction models: Effects of partial pore blockage and polymer chain rigidification, Journal of Membrane Science. 427 (2013) 399–410.

[17] K. Tanaka, H. Kita, M. Okano, K. Okamoto, Permeability and permselectivity of gases in fluorinated and non-fluorinated polyimides, Polymer. 33 (1992) 585-592.

[18] J. Fang, X. Guo, S. Harada, T. Watari, K. Tanaka, H. Kita, K. Okamoto, Novel

sulfonated polyimides as polyelectrolytes for fuel cell application: 1. Synthesis, proton conductivity, and water stability of polyimides from 4,4′-diaminodiphenyl ether-2,2′-disulfonic acid, Macromolecules. 35 (2002) 9022-9028.

[19] K. Tanaka, M. Okano, H. Toshino, H. Kita, K. Okamoto, Effect of methyl substituents on permeability and permselectivity of gases in polyimides prepared from methyl-substituted phenylenediamines, Journal of Polymer Science Part B: Polymer Physics. 30 (1992) 907-914.

[20] M. Safak Boroglu, A.B. Yumru, Gas separation performance of 6FDA-DAM-ZIF-11 mixed-matrix membranes for H_2/CH_4 and CO_2/CH_4 separation, Separation and Purification Technology. 173 (2017) 269-279.

[21] J.H. Kim, S.B. Lee, S.Y. Kim, Incorporation effects of fluorinated side groups into polyimide membranes on their physical and gas permeation properties, Journal of Applied Polymer Science. 77 (2000) 2756-2767.

[22] K. Tanaka, M. Okano, H. Toshino, H. Kita, K. Okamoto, Effect of methyl substituents on permeability and permselectivity of gases in polyimides prepared from methyl-substituted phenylenediamines, Journal of Polymer Science Part B: Polymer Physics. 30 (1992) 907-914.

[23] K. Tanaka, H. Kita, K. Okamoto, A. Nakamura, Y. Kusuki, The Effect of Morphology on Gas Permeability and Permselectivity in Polyimide Based on 3,3′,4,4′-Biphenyltetracarboxylic Dianhydride and 4,4′-Oxydianiline, Polymer Journal. 21 (1989) 127-135.

[24] J. Liu, T.H. Bae, W. Qiu, S. Husain, S. Nair, C.W. Jones, R.R. Chance, W.J. Koros, Butane isomer transport properties of 6FDA-DAM and MFI-6FDA-DAM mixed matrix membranes, Journal of Membrane Science. 343 (2009) 157-163.

[25] H. Vinh-Thang, S. Kaliaguine, Predictive models for mixed-matrix membrane performance: A review, Chemical Reviews. 113 (2013) 4980-5028.

[26] Z. Wang, D. Wang, S. Zhang, L. Hu, J. Jin, Interfacial Design of Mixed Matrix Membranes for Improved Gas Separation Performance, Advanced Materials. 28 (2016) 3399-3405.

Chapter 7 Conclusions and Future Works

7.1 Conclusions

In this thesis, gas separation membrane: AEI type zeolite AlPO-18 membranes, PESU and PI-based mixed matrix membranes with filling CHA type SAPO-34, SSZ-13 and AEI type AlPO-18 zeolites. And the gas permeation properties on those gas permeation membranes were investigated, meanwhile, the effects of temperature and pressure on AEI type zeolite AlPO-18 membranes for gas separation were also been discussed.

The first object was aimed at preparing the AEI type and CHA type zeolites with different sizes for the AlPO-18 zeolite membranes and mixed matrix membranes, which is shown in **Chapter 2**.

The second object was aimed at investigating the gas permeation properties on gas separation membranes, which can be divided into four parts:

(1): The first part was to study gas permeation properties on AEI type zeolite AlPO-18 membranes, as shown in **Chapter 3**. The AlPO-18 zeolite membranes were prepared by single TEAOH, single DIPEA template and dual TEAOH and DIPEA templates, respectively. The AlPO-5 impurity formed sometimes when performed the AlPO-18 membranes with single TEAOH and single DIPEA template. The AlPO-18 membranes prepared by single TEAOH template displayed highest CO_2/CH_4 selectivity however lowest CO_2 single gas permeance, by single DIPEA template displayed highest CO_2 single gas permeance with moderate CO_2/CH_4 ideal selectivity, and prepared by combined TEAOH and DIPEA templates displayed moderate CO_2 single gas permeance with lowest CO_2/CH_4 ideal selectivity. Meanwhile, temperature decreased dramatically for CO_2 and N_2 single gas permeance, while the CH_4 is almost independent of temperature, as a result, the CO_2/CH_4 and N_2/CH_4 ideal selectivity was decreased as increasing temperature. Pressure decreased CO_2 single gas permeance while increased a little for N_2 and CH_4 single gas permeances, which finally CO_2/CH_4 ideal selectivity

decreased as increasing pressure and N_2/CH_4 ideal selectivity is almost stable.

(2): The second part was to study gas permeation properties on CHA type zeolite SAPO-34 and SSZ-13 membranes, as shown in **Chapter 4**. SSZ-13 and SAPO-34 membranes can be prepared with few defects larger than 0.5 nm, as indicated by the high CO_2/i-butane separation selectivities (> 500,000 for SAPO-34, 20,000 for SSZ-13). SSZ-13 membranes separate N_2/CH_4 mixtures with higher selectivities of 9-13 at low pressure. The highest N_2/CH_4 selectivity for SAPO-34 membranes was 7. SSZ-13 membranes separate CO_2/CH_4 mixtures with higher selectivities (> 200 at high pressure) than SAPO-34 membranes, but their permeances are only ~10% of the SAPO-34 membrane permeances because the SSZ-13 membranes are thicker. Propane continuously decreases CO_2 and N_2 permeances for both SSZ-13 and SAPO-34 membranes at low pressures, but permeances decreased ten times faster for SAPO-34 membranes. Propane only changed selectivities slightly but steady state was not reached even after seven days. At high pressures, CO_2 permeances and CO_2/CH_4 selectivities initially increased for SSZ-13 membrane, and then CO_2 permeances decreased a few percent per day. For 9% propane in the feed, the CO_2/CH_4 selectivity initially increased 40%. Propane decreases N_2 permeance more than CO_2 permeance, because CO_2 competes better for adsorption sites than N_2 in the zeolite pores as a result of its higher heat of adsorption. Propane adsorbs in SSZ-13 and SAPO-34 pores, but essentially all its permeance is through defects.

(3): The third part was to study gas permeation properties on PESU based mixed matrix membranes by filling CHA type SAPO-34, SSZ-13 and AEI type AlPO-18 zeolites, which is shown in **Chapter 5**. Gas permeability of all test six gases are improved by loading these three type zeolites from compared with neat PESU polymer. While loading with the smallest SAPO-34 zeolites (~100nm) decreased the ideal selectivity due to the crystals aggregation, and loading 20 wt.% bigger and homogeneous SAPO-34 (~200nm) and SSZ-13 (~400nm) zeolites can improve both gas permeability and selectivity. Meanwhile, CO_2 single gas permeability and CO_2/CH_4 ideal selectivity are increased by increasing the filler loading from 20 wt.% to 30 wt.% for SAPO-34 with ~200nm crystals size.

(4): The fourth part was to study gas permeation properties on 6FDA-TrMPD (PI) based mixed matrix membranes by filling CHA type SAPO-34 zeolites, which is shown in **Chapter 6**. One homogeneous SAPO-34 zeolite (~200nm) and one heterogeneous SAPO-34 zeolite (100nm-500nm) were added into homo-made 6FDA-TrMPD (PI) polymer, the single gas permeability. Gas permeability was dramatically improved by filling both zeolites along with decreasing a little ideal selectivity and increased as increasing the filler loading with 20 wt.%, 30 wt.% and 40 wt.%. Higher permeability membrane can be obtained by loading homogeneous zeolites, meanwhile, using milling method to prepare 6FDA-TrMPD (PI)/SAPO-34 MMMs can improve both CO_2 permeability and CO_2/CH_4 selectivity.

7.2 Future works

(1) AlPO-18 membrane is a good candidate for light gas separation as with the excellent pore structure of 0.38nm. Until now, all the reported AlPO-18 membranes were prepared by using the structure-directing agent (SDA), it need to remove the SDA before applying to the usage. If the AlPO-18 membrane can be prepared without using the SDA and keeps the good performance for light gas separation, it will reduce the cost and avoiding some defects that formed when removing the SDA. Microwave irradiation should be a good way for preparing the AlPO-18 membrane without using the SDA.

(2) For preparing the mixed matrix membranes (MMMs), the crystals that difficult to aggregate should be a good candidate to fabricate high gas separation performance membranes. All-silica or high silica zeolites with appropriate pore system might be a good choice. Meanwhile, before loading the zeolites into the polymer, the modification of both filler and polymer may improve the connection of the filler and polymer, for example, amino-functionalized of the filler and polymer.

List of publications

1. **Ting Wu,** Bin Wang, Zhanghui Lu, Rongfei Zhou, Xiangshu Chen, "Alumina-supported AlPO-18 membranes for CO_2/CH_4 separation", *Journal of Membrane Science*. 471, 338-346, 2014.

2. **Ting Wu,** Merritt C. Diaz, Yihong Zheng, Rongfei Zhou, Hans H. Funke, John L. Falconer, Richard D. Noble, "Influence of propane on CO_2/CH_4 and N_2/CH_4 separations in CHA zeolite membranes", *Journal of Membrane Science.* 473, 201-219, 2015.

3. **Ting Wu,** Kazuhiro Tanaka, Xiangshu Chen, Izumi Kumakiri, Hidetoshi Kita, "Synthesis and gas permeation properties of AEI zeolite membranes by DIPEA as a template", *Membrane.* (Accepted)

4. **Ting Wu,** Izumi Kumakiri, Kazuhiro Tanaka, Xiangshu Chen, Hidetoshi Kita, "Preparation and gas permeation properties of PESU-based mixed matrix membranes with nano-sized CHA-type zeolites", (In preparation for submission)

Acknowledgements